SOLID STATE CHANGES IN THE LEACHING OF COPPER SULPHIDES

A Thesis

presented for the degree of

Doctor of Philosophy

in the

University of London

by

James Anthony King, B.Sc.(Eng)., ARSM.

London, November 1966

ABSTRACT

Particulate chalcocite (Cu_2S) was leached in acidified ferric chloride solution and kinetic rate-curves obtained. Chalcocite dissolved in two distinct stages; firstly the chalcocite rapidly lost one half of its copper and transformed to covellite (CuS), secondly the covellite transformed to elemental sulphur. The apparent activation energies of each half of the leach were determined. Interpretation of the rate-curves gave the rate-controlling steps and mechanisms of the two halves of the leaching process.

X-ray powder photographs of residues representing the whole range of the leach from Cu_2S to sulphur showed the phases and phase changes that occurred throughout the leaching process.

Electron probe microanalyser scans across a section of a leached chalcocite disc illustrated the non-stoichiometry of the residue phases.

Microscopic examination of sectioned leached cubes of chalcocite showed the porous nature of the artificially produced covellite and the formation of elemental sulphur in the pores of the porous covellite phase.

CONTENTS

		Page
SECTION 1		
LITERATURE SURVEY		
1.1	Previous Work on the Leaching of Chalcocite and Covellite	1
1.2	Crystal Structures of Chalcocite, Covellite and Orthorhombic Sulphur	15
1.2.1	Structure of Chalcocite	15
1.2.2	Structure of Covellite	20
1.2.3	Structure of Orthorhombic Sulphur	20
1.3	Phase Diagram of the Cu-S System	27
1.4	Complexing of the Ferrous and Ferric Ions in the Leach Solution	33
1.4.1	Hydrolysis of Ferric Ion	33
1.4.2	Hydrolysis of Ferrous Ion	38
1.4.3	Ferric-Chloro Complexes	39
1.4.4	Ferrous-Chloro Complexes	43
1.4.5	Ferric-Ferrous Chloro complexes	44
1.4.6	Electron Transfer between Ferric and Ferrous Ions in Aqueous Chloride Solutions	44
SECTION 2		
EXPERIMENTAL PROCEDURE		
2.1	Preparation of Chalcocite, Cu_2S	46
2.2	Recrystallization of the Chalcocite	48
2.3	Leaching Apparatus and Experimental Procedure	50
2.4	Analysis	54
2.4.1	Analytical Technique	54

Page

2.4.2 Analytical Procedure 55
2.4.3 Absorption Spectra of the Ions present in the Analysis 55
2.4.4 Beers Law Plot 59
2.4.5 The effect of Ferric Hydroxide Precipitate Volume on the Absorbance 62
2.4.6 Copper Adsorption onto the Ferric Hydroxide Precipitate. 64
2.4.7 Pipette Calibration 64
2.4.8 Purity of Materials 66

SECTION 3

RESULTS AND DISCUSSION

3.1 Kinetic Rate-Curves of the Leaching of Chalcocite. Effect of the Leach Variables on the Rate of Reaction 69
3.1.1 Temperature 69
3.1.2 Particle Size 77
3.1.3 Stirring Speed 81
3.1.4 Ferric Ion Concentration 84
3.1.5 Ferrous Ion Concentration 86
3.1.6 Ferrous Ion in the presence of Ferric Ion 88
3.1.7 Acid Concentration 90
3.1.8 Sample Weight 91
3.2 Microscopic Examination of Leached Chalcocite Discs 93
3.3 X-ray Powder Diffraction Study of the Leach Residues 109
3.3.1 First Reaction-half 118
3.3.2 Second Reaction-half 123
3.4 Electron Probe Work 125
3.4.1 Theory of the Electron Probe Microanalyser 125

Page

3.4.2 Experimental Procedure 128

3.4.3 Results and Discussion 133

SECTION 4

CONCLUSIONS

4.1 Summary of Results 143

4.2 Comparison of the Present Investigation with Previous Work 145

SECTION 5

APPENDIXES 150

ACKNOWLEDGEMENTS 193

REFERENCES 194

SECTION 1

LITERATURE SURVEY

1.1 Previous Work on the Leaching of Chalcocite and Covellite

J. D. Sullivan[1] studied the chemical and physical features of the leaching of these particulate minerals with an acidified ferric sulphate solution. He found the following phenomena:

i) Chalcocite dissolved in two stages, the first being much more rapid than the second (fig. 1). The two stages were represented by the Cu_2S rapidly giving up one half of its copper and changing to a form approximating to CuS, which then dissolved at a slower rate. The reactions may be written:

$$Cu_2S + Fe_2(SO_4)_3 = CuS + CuSO_4 + 2FeSO_4$$

$$CuS + Fe_2(SO_4)_3 = CuSO_4 + 2FeSO_4 + S$$

or combining the two halves of the reaction:

$$Cu_2S + 2Fe_2(SO_4)_3 = 2CuSO_4 + 4FeSO_4 + S$$

The rate of the first reaction-half was markedly increased by a decrease in the particle size; the rate of the second reaction-half was virtually independent of particle size (fig. 1). Sullivan inferred from the fact that the rate of the second reaction-half was virtually independent of particle size that either chalcocite contained in its normal condition, sufficient capillary

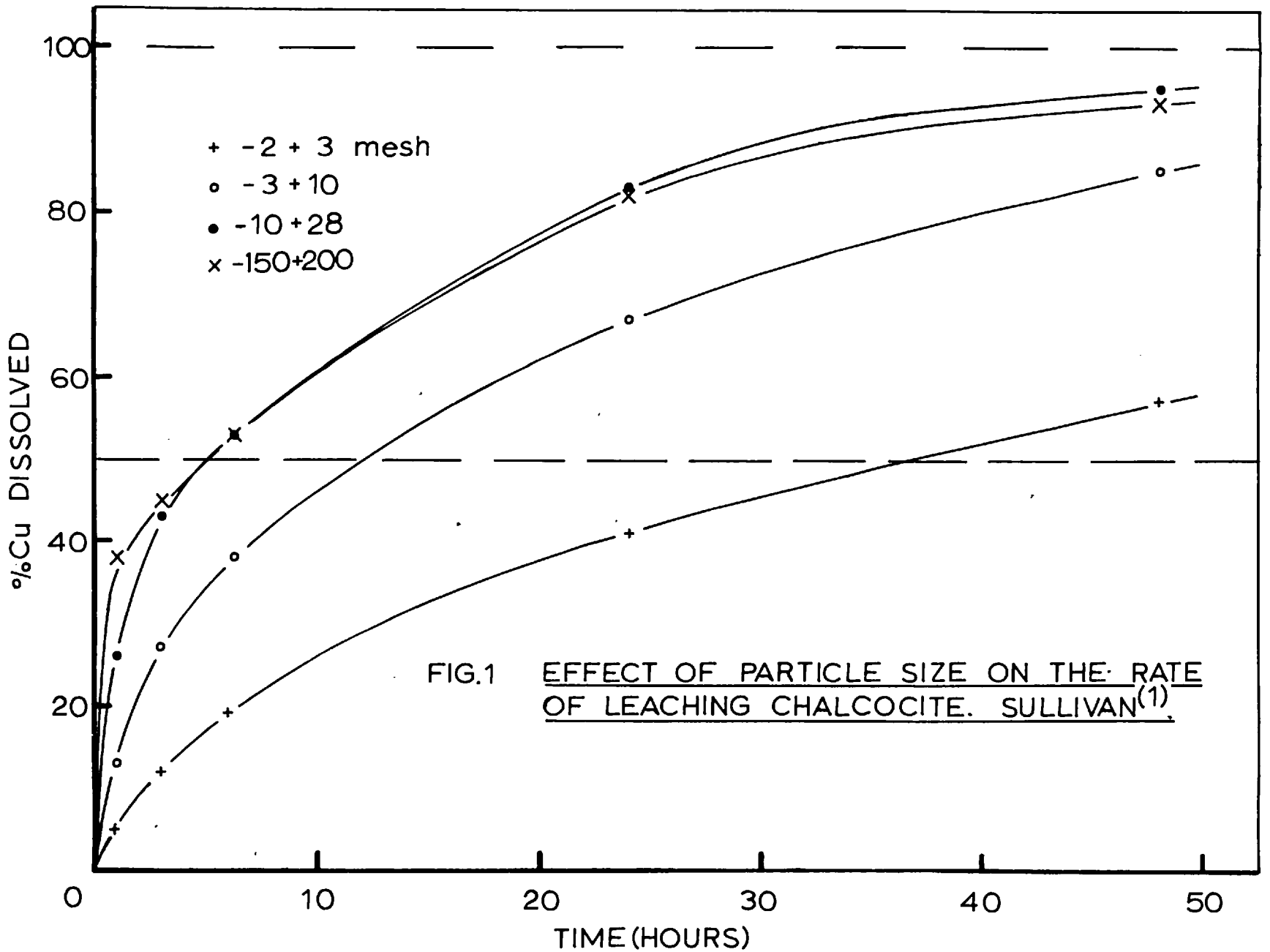


FIG.1 EFFECT OF PARTICLE SIZE ON THE RATE OF LEACHING CHALCOCITE. SULLIVAN[1].

pores or openings to permit ingress of solution, or that internal fractures are opened during the crushing process. He thought the latter unlikely since the larger pieces received scarcely any breaking or crushing treatment.

ii) Over the range 0.2 to 1.0 g.ion Fe^{3+} per litre, the rate of the first reaction-half was virtually independent of ferric ion concentration; over the range 0.2 to 0.6 g.ion Fe^{3+} per litre, the rate of the second reaction-half increased with increasing ferric ion concentration. The rates of both halves were independent of sulphuric acid concentration over a wide range. In very dilute ferric sulphate solutions, the addition of ferrous sulphate in large quantities retarded the rate of both halves of the leach.

iii) Sullivan believed that the artificially produced CuS was not the same as natural covellite. The reasons behind this argument were that a) the rate of dissolution of artificial covellite is markedly different from that of natural covellite and b) the bluish colour of the polished leached mineral surface was of a much paler blue than true natural covellite. Sullivan thought it resembled the colour often classified by mineralogists as blue chalcocite, which is claimed to be an intimate mixture of white chalcocite and blue covellite and which

gives a paler colour than that of true covellite.

iv) An increase in the leaching temperature markedly increased the rate of the second half of the reaction (fig. 2).

v) After leaching, the particles retained nearly their original outline, the sulphur remaining behind retaining the form of the original chalcocite. Addition of carbon bisulphide dissolved the sulphur and the particles collapsed.

vi) Covellite was found to dissolve at a much slower rate than chalcocite. Particle size had a significant effect on the leaching rate and the smaller size fraction dissolved more rapidly than larger ones (fig .3). Sullivan thought that the difference, however, was not as great as would be expected from the new area of surface exposed during grinding. He thought this might be explained by covellite being somewhat porous by nature, or internal fractures being formed during grinding and crushing, which would permit influx of leaching solution into the particles.

vii) The rate of dissolution was increased by increases in temperature, (fig. 4). Using Sullivan's data, the activation energy of the dissolution of covellite is calculated to be 8.6 ± 2.2 kcals.

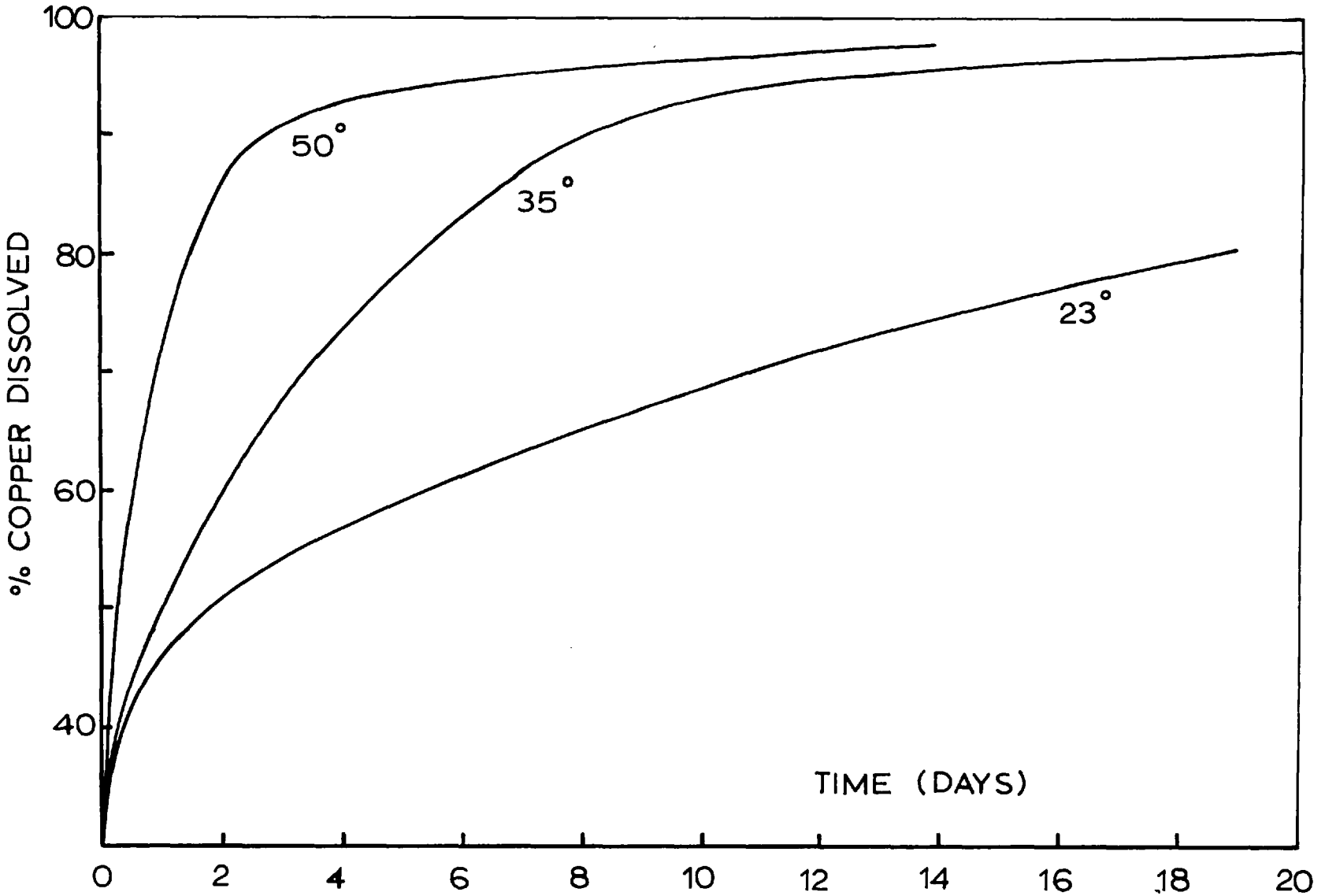


FIG.2 EFFECT OF TEMPERATURE ON THE RATE OF LEACHING -100 + 200 MESH CHALCOCITE IN ACIDIFIED $Fe_2(SO_4)_3$ AQ. J.D. SULLIVAN[1].

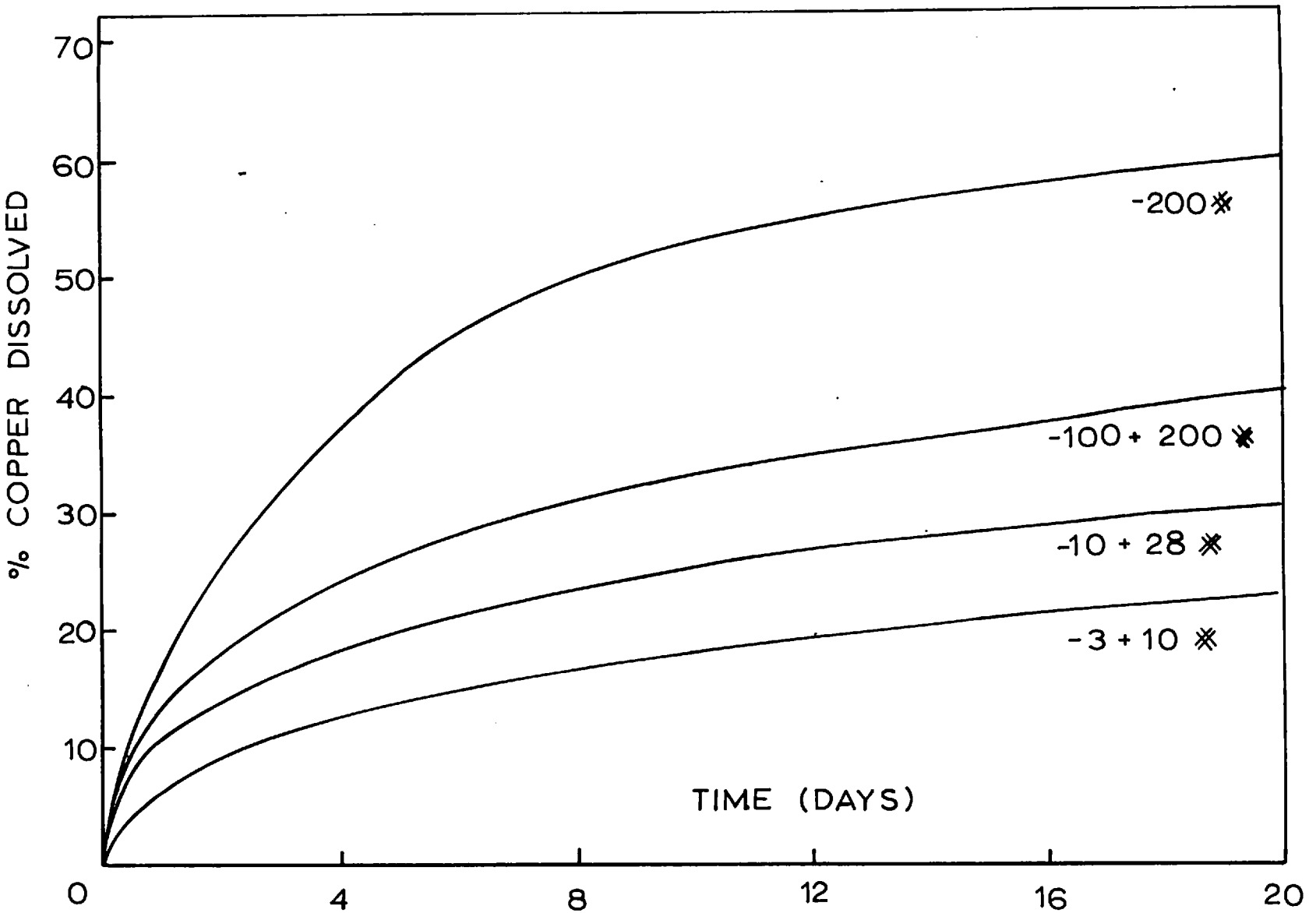


FIG.3 EFFECT OF MESH SIZE ON THE RATE OF LEACHING COVELLITE IN ACIDIFIED $Fe_2(SO_4)_3$ AT 35°C. J.D.SULLIVAN[1].

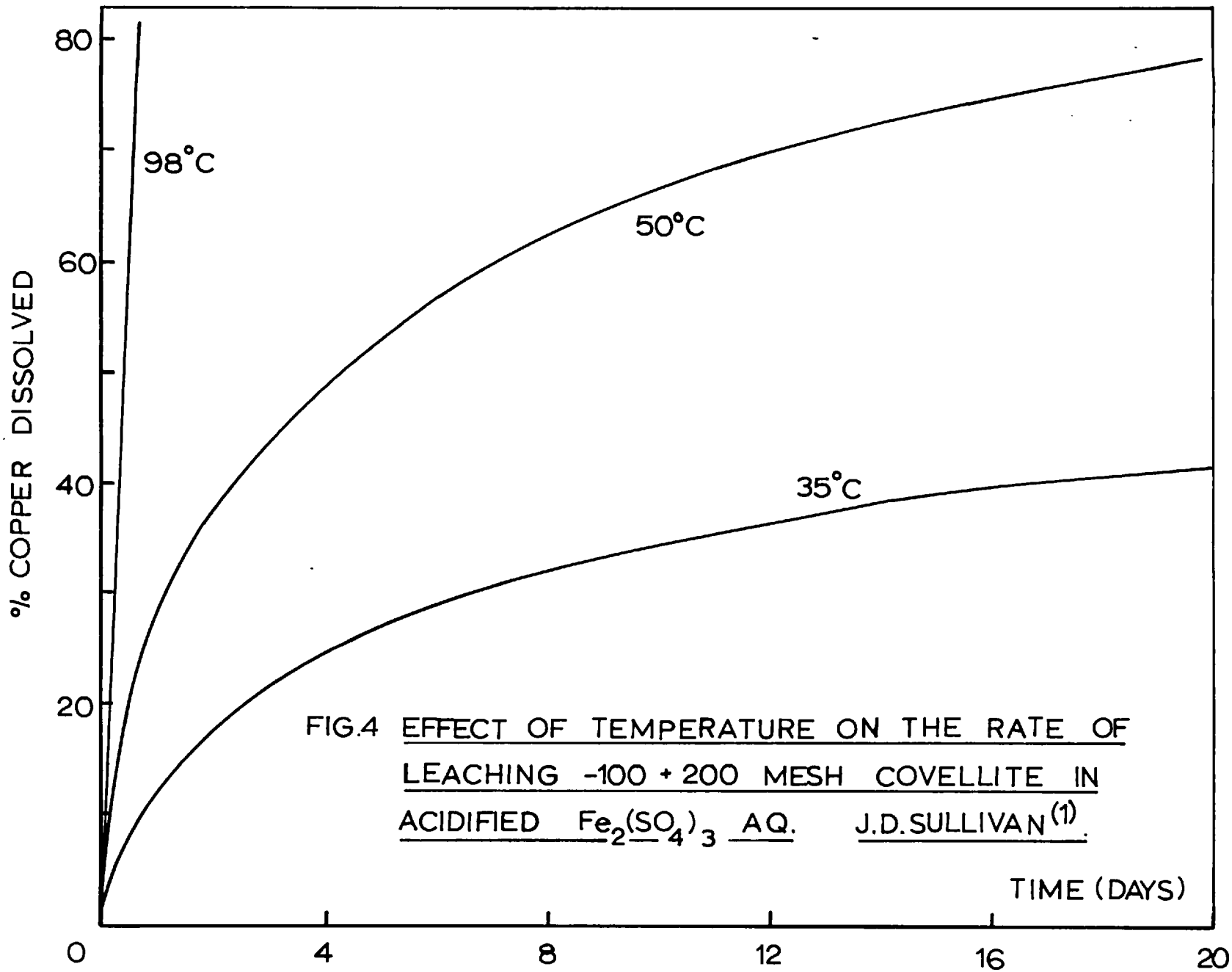


FIG.4 EFFECT OF TEMPERATURE ON THE RATE OF LEACHING -100 + 200 MESH COVELLITE IN ACIDIFIED $Fe_2(SO_4)_3$ AQ. J.D.SULLIVAN[1].

Sullivan's results showed that artificial covellite, produced by leaching 50% of the copper from chalcocite, dissolved much more rapidly than natural covellite (fig. 5). This behaviour, coupled with the fact that the 'artificial' covellite was not as dark a blue as he thought it should have been, led Sullivan to state that one cannot say that when chalcocite is leached with ferric sulphate, one half of the copper is rapidly dissolved leaving a residue of covellite which dissolves at a slower rate.

I. H. Warren[2] studied the acid pressure leaching of chalcocite and covellite. The experimental conditions were high temperatures (100-200°C), high oxygen partial pressures (10-100 psi.), and an acidity of 20-50g H_2SO_4/l. The two half-stages of the chalcocite leach reaction were evident. The rate of both halves of the reaction increased with an increase in temperature (fig. 6) and the activation energies for the processes controlling the first and second stages of leaching of the copper were calculated to be 6.6 and 1.8 kcal/mole respectively.

The amount of copper leached after a given time was directly proportional to the weight of the Cu_2S sample and hence to its surface area.

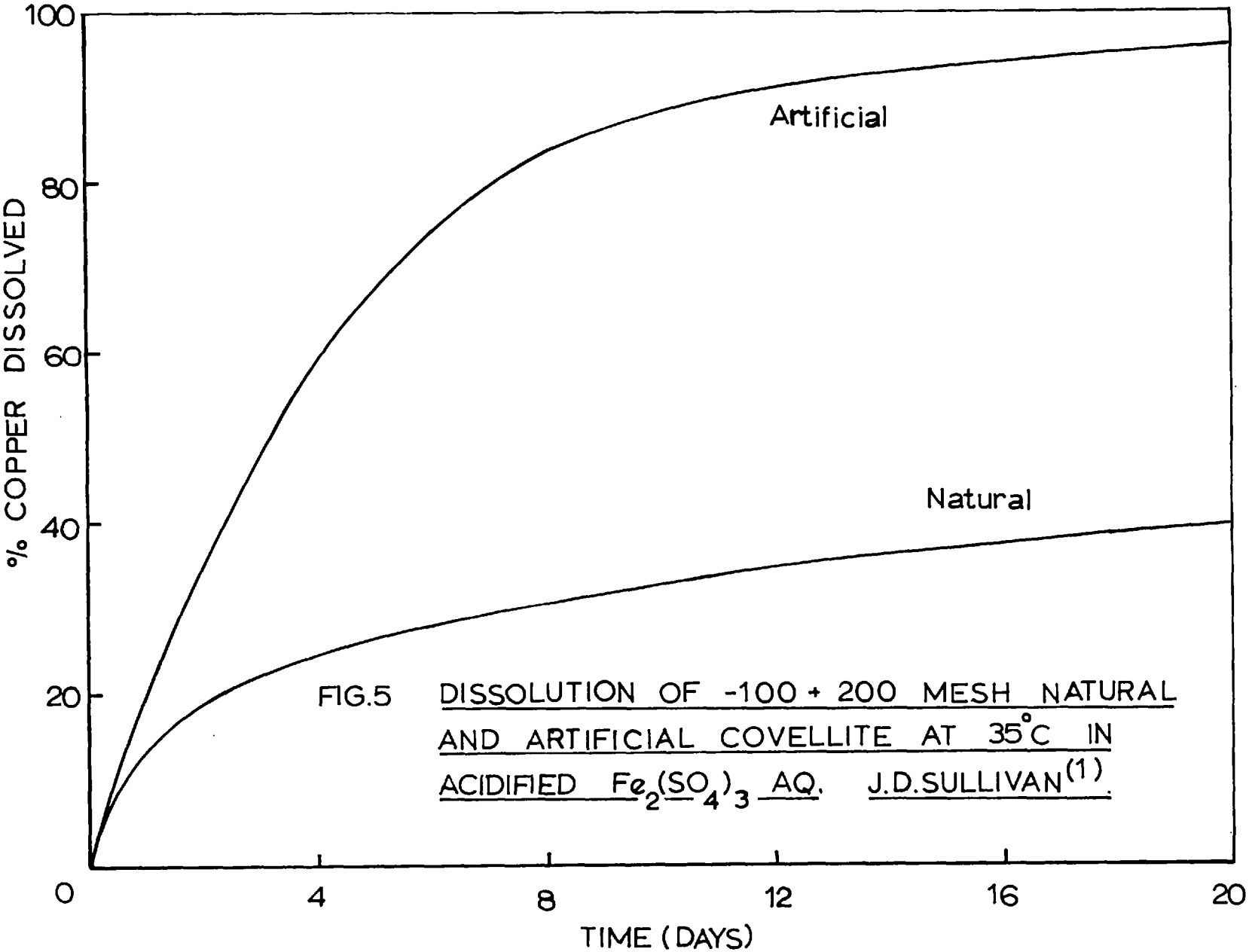


FIG.5 DISSOLUTION OF -100 + 200 MESH NATURAL AND ARTIFICIAL COVELLITE AT 35°C IN ACIDIFIED $Fe_2(SO_4)_3$ AQ. J.D.SULLIVAN[1].

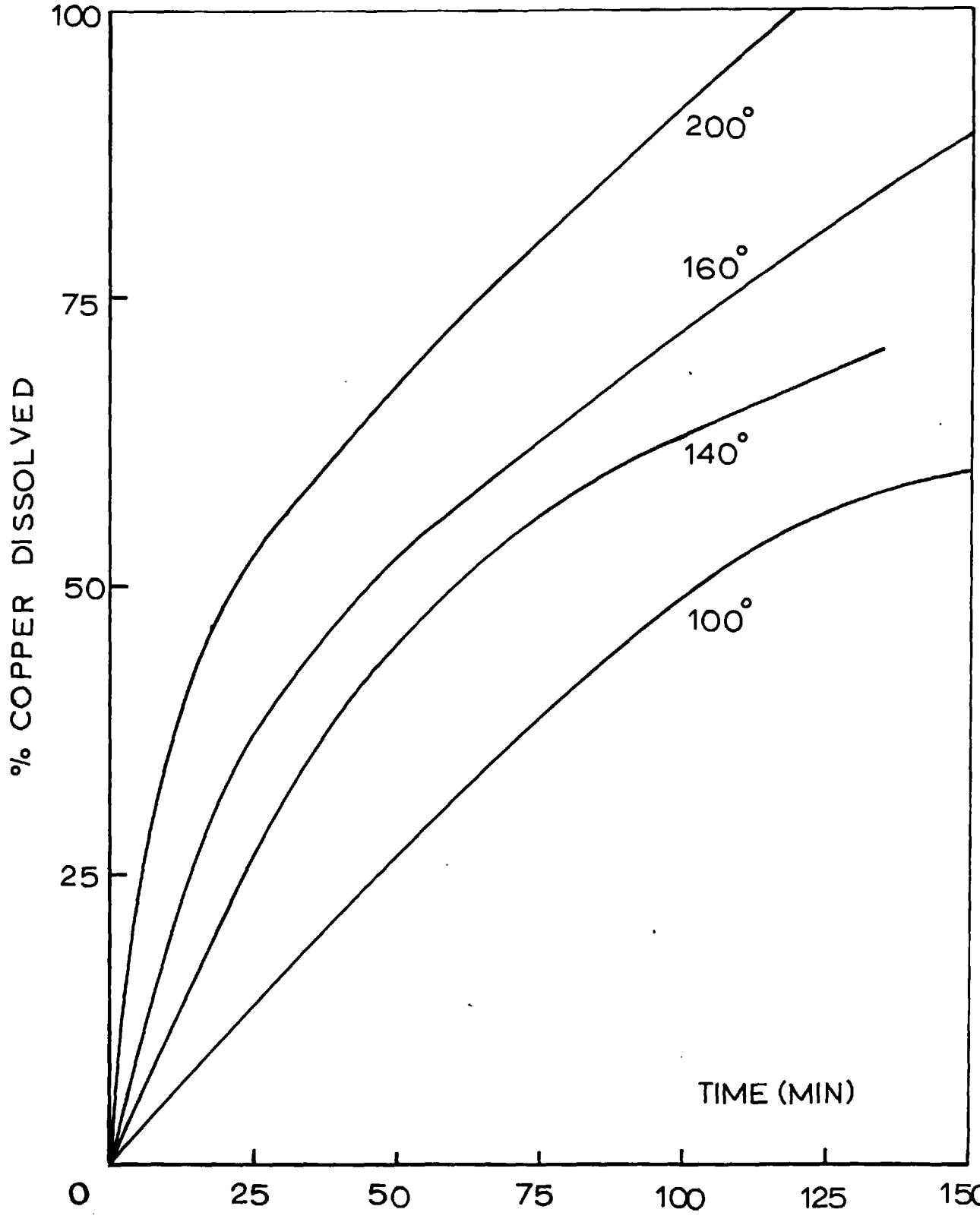


FIG.6 EFFECT OF TEMPERATURE ON THE RATE OF LEACHING CHALCOCITE AT 40 P.S.I. O_2 IN 30g H_2SO_4/l. I.H.WARREN[2].

The value of the activation energy (6.6 kcals/mole) for the first half of the leach, and the dependence of rate on the surface area, led Warren to suggest that the process controlling the first stage of oxidation of chalcocite is a heterogeneous process at the surface of the mineral. He dismissed the possibility of copper ion diffusion in the mineral lattice as the controlling step since Jost[94] had shown this diffusion process to have a low activation energy, of value approximately 1 kcal/mole.

Warren suggested that the low temperature coefficient of the second stage of the leaching may have been due to coating of the mineral surface with molten elemental sulphur.

Increasing the oxygen pressure increased the rate of the first half of the leach until at a critical value, any further increase in oxygen pressure had no significant effect on copper dissolution. The rate of the second half of the reaction increased with an increase in oxygen pressure over the whole range of pressure studied.

Acid concentration had a nominal effect on the leach rate, and this variation was probably due to the effect of acid concentration on oxygen dissolution.

Covellite was leached under similar conditions to those of chalcocite. A typical rate curve showed the rate of copper dissolution to decrease as copper was removed (fig. 7).

Increasing the temperature of the leach solution increased the rate of copper dissolution significantly, (fig. 7), giving an activation energy of 11.7 kcal/mole. Warren thought this too high a value for a diffusion controlled process.

The rate was also increased by increasing a) the oxygen partial pressure and b) the sample weight, i.e. the surface area, (fig. 8). As in the case of the first half of the chalcocite leach, Warren thought that the rather high activation energy value of 11.7 kcal/mole, and the dependence of leach rate on surface area, suggested the rate-controlling step to be a heterogeneous process at the surface.

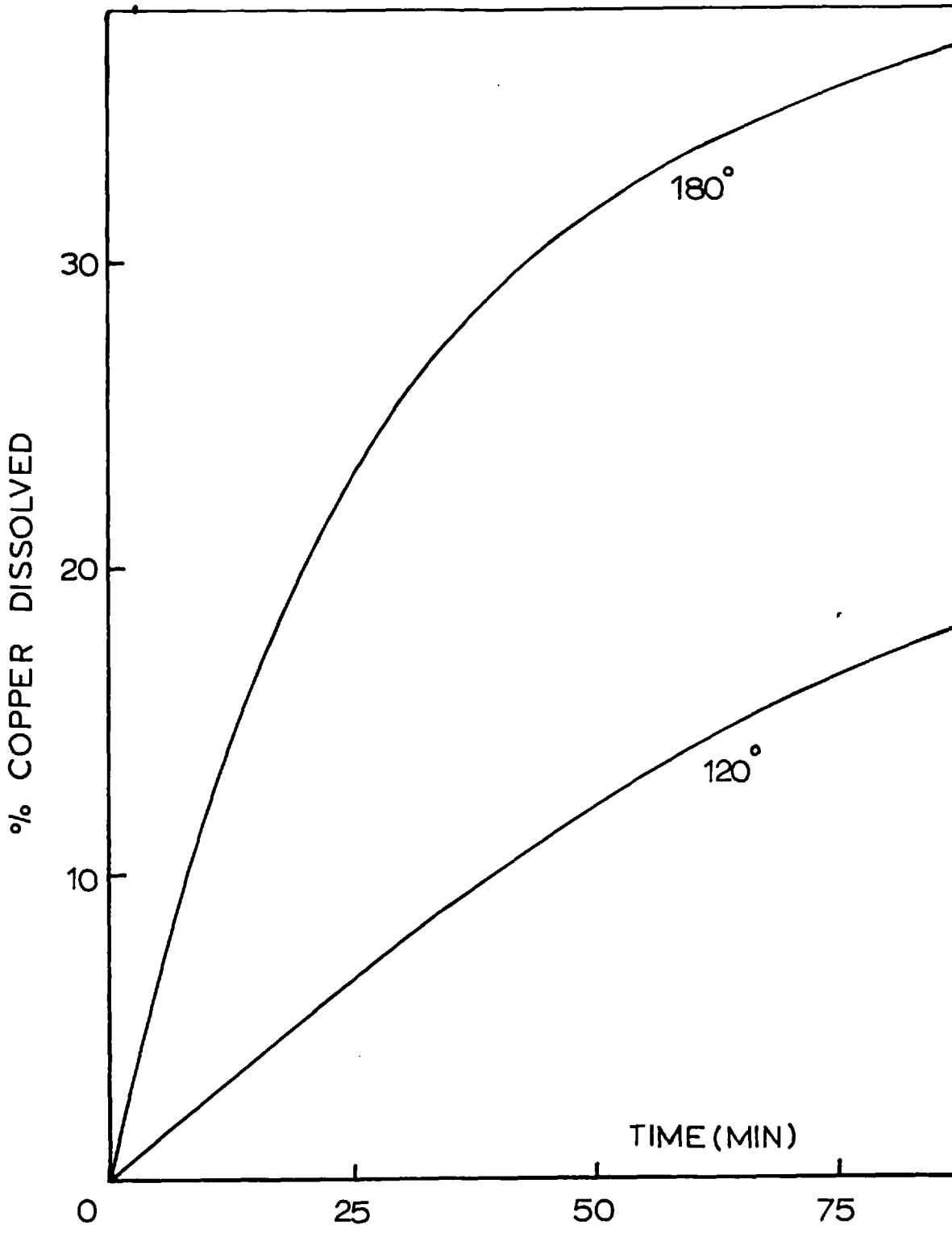


FIG.7 EFFECT OF TEMPERATURE ON THE RATE OF LEACHING COVELLITE AT 100 P.S.I. O_2 AND pH = 0.75 I.H.WARREN.

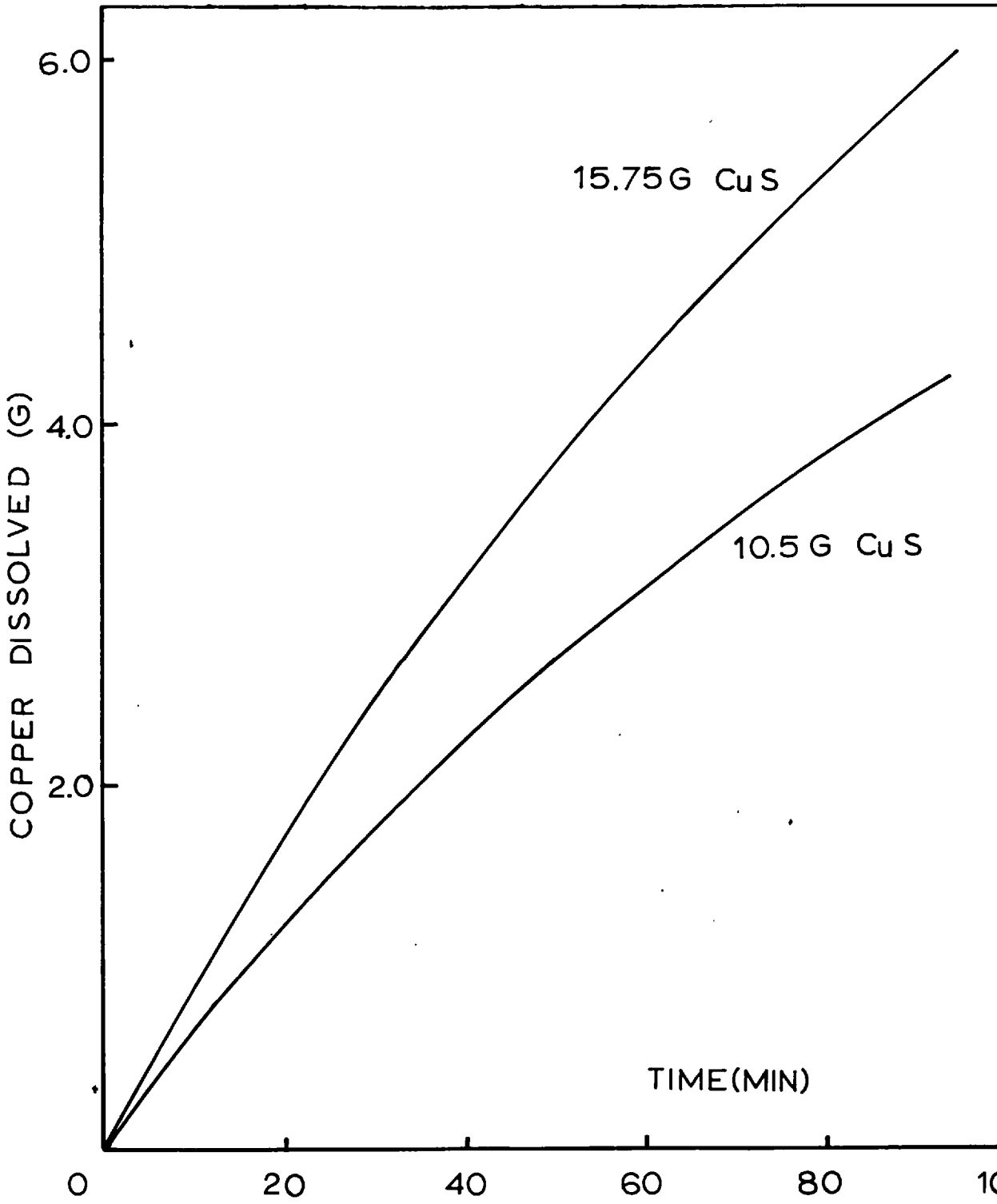


FIG.8 EFFECT OF SAMPLE WEIGHT ON THE RATE OF LEACHING COVELLITE AT 180°C 100 P.S.I. O_2 AND MODERATE ACIDITY. I.H.WARREN[2].

1.2. Crystal Structures of Chalcocite, Covellite and Orthorhombic Sulphur

1.2.1. Structure of Chalcocite

The structure of this mineral has been the subject of many investigations (10-18).

Djurle[18], using high temperature X-ray analysis, revealed two phase transitions in Cu_2S. The low temperature transition is gradual at about 110°C, in agreement with previous workers (11,16,17); the upper transition occurs at 465 to 475°C, in agreement with the value of Hirahara[16].

Djurle indicated that the low temperature form Cu_2S III has an A-centred orthorhombic cell and that the intermediate phase Cu_2S II has a hexagonal unit cell.

The high temperature phase Cu_2S I was indexed as having a face-centred cubic lattice with a cell edge of:

$a = 5.725\text{Å}$ 465°C

$a = 5.735\text{Å}$ 500°C

A cell content of $4Cu_2S$ is consistent with the cube edge.

The cell dimensions of the orthorhombic cell are:

$a = 11.82\text{Å}$, $b = 27.05\text{Å}$, $c = 13.43\text{Å}$

The cell dimensions of the hexagonal cell are:

$a = 3.89\text{Å}$, $c = 6.88\text{Å}$

The orthorhombic and hexagonal phases are related by a reversible transformation and it has been shown that a substructure - superstructure relationship exists between the unit cells of the two structures[12]. The axes of the A-centred orthorhombic unit cell were multiples of 3, 4 and 2 of the cell edges of the orthohexagonal cell in the a, b, and c directions respectively, (fig. 9). Assuming that one structure could be derived from the other, Wuensch and Buerger[15] assigned the space group Ab2m (C_{2v}^{15}) to the orthorhombic form and $P6_3/mmc$ (D_{6h}^{4}) to the hexagonal form. The orthorhombic structure contains 96 Cu_2S per unit cell and is complex, whereas the hexagonal cell contains only 2 Cu_2S per unit cell.

Early attempts to solve satisfactorily the relatively simple hexagonal structure were unsuccessful, (12,13,17). The difficulty in finding a structure for hexagonal chalcocite was due to the disordered structure, so that the four copper atoms in the unit cell could not be placed merely on a four-fold, or two, two-fold equipoints.

To find the distribution of the disordered copper atoms, Wuensch and Buerger employed intricate and complicated crystallographic methods. The disordered hexagonal chalcocite structure was found to contain

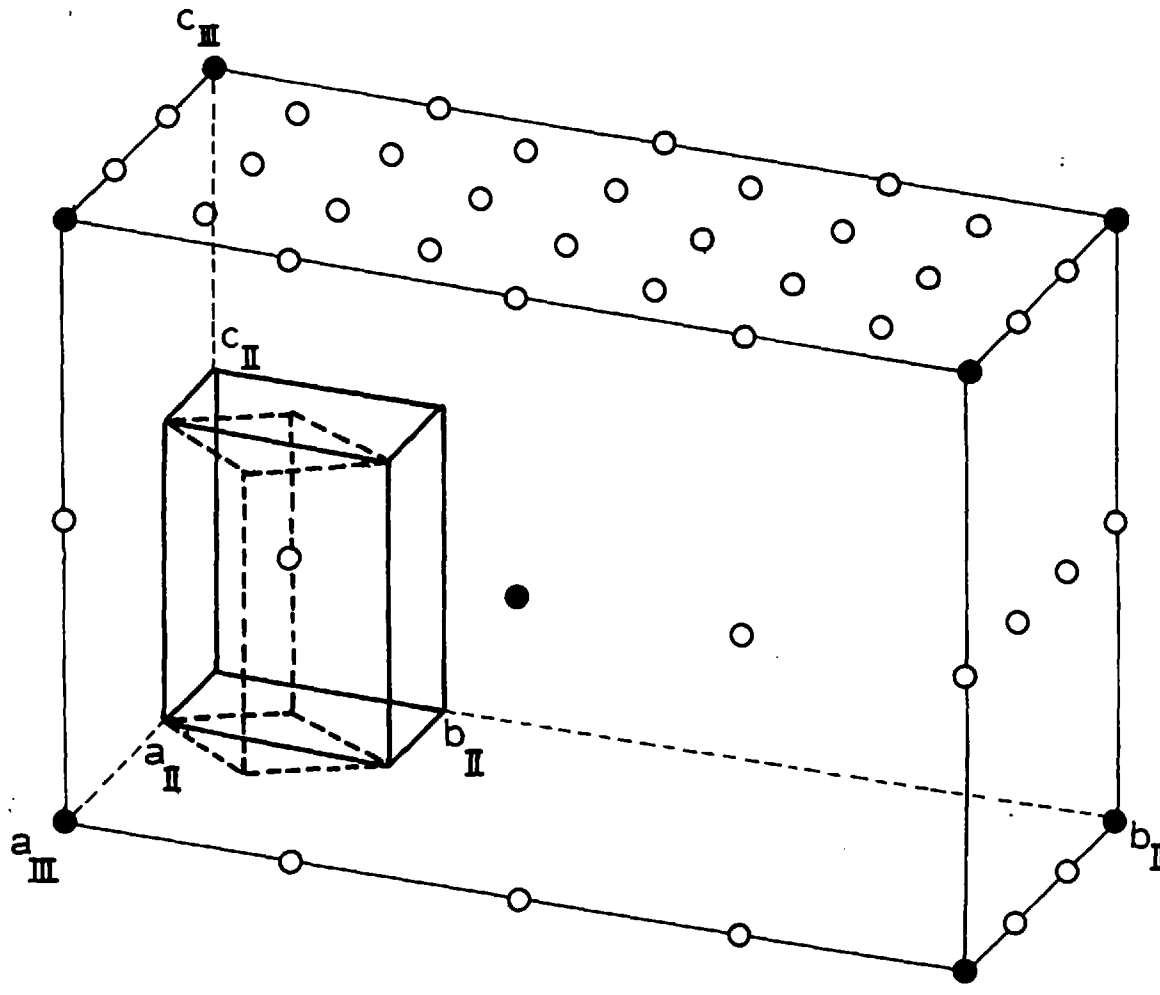


FIG.9 RELATION BETWEEN THE ORTHOHEXAGONAL UNIT CELL OF Cu_2SII CHALCOCITE AND THE A-CENTRED ORTHORHOMBIC CELL OF Cu_2SIII CHALCOCITE. (The lattice points of Cu_2SII chalcocite are indicated by open points and those of Cu_2SIII chalcocite by solid points. The hexagonal cell of Cu_2SII chalcocite is indicated by heavy dotted lines.)

sulphur atoms in hexagonal close packing and mobile Cu atoms statistically occupying 3 types of sites, Table 1.

TABLE 1.

Co-ordinates of atom positions in hexagonal chalcocite.

Atom	Equipoint	Co-ordinates	Temperature Factor
1S	2d	$\frac{2}{3}$, $\frac{1}{3}$, $\frac{1}{4}$	0.43
0.870 Cu^{1}	2b	0, 0, $\frac{1}{4}$	0.15
0.355 Cu^{11}	4f	$\frac{1}{3}$, $\frac{2}{3}$, 0.568	4.73
0.140 Cu^{111}	6g	0, $\frac{1}{2}$, 0	3.28

Cu^{1} lies in the S layers forming a trigonal CuS sheet. Cu^{11} occupies the available tetrahedral sites. Covellite also exhibits this combination of Cu-S layers and tetrahedrally co-ordinated copper. The remaining Cu^{111} atoms are located on three edges of the S tetrahedron and thus statistically link an S atom to three S atoms in the neighbouring sheet.

The Cu-S bond lengths are 2.28Å and 2.06Å for Cu^{1} and Cu^{111} respectively. Cu^{11} is not located in the centre of the S tetrahedron, but has three neighbours at 2.59Å and one at 2.15Å.

In hexagonal chalcocite, the hexagonal close packed sulphur atoms comprise a substantially fixed structure,

while the copper atoms are mobile through the interstices of this structure. The mobility is possible because the copper atoms can assume tetrahedral, trigonal, and linear co-ordination.

In the orthorhombic form which exists at a lower temperature, the thermal energy is insufficient to maintain mobility and the structure is doubtless characterised by sulphur atoms in hexagonal close-packed array with copper atoms in at least two of the three co-ordinations observed in the high temperature form. The alternation of copper in different co-ordinations accounts for the large superstructure cell of the orthorhombic phase.

Wuensch and Buerger were unable to solve the orthorhombic structure. However, they measured three-dimensional diffraction intensities of orthorhombic chalcocite, which when computed, indicated that the tetrahedral and trigonal sites were occupied.

Although work is still in progress[19], the solution of this structure is still far from complete. The formidable problems are the large number of atoms contained in the unit cell, and the marked substructure.

1.2.2. Structure of Covellite

I. Oftedal[5] first solved the structure of covellite using lattice dimensions taken from earlier work[6,7]. His investigation showed a highly symmetrical space group D^4_{6h} $P6_3/mmc$. The hexagonal unit cell is shown in fig. 10[8] and contains 6CuS. It has the dimensions:

$a = 3.80\text{Å}$, $c = 16.4\text{Å}$, $c/a = 4.32$

The point positions of the atom are:

For Cu $\frac{1}{3}, \frac{2}{3}, u$; $\frac{2}{3}, \frac{1}{3}, \bar{u}$; $\frac{1}{3}, \frac{1}{3}, \frac{1}{2}-u$

$\frac{2}{3}, \frac{1}{3}, \frac{1}{2}+u$; $\frac{1}{3}, \frac{2}{3}, \frac{3}{4}$; and $\frac{1}{3}, \frac{1}{3}, \frac{1}{4}$

$u = 0.107 \pm 0.001$

For S $00v$; $00\bar{v}$; $0,0,\frac{1}{2}-v$; $0,0,\frac{1}{2}+v$;

$\frac{1}{3}, \frac{2}{3}, \frac{1}{4}$; and $\frac{2}{3}, \frac{1}{3}, \frac{3}{4}$;

$v = \frac{1}{16}$

The interatomic distances are:

S-S = 2.05Å, Cu-S = 2.20 to 2.35Å.

A clearer picture of the structure is shown in figs. 11 and 12.

L. B. Berry[9] confirmed the structure of Oftedal, but recommended a slight change in the v parameter of the S point positions, to v = 0.064.

1.2.3. The Structure of Orthorhombic Sulphur

The crystal structure of orthorhombic sulphur has been solved by Warren and Burwell[3]. It comprises

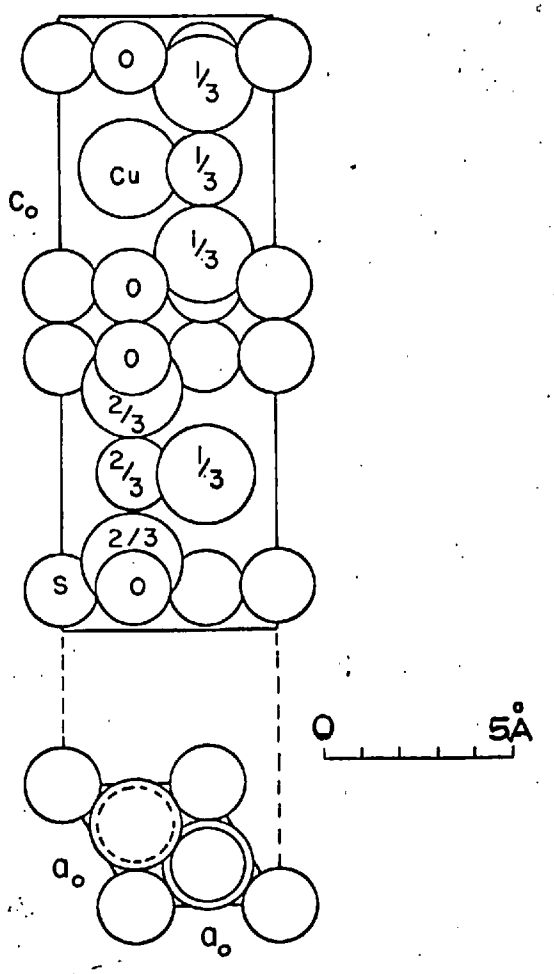
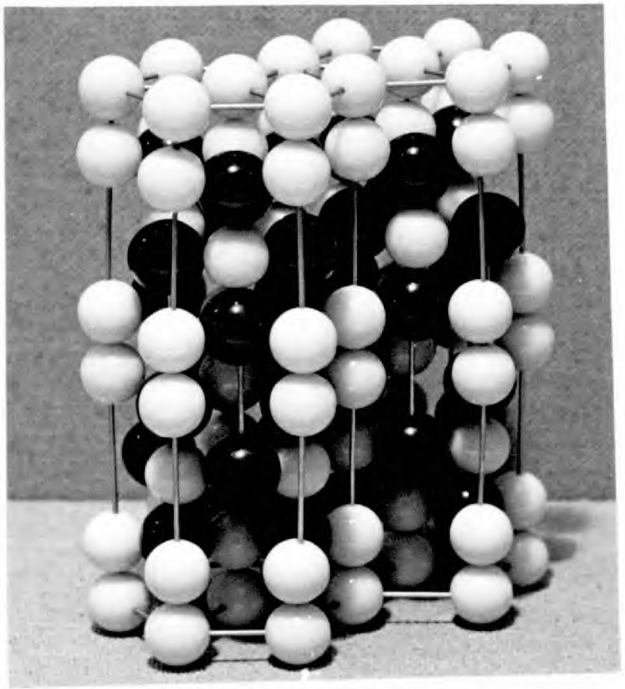
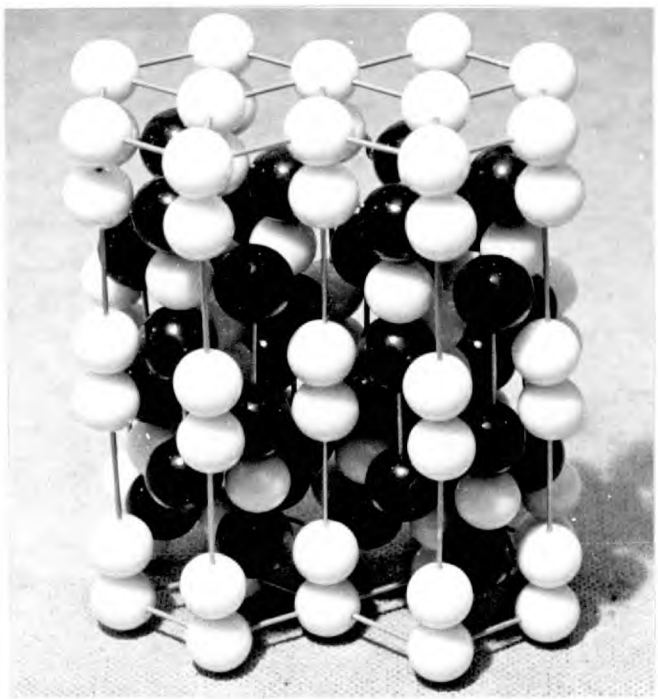


FIG.10 THE HEXAGONAL UNIT CELL OF CuS SHOWN IN TWO PROJECTIONS.





Figs. 11 & 12 Crystal structure of covellite

symmetrically puckered S_8 ring molecules. The space group is D_{2h}^{24} - Fddd, with 16 molecules per unit cell.

The complete structure is shown in fig. 13. The c co-ordinates of the atoms are given in degrees, so that for example 90° means one-fourth of the c axis up from the plane of the paper. To avoid confusion, only part of the molecules in the cell are shown; in the lower left hand portion from $0\text{-}90^\circ$, and in the upper right hand portion from $0\text{-}180^\circ$. The molecules are arranged approximately in layers perpendicular to the c axis, with 4 molecules in each quarter of c.

The molecular and unit cell dimensions have since been determined extremely accurately by S.C. Abrahams[4]. The orthorhombic unit cell measured:

$$a = 10.437 \pm 0.01\text{Å}, \quad b = 12.845 \pm 0.01\text{Å} \text{ and}$$
$$c = 24.369 \pm 0.01\text{Å}$$

(hkl) is present only when h+k, k+l, l+h = 2n;
(0kl) only when k+l = 4n; (h0l) only when h+l = 4n;
(kk0) only when h+k = 4n.

The S_8 molecule (fig. 14) may be described as consisting of two 'squares' formed by atoms $S_1S_2S_3S_4$ and $S_5S_6S_7S_8$, with a distance of 0.99Å between their mean planes. One 'square' is turned through 45° with respect to the other and their two planes are identically parallel.

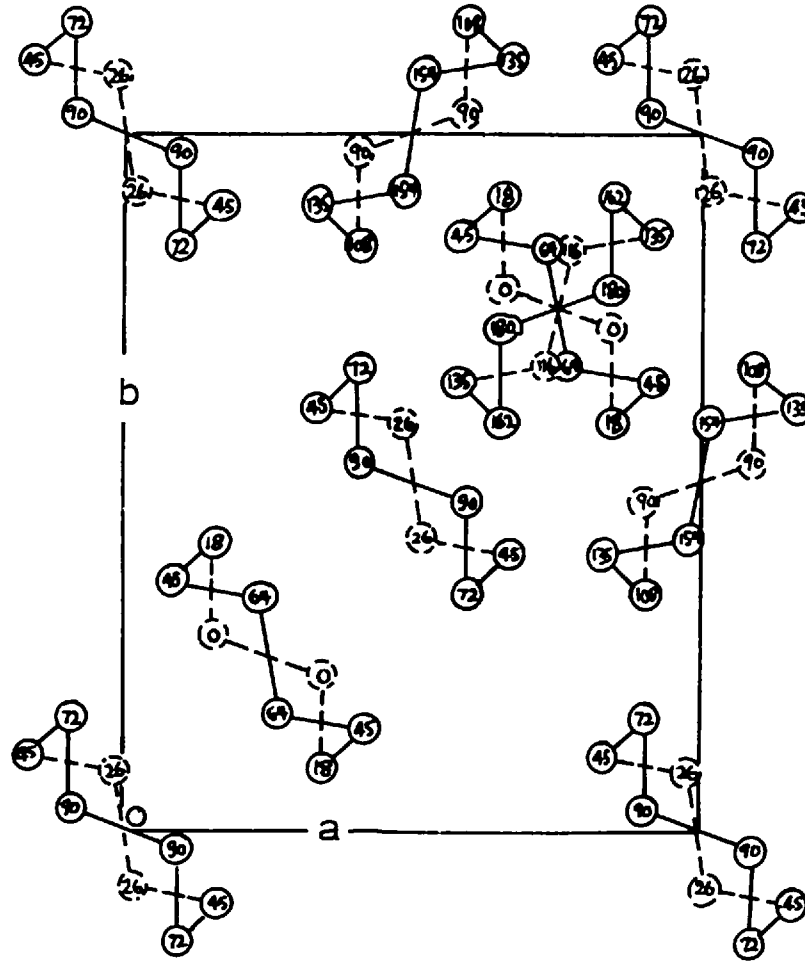
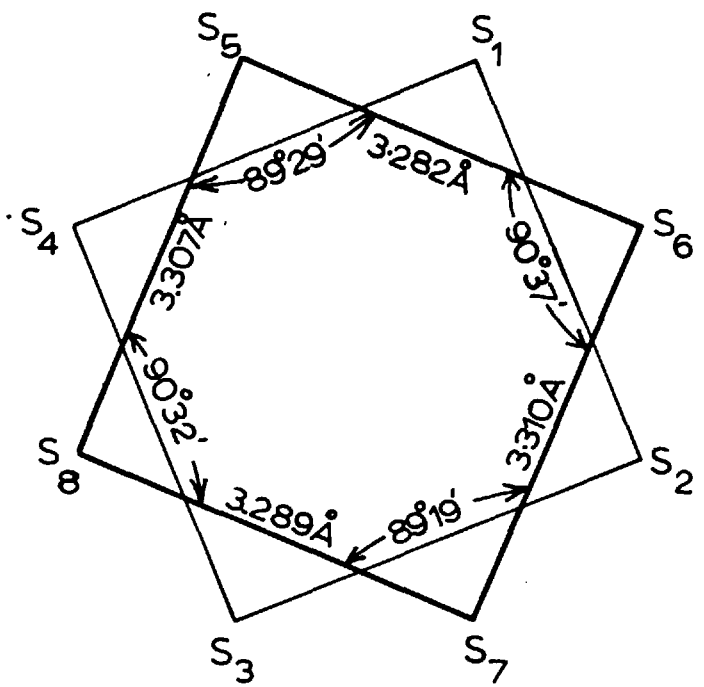


FIG. 13 STRUCTURE OF ORTHORHOMBIC SULPHUR. (Only part ~~of part~~ of the molecules in the cell are shown; the 'c' coordinates are given in degrees.)



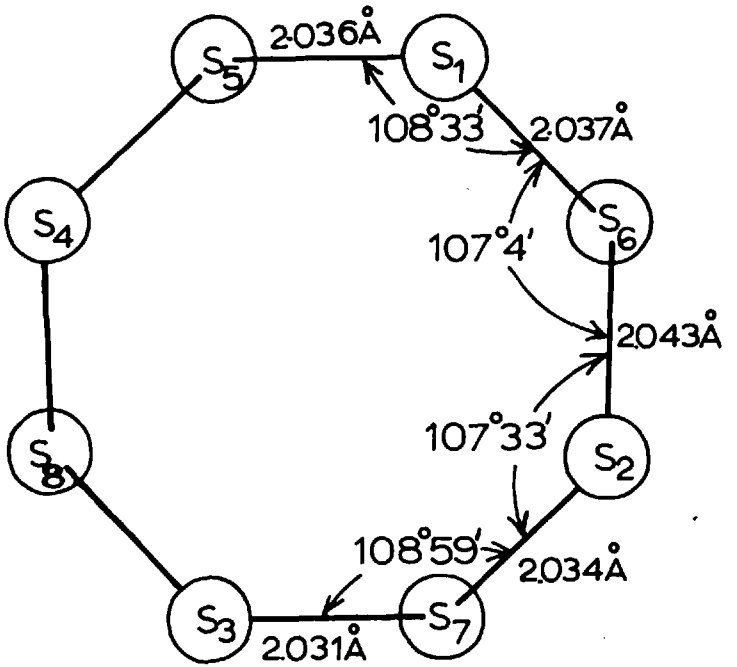


FIG.14 DIMENSIONS IN THE S_8 MOLECULE IN ORTHORHOMBIC SULPHUR.

The mean S-S bond length is 2.037 $\pm$ 0.005Å, the mean S-S-S bond angle is $107^{\circ}48' \pm 25'$, and the mean dihedral angle is $99^{\circ}16' \pm 31'$.

1.3. Phase Diagram of the Cu-S system

The $Cu-Cu_2S$ system has been investigated by Johannsen and Vollmer[20]. Their results and those of earlier workers[21-32] are shown in fig. 15. Liquid copper and Cu_2S are seen to be immiscible over a great range of composition.

There is a descrepancy between the results of Jensen[30], and Johannsen and Vollmer[20] over the range of non-stoichiometry in Cu_2S during solidification (cf figs. 15 and 16). Johannsen and Vollmer found no non-stoichiometry, whereas Jensen found that the Cu_2S precipitated from the melt at 1129°C contained 79.76wt% Cu, compared with the stoichiometric requirement of 79.86wt% Cu. The initially precipitated Cu_2S gains copper from the melt liquid as it cools, and at 1108°C it contains the stoichiometric 79.86wt% Cu.

The equilibria in the range Cu_2S - CuS have been clarified by the high temperature X-ray work of Djurle[18] and Ruhl and Saur[32]. The phases present in this range are Cu_2S, $Cu_{1.96}S$, $Cu_{1.8}S$ and CuS. Cu_2S and $Cu_{1.96}S$ are trimorphic, and $Cu_{1.8}S$ dimorphic.

The high temperature phases of Cu_2S, $Cu_{1.96}S$ and $Cu_{1.8}S$ have a f.c.c lattice, with unit cells of

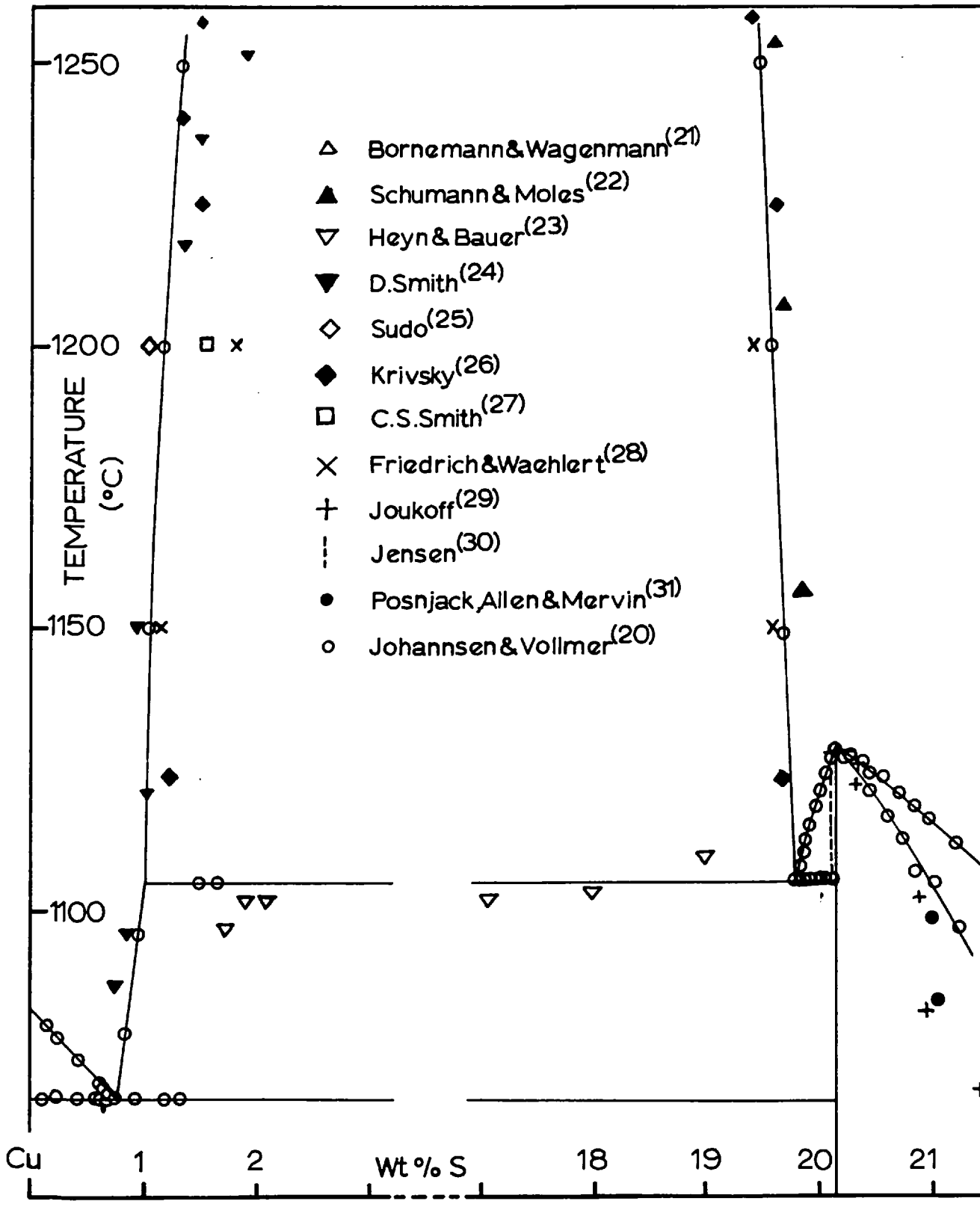


FIG.15 PHASE DIAGRAM OF THE Cu-CuS SYSTEM.

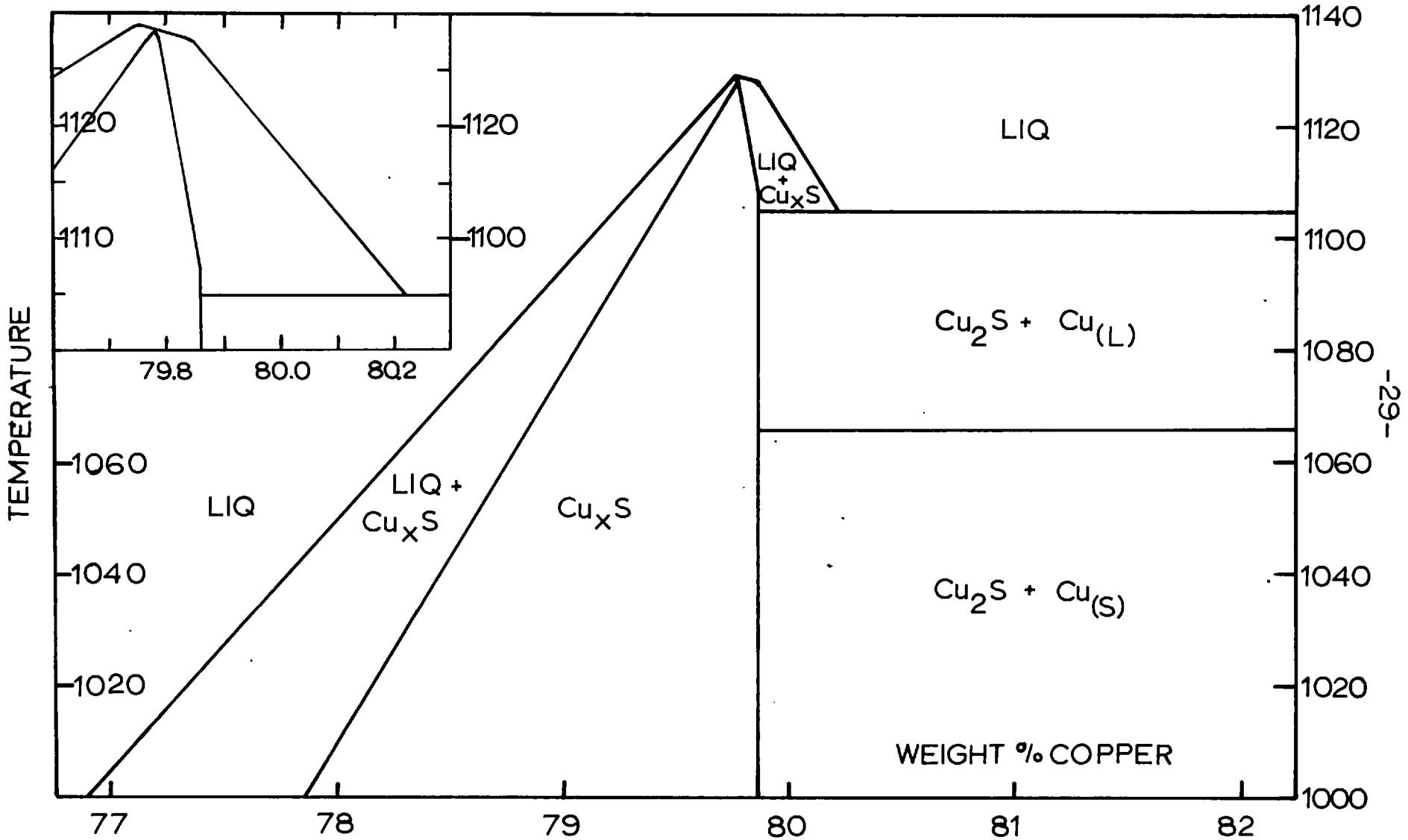


FIG.16 PHASE DIAGRAM OF THE Cu-S SYSTEM IN THE Cu_2S REGION. E. JENSEN (30).

approximately the same length and $Cu_{2-x}S$ molecule content. The small variation in unit cell length was a direct function of composition, and this suggests a continuity in the $Cu_{2-x}S$ ($x = 0 - 0.2$) phase that solidifies at high temperatures[18]. The low temperature $Cu_{1.80}S$ phase, $Cu_{1.80}S$ II, itself has a compositional range of existence. Sulphides of composition $Cu_{1.82}S$ II, $Cu_{1.78}S$ II, $Cu_{1.74}S$ II and $Cu_{1.70}S$ II give powder photographs with regular displacements in the lines with composition variation; the strongest lines of the photographs correspond to a f.c.c basic lattice, and the basic cube edge for the various compositions are:

$Cu_{1.82}S$	$Cu_{1.78}S$	$Cu_{1.74}S$	$Cu_{1.70}S$
$a = 5.570$	$a = 5.564$	$a = 5.556$	$a = 5.551 \pm 0.003$Å

The displacements of most of the other lines when the composition is varied shows, however, that the real lattice cannot be cubic.

Since the low temperature phase $Cu_{1.8}S$ II is derived from the high temperature phase $Cu_{1.8}S$ I, the high temperature f.c.c. phase should have a homogeneity range corresponding to $Cu_{2-x}S$ where $x = 0 - 0.3$. Beyond the limit of the $Cu_{1.8}S$ homogeneity range, '$Cu_{1.8}S$' and CuS are found to be in equilibrium.

The low temperature equilibrium phase-diagram for the range Cu_2S - $Cu_{1.5}S$ is shown in fig. 17. It has been

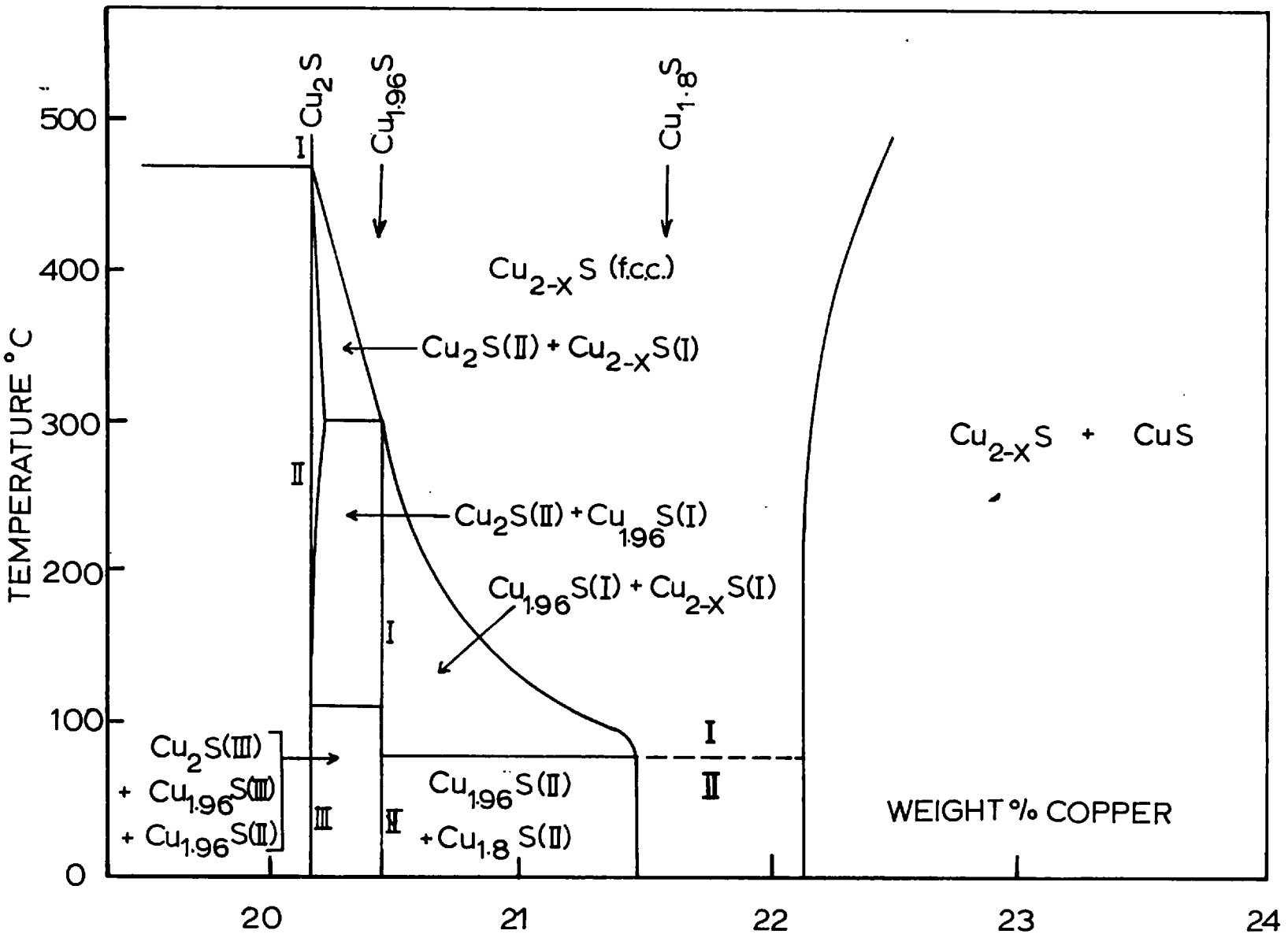


FIG.17 SOLID-STATE PHASE EQUILIBRIA IN THE Cu_2S REGION.

compiled[33] mainly from the information of Djurle[18] and Ruhl and Saur[32]. It assumes that $Cu_{1.96}S$ decomposes peritectoidally. The phases shown in fig. 17 are:

Cu_2S(III) stable below 110°C. Orthorhombic
a = 11.881Å, b = 27.323Å, c = 13.491Å

Cu_2S(II) stable 110 - 470°C. Hexagonal
a = 3.981Å, c = 6.76Å

CuS(I) stable above 470°C. F.C.C.
a = 5.735Å (500°C)

$Cu_{1.96}S$(III) stable below 100°C. Low symmetry.

$Cu_{1.96}S$(II) metastable. Primitive tetragonal
a = 4.008Å, c = 11.268Å

$Cu_{1.96}S$(I) stable above 100°C. F.C.C.
a = 5.707Å (500°C)

$Cu_{1.8}S$(II) stable below 78°C. F.C.C. with a superlattice.
a = 5.570Å ($Cu_{1.82}S$)
to a = 5.551Å ($Cu_{1.70}S$)

$Cu_{1.8}S$(I) stable above 78°C. F.C.C.
a = 4.610Å (300°C)

CuS Hexagonal.
a = 3.794Å, c = 16.332Å

1.4. Complexing of the Ferrous and Ferric Ions in the Leach Solution.

1.4.1. Hydrolysis of Ferric Ion

The hydrolysis of ferric salts has been investigated by many workers (34-58).

The Fe^{3+} ion hydrolyses in three stages, to $FeOH^{2+}$, $Fe(OH)_2^+$, and a precipitate whose composition varies according to the dilution.

$$Fe^{3+} + H_2O = FeOH^{2+} + H^+$$
$$FeOH^{2+}\ H_2O = Fe(OH)_2^+ + H^+$$
$$Fe(OH)_2^+ + H_2O = Fe(OH)_3 + H^+$$

There is also evidence of dimerisation of the product of the first stage in solutions whose Fe^{3+} concentration is greater than 10^{-4} moles/litre:

$$2FeOH^{2+} = Fe(OH)_2Fe^{4+}$$
$$\text{or } Fe_2(OH)_2^{4+}$$

The results of the determination of the first stage hydrolysis constant at 25°C are shown in fig. 18. The hydrolysis constant varies with ionic strength and the results of workers who have not taken this into consideration have been neglected.

The results of Milburn and Vosburgh[40] are representative of the other workers over the range of ionic strength μ = 0 - 3.0. They follow the equation:

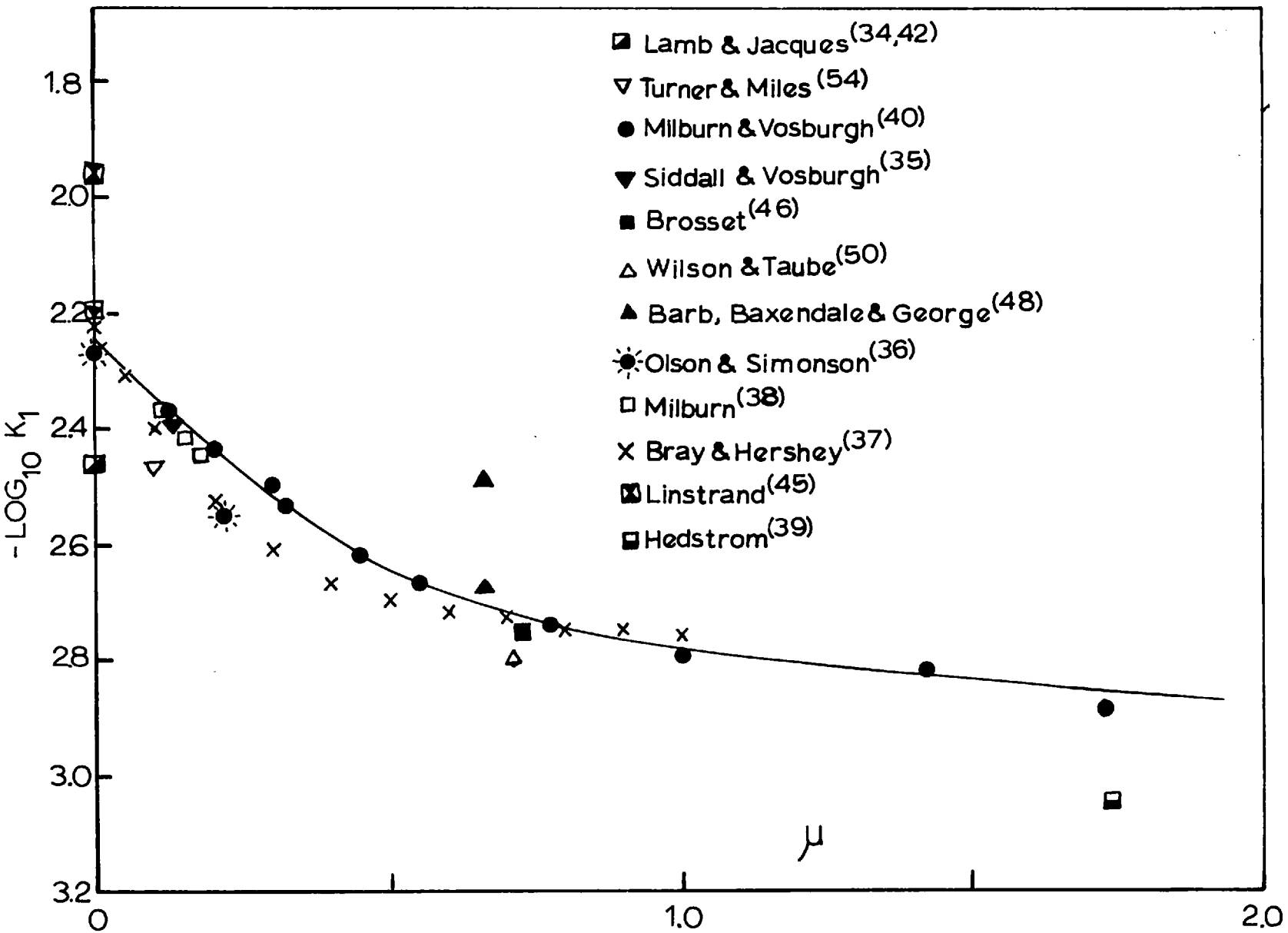


FIG.18 VARIATION OF THE FIRST HYDROLYSIS CONSTANT OF IRON, K_1, WITH IONIC STRENGTH, μ, AT 25°C.

$$\text{Log } K_1 = -2.172 - \frac{2.04\mu^{\frac{1}{2}}}{1 + 2.4\mu^{\frac{1}{2}}} - 0.01\mu$$

Richards and Sykes [56] studied the first stage of hydrolysis over a range of temperature 18.2° - 35.5°C. Having determined the enthalpy change, ΔH, they extrapolated the results of Milburn and Vosburgh to their range of temperatures and found the two investigations to be in excellent agreement.

The dimer formation equilibrium constant K_1^+ is given by

$$K_1^+ = \frac{\left[Fe_2(OH)_2^{2+}\right]}{\left[Fe(OH)^+\right]^2}$$

It has been determined by Hedstrom [39], Milburn and Vosburgh [40], Milburn [38], and Mulay and Selwood [43]. Their results are shown in fig. 19. K_1^+ is related to μ [40] by

$$\text{Log } K_1^+ = 1.46 + \frac{4.08\mu^{\frac{1}{2}}}{(1 + 2.1\mu^{\frac{1}{2}})} + 0.075\mu$$

With the exception of Mulay and Selwood [43], the results are in excellent agreement. The results of Milburn [38] and Hedstrom [39] follow precisely the equation relating K_1^+ and μ proposed by Milburn and Vosburgh [40].

The equilibrium constant for the second stage of the hydrolysis is written:

$$K_2 = \frac{\left[Fe(OH)_2^+\right]\left[H^+\right]}{\left[Fe(OH)^{2+}\right]\left[H_2O\right]}$$

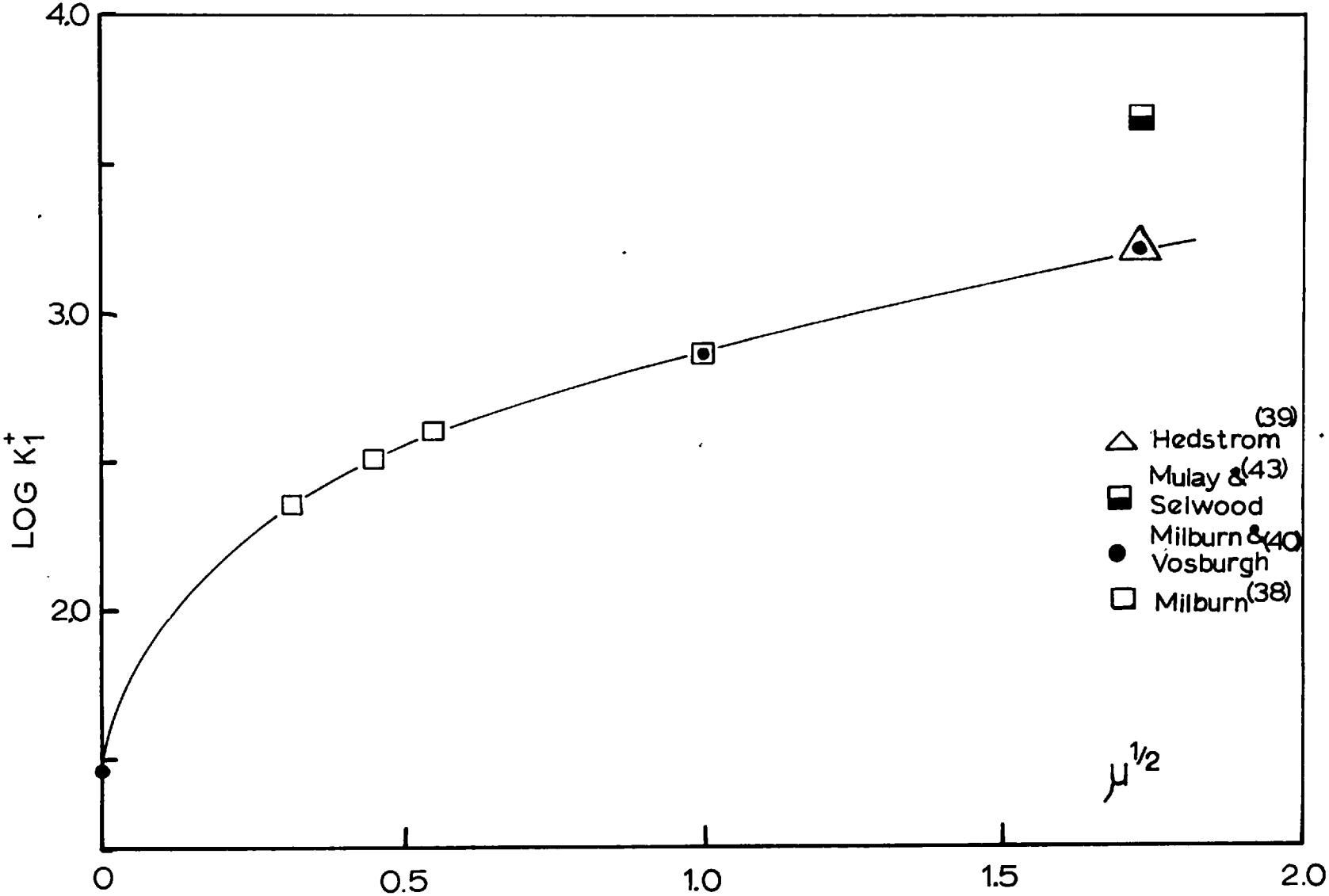


FIG.19 VARIATION OF THE DIMERISATION CONSTANT OF THE FIRST HYDROLYSIS PRODUCT OF IRON, K_1^+, WITH IONIC STRENGTH, μ, AT 25°C.

Lamb and Jacques[42] determined an approximate value of $K_2 = 2 \times 10^{-5}$ at 25°C and corrected to $\mu = 0$.

Hedstrom[39] measured $K_2 = 5.4 \times 10^{-4}$ at 25°C and $\mu = 3.0$. Biedermann[59] is in agreement with Hedstrom. His value of $K_2 = 5.5 \times 10^{-4}$ was also measured at 25°C and $\mu = 3.0$.

Arden[47] measured K_2 in sulphate solutions of different ionic strengths and obtained an average value of $K_2 = 4.2 \times 10^{-4}$. Arden however neglected the formation of Fe^{3+} - sulphate complexes and his result is therefore suspect.

Broersma[53] measured $K_2 = 5.0 \times 10^{-4}$ at 20°C and $\mu = 3.0$. Perrin[55] determined $K_2 = 4.9 \times 10^{-4}$ at the same temperature and $\mu = 1.0$.

Neglecting Lamb and Jaques approximate value, K_2 does not appear to be affected significantly by the ionic strength or by the temperature of the solution. A value of $K_2 = 5 \times 10^{-4}$ seems representative of the experimentally determined values.

The third stage of the hydrolysis

$$Fe(OH)_2^+ + H_2O = Fe(OH)_3 \text{ ppt} + H^+$$

where $$K_3 = \frac{[Fe(OH)_3] \cdot [H^+]}{[Fe(OH)_2^+] \cdot [H_2O]} = \frac{[H^+]}{[Fe(OH)_2^+]}$$

has received little attention experimentally and only an

estimate of K_3 = 95 has been proposed by Arden[47], but again this is suspect because of his neglect of sulphate complex formation.

1.4.2. Hydrolysis of Ferrous Ion

Hydrolysis of the ferrous ion proceeds in two stages

$$Fe^{2+} + H_2O = FeOH^+ + H^+$$

and $$FeOH^+ + H_2O = Fe(OH)_2 + H^+$$

$FeOH^+$ is the only hydrolysis product found in solution[60-64]. Since hydroxyl ion is a ligand that tends to form polynuclear complexes, it is possible that other existing ionic complexes are present in minor amounts but have not been detected. There is little variation in K_1' with ionic strength and the temperature dependence of K_1' is expressed[64] by

$$pK_1' = \frac{2625}{T} - 2.037$$

Literature values of K_1' are assembled in Table 2.

Table 2 The first hydrolysis constant of ferrous ion

Temp(°C)	K_1'	ionic system	Reference
20	1.3×10^{-6}	$\mu \rightarrow 0$ (corr)	60
25	3.2×10^{-10}	μ = 1 ($NaClO_4$)	61
25	5.0×10^{-10}	$\mu \rightarrow 0$ (corr)	62
25	1.2×10^{-8}	dil $FeCl_2$Soln	63
	6.8×10^{-8}	μ = 0.5 (KCl)	63
25	1.8×10^{-7}	μ = 0.5 to 2.2	64

There is no satisfactory explanation for the poor agreement between these results. However, for this investigation it is sufficient to know the order of magnitude of K_1'.

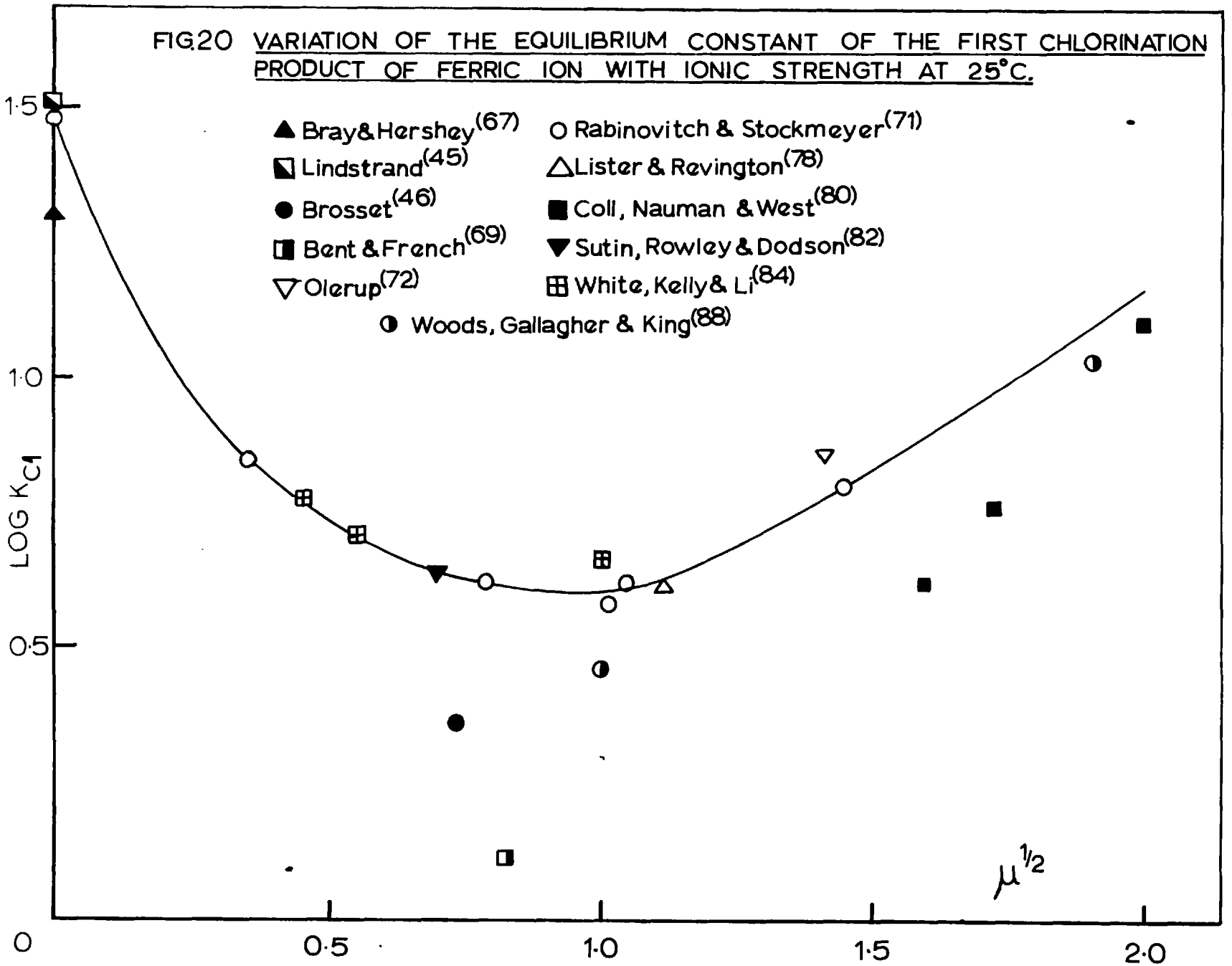
1.4.3. Ferric-Chloro Complexes

In aqueous solution, it has been experimentally shown that a solution of ferric chloride can contain all the species Fe^{3+}, $FeCl^{2+}$, $FeCl_2^+$, $FeCl_3$, and $FeCl_4^-$ (67-85). Much evidence has been presented to the effect that the limiting complex in aqueous solutions is $FeCl_4^-$ (76,77). These chloride complexes form in a stepwise fashion and the stability constant for each complex is represented by

$$K_{cn} = \frac{\left[FeCl_n^{(3-n)+}\right]}{\left[FeCl_{n-1}^{(3-n+1)+}\right]\left[Cl^-\right]}$$

The results of the determination of the equilibrium constant for the first chlorination product $FeCl^{2+}$ are shown in fig. 20.

The results of Lindstrand(85) and Olerup(72) have been extrapolated to 25°C using the enthalpy value $\Delta H = 8.5$ kcals(71). Bent and French(69) used the $FeCNS^{2+}$ ion as a coloured indicator for the concentration of free Fe^{3+} ions and obtained a value of K_{c1}, but owing to their neglect of higher complexes and possible formation of


FIG.20 VARIATION OF THE EQUILIBRIUM CONSTANT OF THE FIRST CHLORINATION PRODUCT OF FERRIC ION WITH IONIC STRENGTH AT 25°C.
Bray & Hershey (67)
Lindstrand (45)
Brosset (46)
Bent & French (69)
Olerup (72)
Rabinovitch & Stockmeyer (71)
Lister & Revington (78)
Coll, Nauman & West (80)
Sutin, Rowley & Dodson (82)
White, Kelly & Li (84)
Woods, Gallagher & King (88)
LOG K_{C1}
$\mu^{1/2}$
1·5
1·0
0·5
0
0·5
1·0
1·5
2·0

mixed chloro- and thiocyanate- complexes, their result must be regarded as approximate. Brosset[70] investigated the complexes potentiometrically in a KNO_3 medium. The nitrate ions may have complexed some of the ferric ions[86] giving an erroneous result. With the exception of Brosset[70] and Bent and French[69], the results of Rabinovitch and Stockmeyer[71] are in good agreement with the other workers over the wide range of ionic strength studied at 25°C and they follow the equation

$$\log K_{c1} = 1.48 - \frac{3\mu^{\frac{1}{2}}}{1 + 1.5\mu^{\frac{1}{2}}} + 0.295\mu$$

whose general form and limiting slope are suggested by the Debye - Hückel theory.

The second complex $FeCl_2^+$ has not been studied as extensively as the first. Since the three investigations (71,72,78) have been performed at different temperatures, and there is no reliable known data for ΔH_{c2}, no definite relationship between K_{c2} and μ is known. However, from Table 3, it may be seen that K_{c2} is of the order of 4.5 at $\mu = 0$, decreasing to a minimum of 1.3 at $\mu = 1.0$, rising to 2.0 at $\mu = 2.0$.

The data available on K_{c3}, the complex constant for $FeCl_3$ formation, is not well reported and the authors do not agree very well (Table 3). However it may be assumed

Table 3. The equilibrium constants of the second, third and fourth ferric-chloro complexes

Reference	Method	Temperature	Ionic Strength	K_{c2}	K_{c3}	K_{c4}
71	Sp	25°	0	4.5	0.10	
		26.7°	1($NaClO_4$)	1.3	0.04	
78	Sp	25°	1.2($NaClO_4$)	1.5		
72	Sp., red	20°	2 ($HClO_4$)	2.0	0.87	
77	Sp	20°	0 corr		0.73	1.0×10^{-2}
81	aix	25°	0 corr		0.04	1.2×10^{-2}

that K_{c3} is of the order 0.5.

Gamlen and Jordan[77] and Marcus[81] both give a value of $K_{c4} = 1 \times 10^{-2}$, (Table 3).

1.4.4. Ferrous-Chloro complexes

There is evidence for the existence of ferrous-chloro complexes[65,66,87].

Using potentiometric and spectrophotometric techniques, Olerup[87] evaluated the first and second complex constants in a 2M $HClO_4$ medium at 20°C.

$K_{c1} = 2.3$ and $K_{c2} = 1.1$

The existence of ferrous-chloro complexes was evident in the work of McConnell and Davidson[66] who studied the adsorption spectra of iron (II) in solutions of varying hydrochloric acid concentration.

Kraus and Moore[65] investigated the anion exchange properties of various divalent chlorides in various HCl concentrations. It was proposed that the complex $FeCl_3^-$ is formed in solutions of greater than 4M HCl, and that as the molarity of the HCl is increased to 12, the $FeCl_4^{2-}$ complex is formed. These workers also observed that the order of complexing of the divalent chlorides as indicated by anion exchange, solubility, and activity coefficient measurements was not in agreement with the order suggested

by the known stability constants. The only known stability constant for $FeCl_2$ as given by Olerup[87] was suspiciously high and Kraus and Moore thought a check on this value desirable.

1.4.5. Ferric-Ferrous Chloride Complexes

A spectrophotometric study[66] of mixed solutions of Fe^{3+} and Fe^{2+} in concentrated hydrochloric acid, gives evidence for the formation of unstable but strongly absorbing interaction complexes, each interaction complex containing one atom of Fe(II), one atom of Fe(III) and a number of co-ordinating chloride ligands.

The existence of the interaction complexes is found to be highly dependent on the HCl concentration and results suggest very little interaction complex formation in HCl of concentration below 5N.

1.4.6 Electron Exchange between Ferric and Ferrous Ions in aqueous Chloride Solutions

The rate of electron transfer between ferrous and ferric ions in perchloric acid solutions has been studied by Betts, Gilmour and Leigh[92]. These workers found that the electron transfer between ferrous and ferric ions in 0.44 - 3.0 N perchloric acid was complete within one

hour at 25°C, and that ferrous ions diffuse 22% more rapidly than ferric ions in perchloric acid media.

Assuming that there was no complexing of the ferrous and ferric ions by ClO_4^- ions, one would expect that because of coulombic repulsion, the factor controlling the speed of the electron transfer was the difficulty that the Fe^{3+} and Fe^{2+} ions have in approaching sufficiently close for the oxidation-reduction reaction to take place.

In HCl, the neutral $FeCl_3$ complex is formed, (Section 1.4.3). Thus in chloride media, the exchange should be considerably easier.

SECTION 2

EXPERIMENTAL PROCEDURE

2.1. Preparation of Chalcocite, Cu_2S

The sulphide was prepared in a two compartment glass-blown vessel, fig. 21.



Fig. 21. Glass-blown vessel containing prepared Cu_2S.

Four 15 cm x 5 mm spectrographically pure copper rods were weighed, and the stoichiometric amount of spec. pure sulphur required for Cu_2S formation was calculated.

This weight of sulphur was weighed out onto a sheet of glossy paper, and transferred to the smaller compartment of the glass vessel. The copper rods were inserted into the large compartment. An oil diffusion pump evacuated the vessel down to a pressure of 0.05 mm Hg.

when the thick walled neck of the vessel was sealed with an oxygen torch.

The vessel was put into a horizontal, Kanthal-wound furnace and heated to 500°C at 100°C per hour. The sulphur distilled over onto the copper and formed Cu_2S. The Cu_2S continued to grow by Cu diffusion through the Cu_2S already formed, to the sulphur on the surface. This was shown to be true by the solid length of crystalline sulphide which had four hollow cores in it. The vessel was left in the furnace for 24 hours to obtain as homogenous and crystalline a product as possible. Fig. 22 shows the crystalline surface of the sulphide.

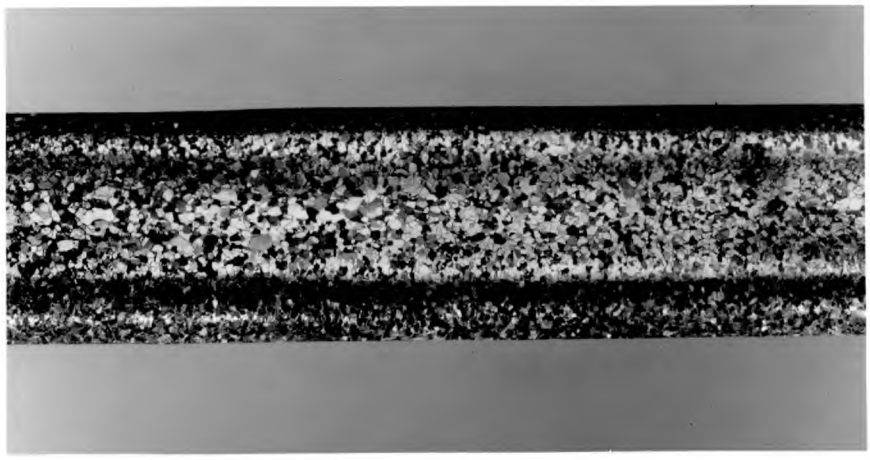


Fig. 22. Crystalline surface of prepared Cu_2S.

This product was then re-crystallised in a vertical furnace to obtain a more massive compact form.

2.2 Recrystallization of the Chalcocite

The chalcocite was recrystallized in the furnace shown in fig. 23.

A temperature profile down the furnace was constructed to find the depth of the maximum temperature of the hot zone. The thermocouple tip was fixed at this depth and the leads connected to a Honeywell automatic temperature controller.

The sulphide was removed from the glass-blown vessel, broken to - $\frac{1}{2}$" pieces and transferred to the Purox alumina tube. The tube was evacuated with an oil diffusion pump, and flushed with Argon. This procedure was repeated three times and the system left under a small positive pressure of Argon. The tube was clamped into the lowering mechanism.

The tube was lowered into the furnace through the hot zone at the rate of $\frac{1}{4}$" per hour. The maximum temperature in the hot zone was 1140°C. This gave 10°C of superheat which was sufficient to ensure complete remelting of the chalcocite and yet minimise the vapourisation of sulphur. Using the Free-energy of metal sulphides diagram of Richardson and Jeffes[93], the vapour pressure of sulphur over Cu_2S at 1140°C is 1 x 10^{-6} atmospheres. At this pressure, sulphur losses from the molten Cu_2S were

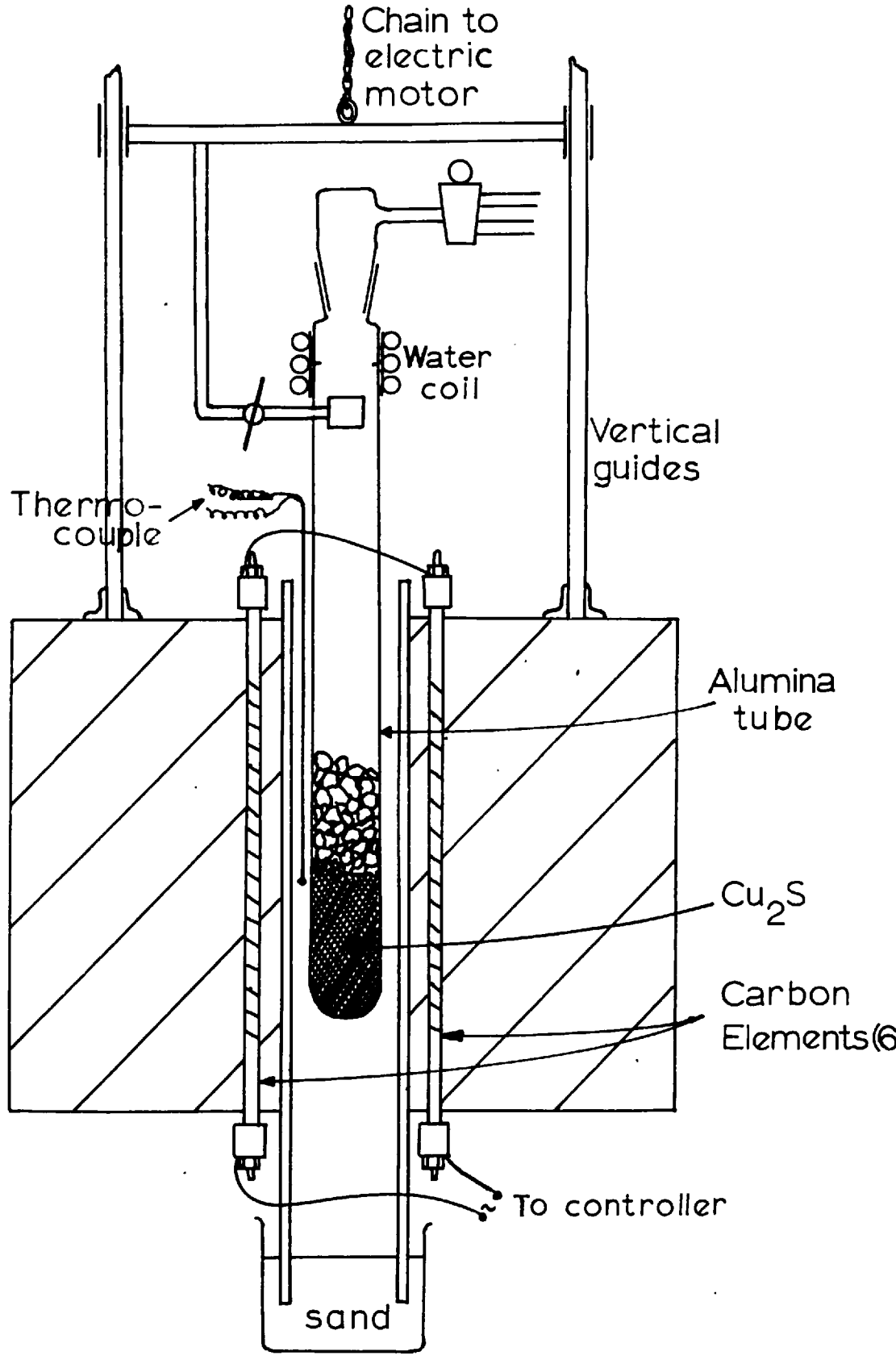


FIG. 23 RECRYSTALLISATION FURNACE

insignificant. An analysis of the recrystallised Cu_2S showed it to contain the stoichiometric requirements of copper and sulphur.

The tube was lowered at $\frac{1}{4}$" per hour to effect controlled slow crystallization. If the phase diagram of Jensen, (fig. 16), as opposed to that of Johannsen and Vollmer (fig. 15), is correct, Cu_2S solidifies over a range of composition. Thus the slow travel through the hot zone and slow subsequent cooling eliminated any coring. Electron probe results (Section 3.4) showed the recrystallized Cu_2S to be perfectly uniform in composition.

2.3. Leaching Apparatus and Experimental Procedure.

The leaching experiments were performed using the apparatus shown in fig. 24.

1 litre of leach liquid was put into the 2 litre leach bath which was then secured into position by the frame assembly. The paraffin-oil bath was raised on vertical guides to the required height and held in position by pins passing through the guides. The thermostatically-controlled paraffin-oil bath controlled the temperature of the leach bath to within $0.1^{\circ}C$. The stirred leaching bath took two hours to come to thermal equilibrium with the oil bath, which was maintained at

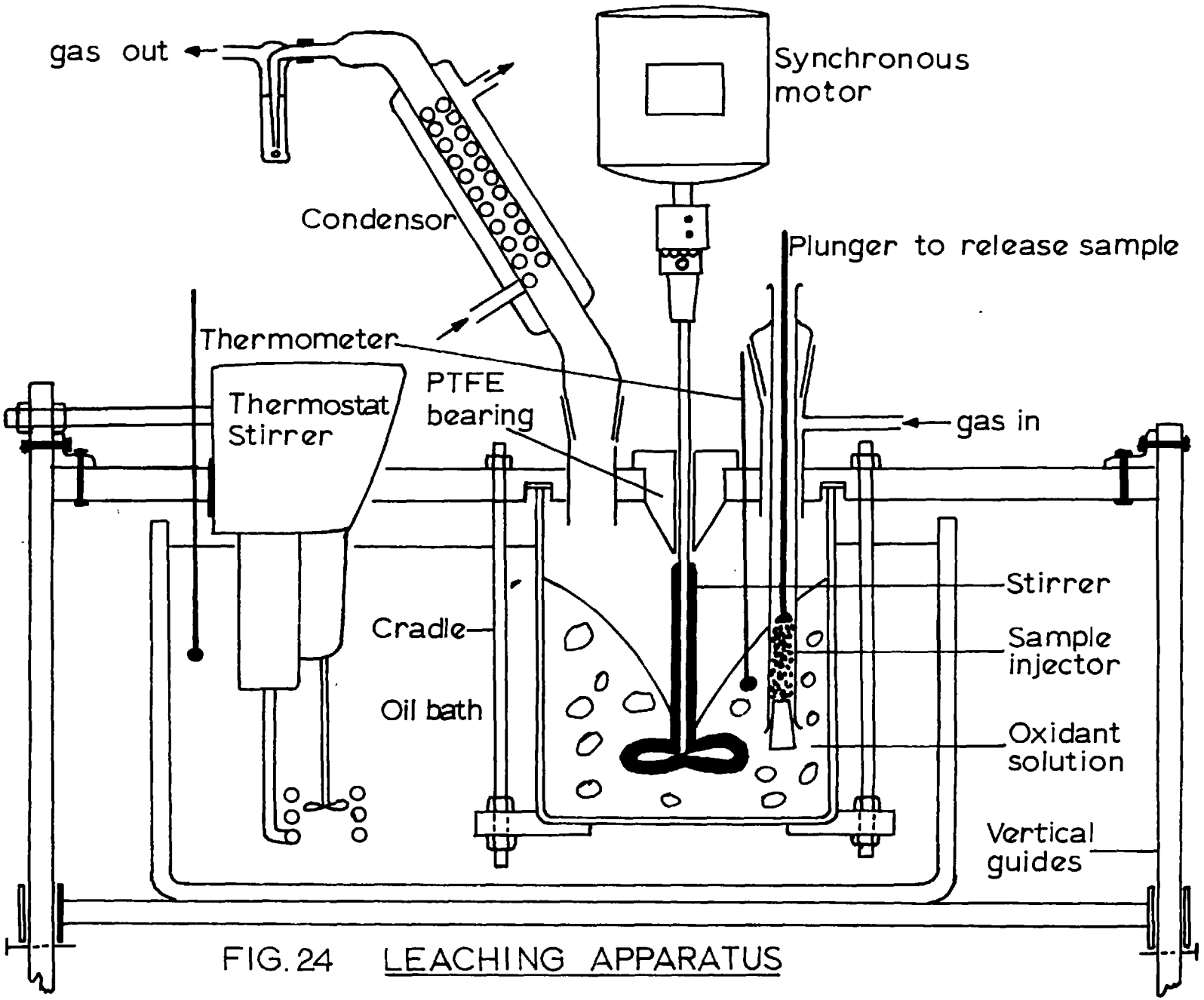


FIG. 24 LEACHING APPARATUS

0.1 - 0.3°C above the temperature in the leach bath, depending on the leaching bath temperature required.

With the leach bath at the required temperature, the Cu_2S sample was injected into the solution. Aliquots of leach liquor were extracted from the bath at set time intervals and analysed for copper content as described in Section 2.4. A specimen calculation of the amount of copper dissolved is given in Appendix 1.

Initially nitrogen was passed through the leach bath to maintain an inert atmosphere and prevent oxygen being absorbed into the solution so increasing its oxidation potential. However there was no detectable difference in the rate of copper dissolution with or without nitrogen gas passing through the bath and this refinement was abandoned. This confirms the need for high temperatures and oxygen pressures, as used by Warren[2], before oxygen gas will oxidise copper from chalcocite.

The most striking problem with the apparatus was the stirrer. Glass did not have the required strength for the high degree of stirring required to keep the sulphide particles in suspension. Stainless steel had the required strength but suffered severe attack by the acidified ferric chloride solutions.

Several paints and sprays were used as protective coatings on the steel, including vinyl-based plastics and PTFE, but with the combination of temperature and the shear forces on the edge of the highly rotated stirrer blades, they were quickly removed. 'Araldite' proved the most strong and enduring coating, but this failed by liquid penetrating pin holes of an imperfect coating and fine cracks due to stresses in the stirrer blades. The problem was overcome by casting the impeller in a block of 'Araldite' and then filing away 'Araldite' to leave a $\frac{1}{4}$" coating around the blades. 'Araldite' was also cast around the stirrer shaft.

2.4 ANALYSIS

2.4.1 Analytical Technique

A colourimetric technique was used to determine the copper concentration in the Fe^{3+}/Fe^{2+} leach solution. Since only a very small aliquot of leach liquor was available for analysis, the analytical technique had to be extremely sensitive to copper, and at the same time be unaffected by the very high ratio of iron to copper present in the leach solution.

Gravimetric techinques were not suitable, as the weight of copper to be analysed in each aliquot was as little as 0.0025 g. Complexing agents could have been used but they would have suffered from iron interference unless a separation of copper from the iron was first effected, rendering the analysis lengthy and tedious. Thus a colourimetric determination was developed.

The two most important colourimetric reagents for copper are dithizone and sodium diethyldithiocarbanate. Unfortunately, both are interfered with by the presence of large quantities of iron, and special measures must be taken involving a complicated analysis.

A far simpler and quicker method was used. The iron and copper were oxidised completely to their ferric and

cupric states by hydrogen peroxide. Ammonia was added in excess, precipitating the iron as ferric hydroxide, leaving the copper in the solution as the blue cuprammonium complex. This was examined spectrophotometrically.

2.4.2 Analytical Procedure

A 5 ml. aliquot of the leach solution was pipetted into a 100 ml. graduated flask, and 20 ml. of 20 vol H_2O_2 added. The solution was left to stand for 12 hours to ensure complete oxidation. 50 ml. of 0.880 NH_3aq. were added to precipitate the iron and leave the cuprammonium complex in solution. The flasks were made up to the mark with distilled water.

The solution was filtered with 'Whattman' No.541 filter paper, and the filtrate examined spectrophotometrically using a Unicam SP500 spectrophotometer and silica 4 cm light path cells, at 576 mμ wavelength. The blank was 50% 0.880 NH_3aq.

2.4.3 Absorption spectra of the Ions present in the Analysis

Absorption spectra were investigated with a Unicam SP800 spectrophotometer, using silica 1 cm cells.

i) conc. HCl (cHCl) No absorption 225 - 700 mμ

ii) 0.880 NH_3aq No absorption 250 - 700 mμ

iii) Cuprammonium complex

The cuprammonium complex was made by dissolving spectrographically pure copper in cHNO_3, heating this solution until there was no further fuming, and dissolving the residue in the minimum amount of cHCl. The complex was formed on addition of excess NH_3aq. The trace from the spectrophotometer showed a peak at about 630 mμ. There was no absorption between 300 and 450 mμ.

The effect of the copper concentration, at constant NH_3 concentration is shown in fig. 25. The complex is seen to obey Beers Law over the range of wavelength 500 - 700 mμ.

The effect of the ammonia concentration at constant copper concentration is shown in fig. 26. An increase in the NH_3aq concentration shifts the peak to a higher wavelength, at the same time increasing the absorbance of the solution. The copper complex is formed step-wise fashion:

$$Cu^{2+} + NH_3 = Cu\,NH_3^{2+}$$

$$Cu\,NH_3^{2+} + NH_3 = Cu\,(NH_3)_n^{2+}$$

$$\text{"} + \text{"} = \text{"}$$

$$Cu\,(NH_3)_{n-1}^{2+} + NH_3 = Cu\,(NH_3)_n^{2+}$$

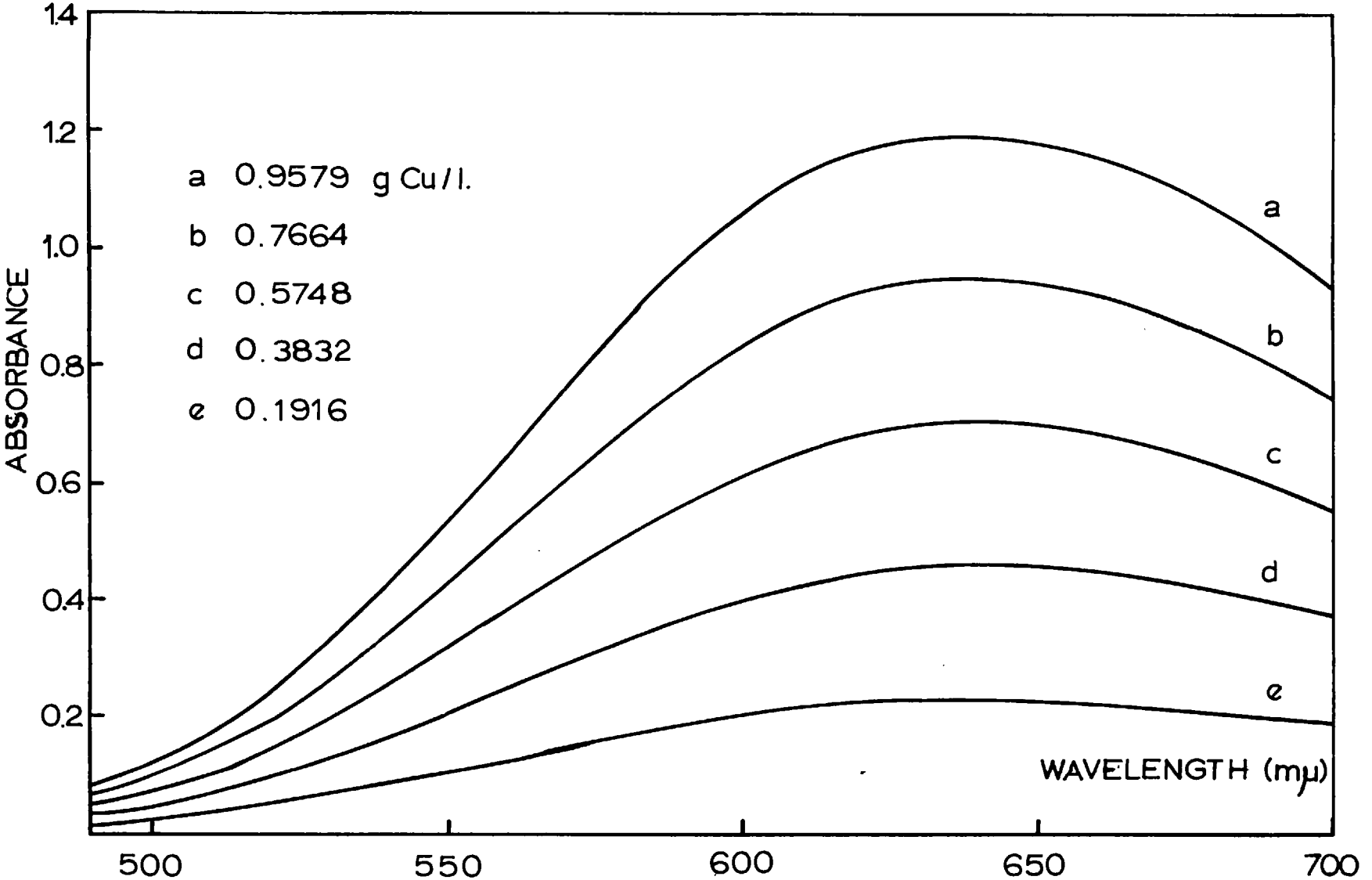


FIG.25 VARIATION OF CUPRAMMONIUM ION ABSORBANCE WITH COPPER CONCENTRATION. AMMONIA CONCENTRATION CONSTANT AT 50% 0.880 AQ. LIGHT PATH = 1 CM.

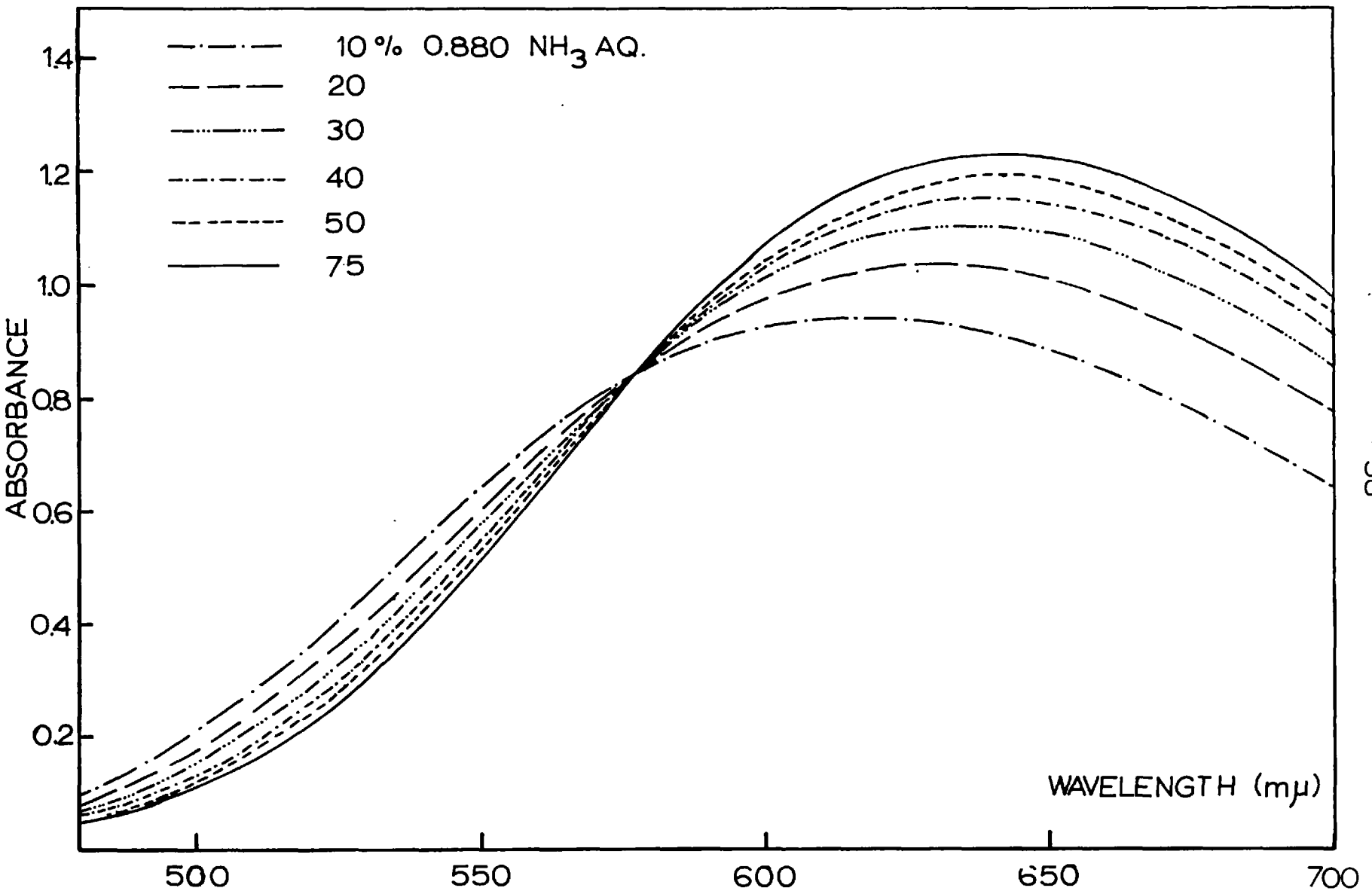


FIG.26 VARIATION OF CUPRAMMONIUM ION ABSORBANCE WITH AMMONIA CONCENTRATION. COPPER CONCENTRATION CONSTANT AT 0.9579 g/l. LIGHT PATH = 1 CM.

The higher complexes, which absorb more strongly and at a higher wavelength, are formed in high ammonia concentrations.

The isobestic point is at 576 mμ (fig. 27), where the absorbance is independent of NH_3 concentration. Since the leach solution can contain varying amounts of iron, the ammonia available for complexing the copper will also vary, affecting the absorbance. Thus to eliminate this error, the analysis was carried out at 576 mμ.

2.4.4 Beers Law Plot

The plot is shown in fig. 28.

Table 4. Optical densities of the cuprammonium ion at 576 mμ

$gCu.l^{-1}$	d (4cm cells)	$d.\ gCu^{-1}.l^{-1}$
0.0668	0.2295	0.858
0.1200	0.411	0.856
0.1708	0.586	0.857
0.2218	0.760	0.856

mean = 0.857 $d.gCu^{-1}.l^{-1}$

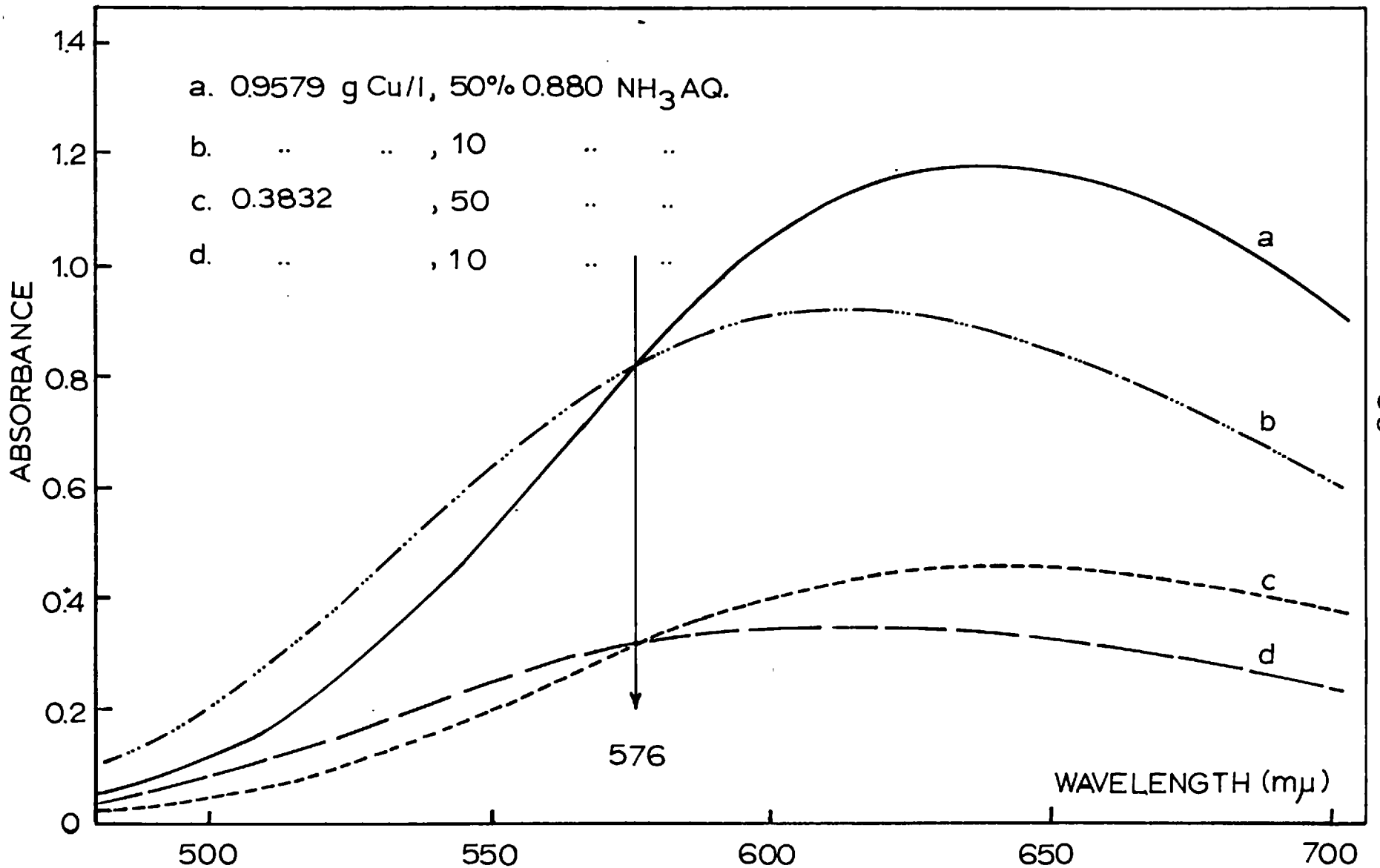


FIG.27 WAVELENGTH DETERMINATION OF THE ISOBESTIC POINT. LIGHT PATH 1 CM.

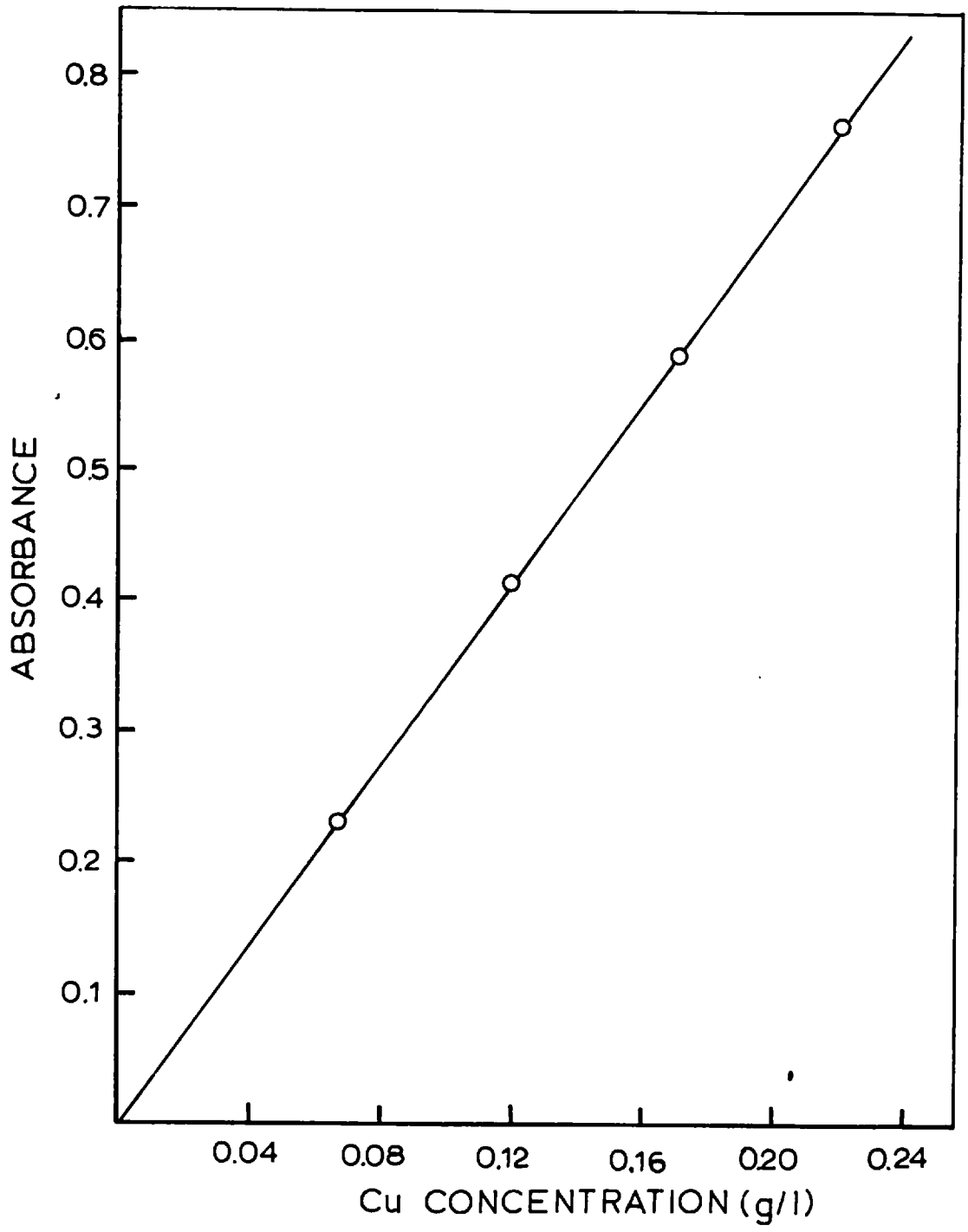


FIG.28 BEERS LAW PLOT. LIGHT PATH 4 CMS. WAVELENGTH 576mμ.

2.4.5 The effect of Ferric Hydroxide Precipitate Volume on the Absorbance

Two solutions of the same iron but different copper content were made up in 500 ml. flasks. They contained:

A. 0.0375 gCu, 6.75 g $FeCl_3.6H_2O$
(i.e 0.025 g.ion Fe^{3+}/litre)

B. 0.07165 gCu, 6.75 g $FeCl_3.6H_2O$
(i.e 0.025 g.ion Fe^{3+}/litre)

The copper impurity introduced by the $FeCl_3.6H_2O$ was 0.00016875 g. 250ml. 0.880 NH_3aq. were added to each flask, precipitating the iron and leaving the copper in solution. The flask was made up to the mark with distilled water.

The solutions were filtered with No. 541 'Whattman' filter papers and the filtrates examined spectrophotometrically at 576 mμ, in 4 cm cells.

Solution	d	gCu/500 ml
A	0.262	0.382
B	0.499	0.0728

Considering the precipitation to be instantaneous, and that there is no adsorption of copper onto the hydroxide precipitate, then:

$$\begin{bmatrix}\text{volume occupied by}\\ \text{solution before pptn.}\end{bmatrix} \times \begin{bmatrix}\text{copper concentration}\\ \text{before pptn.}\end{bmatrix}$$

$$= \begin{bmatrix}\text{volume occupied by}\\ \text{solution after pptn.}\end{bmatrix} \times \begin{bmatrix}\text{copper concentration}\\ \text{after pptn.}\end{bmatrix}$$

For A :

$$500 \times \frac{0.0375 + 0.00016875}{500} = V_A \times \frac{0.0381978}{500}$$

$$V_A = \underline{493.\overset{1}{\cancel{675}}\ \text{ml.}}$$

Similarly for B :

$$500 \times \frac{0.07165 + 0.00016875}{500} = V_A \times \frac{0.072751}{500}$$

$$V_B = \underline{493.\overset{6}{\cancel{503}}\ \text{ml.}}$$

Therefore the average volume of the precipitate is 6.67 ml. Thus N/40 Fe^{3+}, i.e 2.675g $Fe(OH)_3$, occupies an effective volume of 6.67 ml., and the effective density of $Fe(OH)_3$ is calculated stoichiometrically to be 2.675/6.667, i.e. 0.40 g/ml.

There is considerable water of hydration attached to the $Fe(OH)_3$ and the density of the hydrated precipitate is now calculated.

The density of solid dry $Fe(OH)_3$ is 3.6 g/ml. Thus the 2.675g $Fe(OH)_3$ occupies only 0.75 ml. of the 6.67 ml. precipitate volume, water being the remaining 5.92 ml.

True density of the hydrated precipitate.

$$= \frac{\left[\text{Wt of } Fe(OH)_3\right] + \left[\text{Vol. of water of hydration}\right] \times \left[\text{density of water}\right]}{\left[\text{volume of precipitate}\right] + \left[\text{water of hydration}\right]}$$

$$= \frac{2.675 + 5.92 \times 1}{6.67}$$

$$= \underline{1.3 \text{ g/ml.}}$$

2.4.6 Cu Adsorption onto the Ferric Hydroxide Precipitate

The fact that there is an apparent increase in copper concentration caused by the presence of the precipitate, and that the volume occupied by the precipitate is calculated to be the same for different Cu concentrations, shows that there is no adsorption onto the ferric hydroxide precipitate.

2.4.7 Pipette Calibration

The Grade A 5 ml. pipette that was used to remove samples of leach liquot for analysis, was calibrated.

A bath of distilled water was thermostatically maintained at temperature T. Using the pipette, 5 ml. of water from the water bath at temperature T were pipetted into a weighed dry stoppered bottle. The equivalent volume of water at 20°C, delivered from the pipette, was calculated - Table 5, fig. 29.

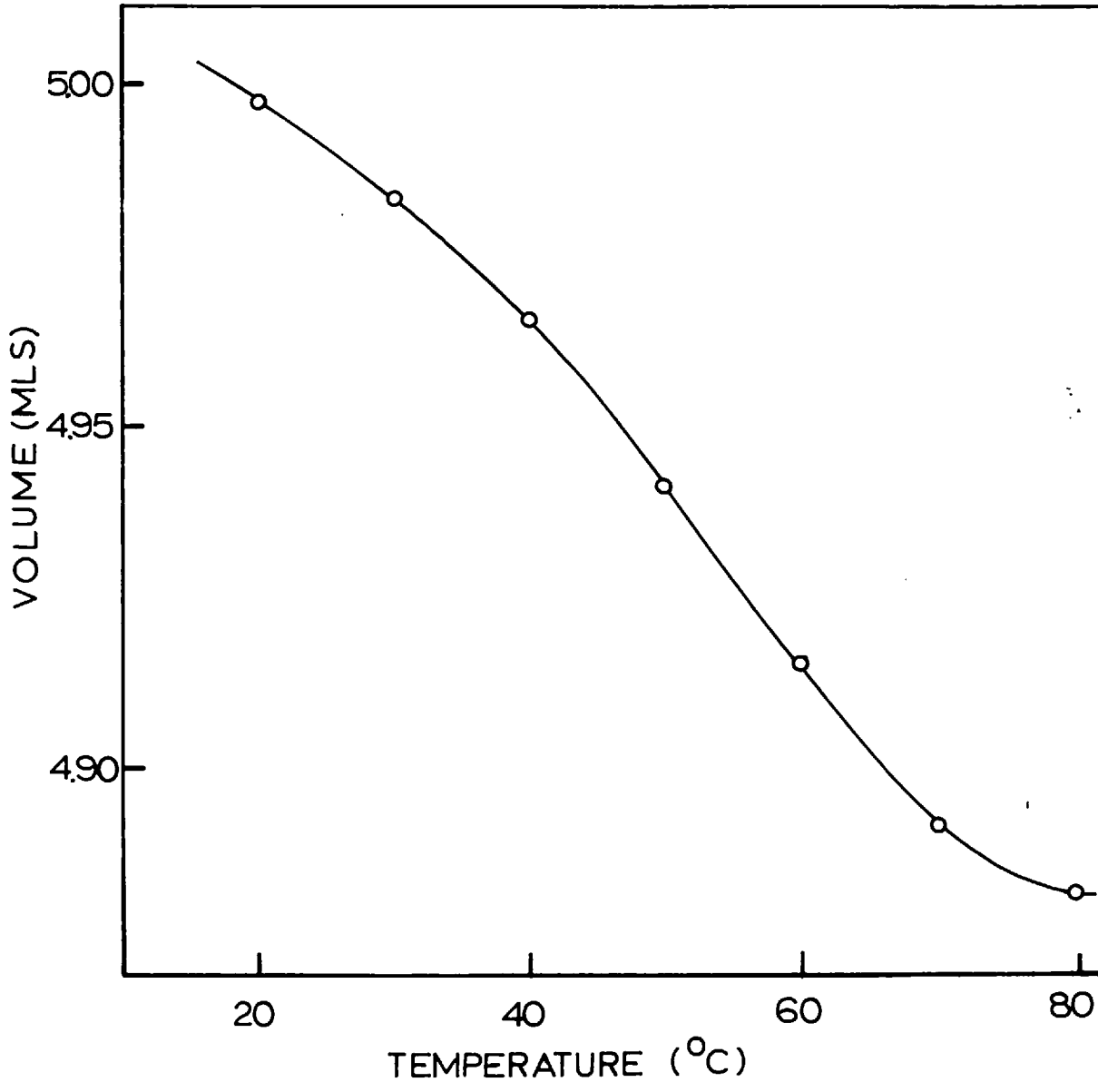


FIG.29 PIPETTE CALIBRATION. VOLUME OF WATER (AT 20°C) DELIVERED FROM PIPETTE AT A GIVEN TEMPERATURE.

Table 5. Volume delivered from pipette at at $T^{o}C$ and $20^{o}C$.

$T^{o}C$	Weight of H_2O	H_2O_T	$^{Wt}H_2O_T$	$^{Wt}H_2O_{20^{o}C}$
20	4.9886	0.99823	4.9974	4.9974
30	4.9746	0.99568	4.9962	4.9834
40	4.9566	0.99222	4.9953	4.9654
50	4.9326	0.98807	4.9922	4.9413
60	4.9066	0.98324	4.9902	4.9153
70	4.8826	0.97781	4.9934	4.8913
80	4.8686	0.97183	5.0097	4.8772

2.4.8 Purity of Materials

(a) $FeCl_2 4H_2O$ GPR grade (Hopkins & Williams Ltd)

A typical analysis gave:

$FeCl_2 4H_2O$	98% min
Sulphate (SO_4)	0.06% max

(b) $\underline{FeCl_3 6H_2O}$ Analar grade (Hopkins & Williams Ltd)

The maximum limits of impurities were:

Free acid (HCl)	0.5%
Free Chlorine (Cl)	0.001
Sulphate (SO_4)	0.005
Nitrate (NO_3)	0.002
Phosphate (PO_4)	0.004
Ferrous salt (Fe)	0.03
Copper (Cu)	0.0025
Lead (Pb)	0.005
Zinc (Zn)	0.01
Manganese(Mn)	0.1
Alkalis (as sulphate)	0.15
Arsenic (As)	0.0004

(c) Copper Rod Spectrographically pure rods (Johnson & (Matthey & Co. Ltd) Cu 99.99%

Spectrographic examination gave the following impurities, expressed in parts per million

Silver (Ag)	3 ppm
Iron (Fe)	2
Lead (Pb)	1
Magnesium (Mg)	1
Silicon (Si)	1

The rods were treated with dil.HNO_3 to remove oxide film before use.

(d) Hydrochloric Acid

Analar grade (Hopkins & Williams Ltd)

HCl not less than 35.4%

Maximum limit of impurities were:

Non volatile matter	0.001%
Free Chlorine (Cl)	0.0002
Sulphate (SO_4)	0.0003
Iron (Fe)	0.0001
Heavy metals (Pb)	0.0002
Arsenic (As)	0.000004

(e) Ammonia (0.880aq.)

GPR 'A' grade (Hopkins & Williams Ltd)

Maximum limit of impurities were:

Non volatile matter	0.005%
Chloride (Cl)	0.0001
Sulphate (SO_4)	0.001
Phosphate (PO_4)	0.0005
Silicate (SiO_2)	0.002
Iron (Fe)	0.0001
Heavy Metals (Pb)	0.0001
Arsenic (As)	0.0000054

SECTION 3

RESULTS AND DISCUSSION

3.1 KINETIC RATE-CURVES OF THE LEACHING OF CHALCOCITE EFFECT OF THE LEACH VARIABLES ON THE RATE OF REACTION

Using the apparatus described in Section 2.3, particulate chalcocite was leached and the kinetic rate-curves obtained. The different kinetic variables were studied to determine the rate-controlling steps and mechanisms of the two halves of the leaching process. The results are given in Appendix 1.

3.1.1 Temperature

The two halves of the leach are evident from fig. 30 and figs 31 and 32 (results from Appendix 5). One half of the copper is extracted and the chalcocite is transformed to covellite, CuS. The existence of the mineral covellite is shown by X-ray powder photographs of the leach residue of composition CuS (Section 3.3) and by the anistropic behaviour exhibited by the microstructure photographs of this composition, (Section 3.2). The artificially produced CuS is further leached to elemental sulphur.

The first reaction-half of the leach from Cu_2S to CuS is extremely fast, complete in 3 to 4 minutes at 40°C, and is not very sensitive to temperature. The second

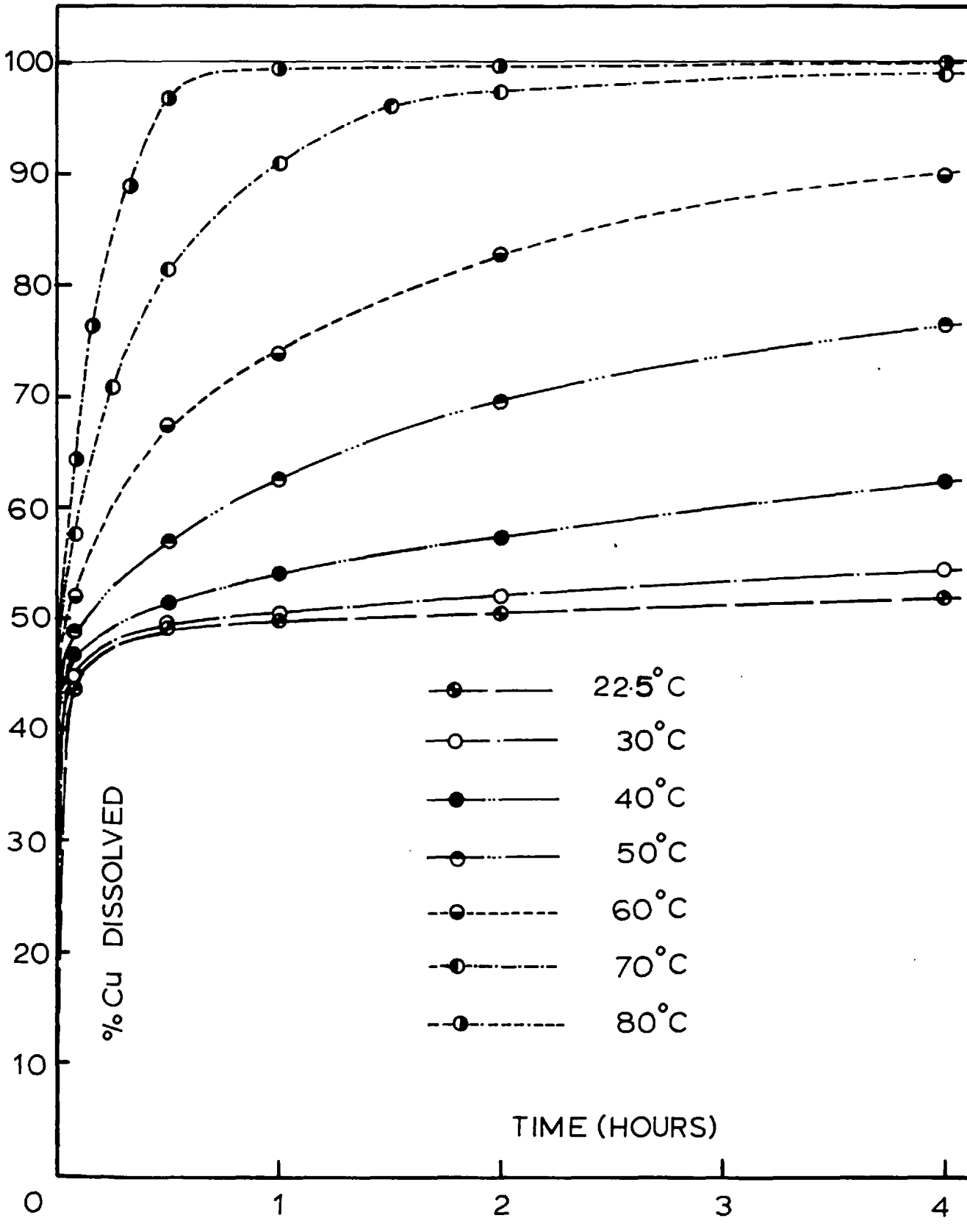


FIG.30 EFFECT OF TEMPERATURE ON THE RATE OF LEACHING CHALCOCITE.

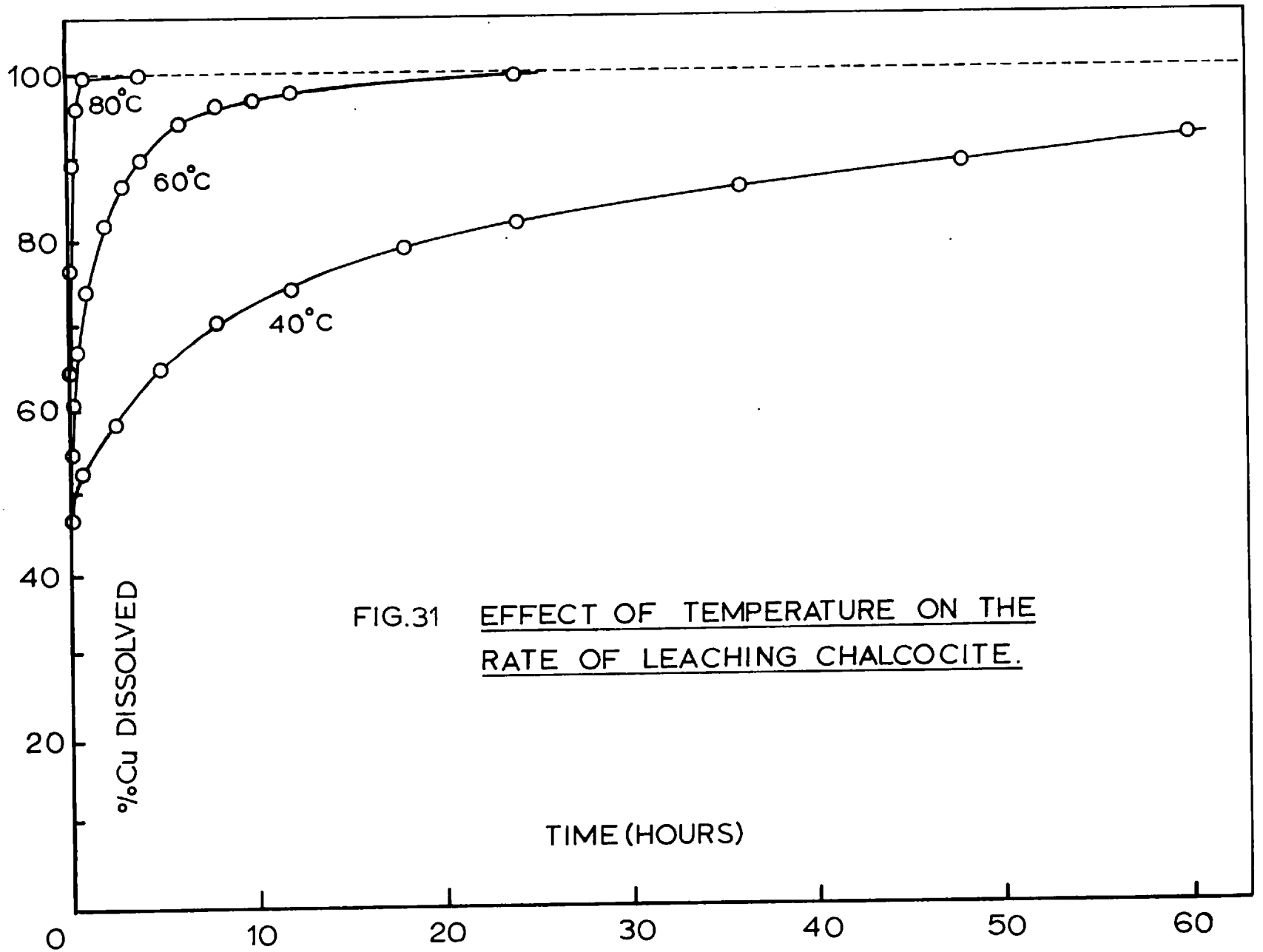


FIG.31 EFFECT OF TEMPERATURE ON THE RATE OF LEACHING CHALCOCITE.

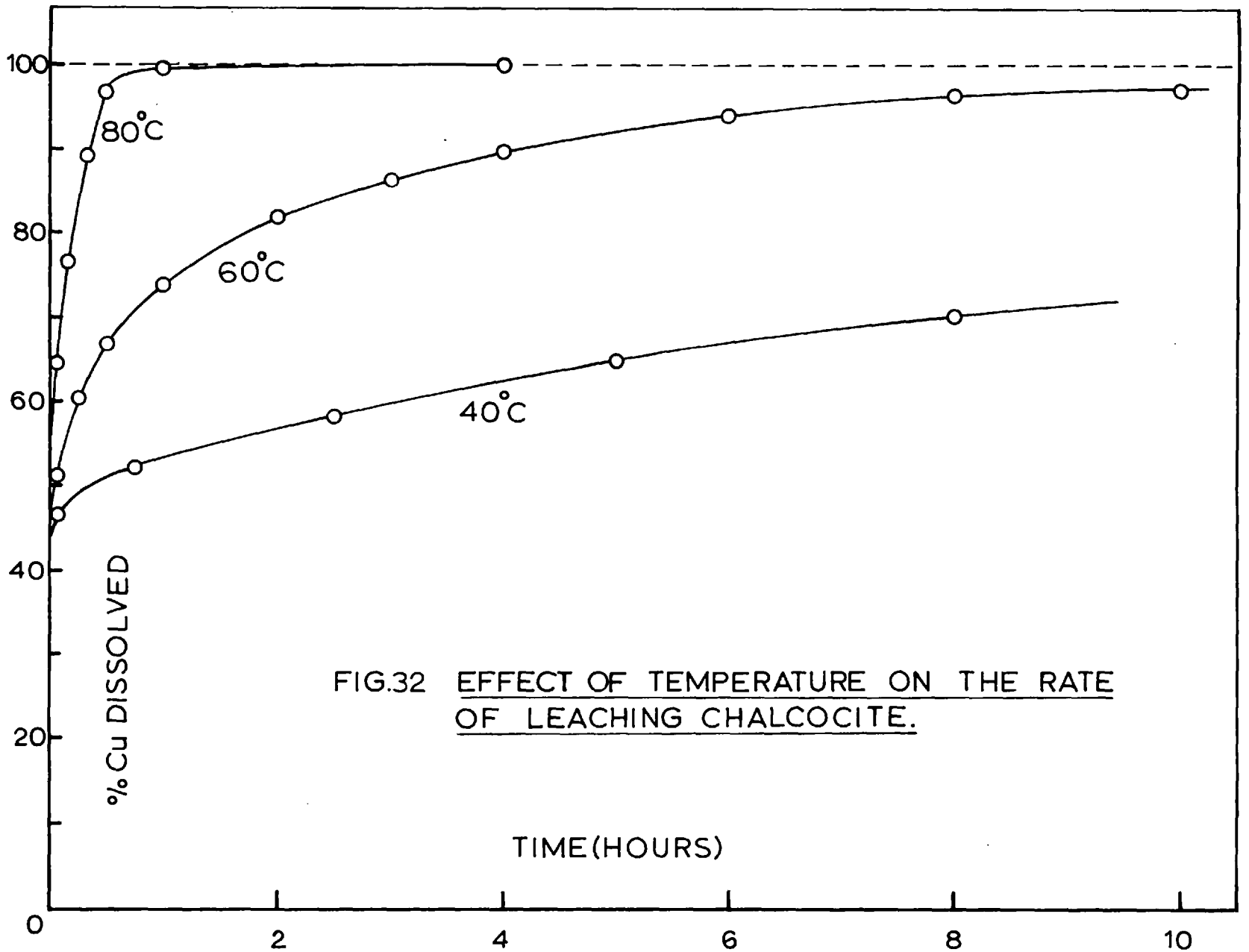


FIG.32 EFFECT OF TEMPERATURE ON THE RATE OF LEACHING CHALCOCITE.

reaction-half from CuS to sulphur is much slower than the first, and highly sensitive to temperature.

Experiments involving the leaching of a rotating disc (Section 3.4) and the leaching of polished cubes of chalcocite (Section 3.2) showed that the sulphide retains its original outline throughout the complete leach from Cu_2S to sulphur. Thus the mechanism for both halves of the reaction must either be diffusion of copper ions in the lattice, straight chemical transformation leaving a product coating to maintain the original outline, or a combination of both.

X-ray powder photographs of leach residues (Section 3.3), and electron probe results over sections of the leached cubes and discs (Section 3.4), show that the chalcocite loses copper by diffusion, and proceeds via the non-stoichiometric $Cu_{1.8}S$ and CuS phases to a residue approximating to the formula $Cu_{0.8}S$ which transforms directly to elemental sulphur.

From the kinetec curves and the relative speed with which the two reaction-halves proceed, it may be inferred that the mechanism of the first reaction-half is by easy diffusion of copper ions in the sulphide lattice and that the mechanism for the second reaction-half is by a more difficult diffusion process of copper ions in the CuS

lattice until the non-stoichiometric $Cu_{0.8}S$ structure is reached, when the $Cu_{0.8}S$ is transformed to elemental sulphur which adheres as a coating.

With these mechanisms, it is apparent that the rate of copper dissolution will be dependent on the amount of copper dissolved, i.e. the rate will be dependent on the diffusion gradient in the lattice or the coating thickness of the transformed phase, whichever mechanism applies. Thus when determing the apparent activation energies of each reaction-half, the rate of copper dissolution at each temperature must be measured when the same amount of copper has been removed, i.e. the particles are in the same physical state.

Since the first half of the reaction is extremely fast, the shape of the curve is difficult to determine, and the rate of the first reaction-half was calculated from the amount of the copper leached from the sulphide after two minutes. The activation energy was determined from the rate of the first reaction-half, i.e. %Cu dissolved in 2 minutes, at 20, 40 and 60°C (Appendix 2). An Arrhenius plot of log rate vs $1/T^{\circ}A$ is shown in fig.74 The three points do not lie on a very satisfactory straight line. This was possibly due to the rate being measured as the %Cu dissolved in a given time instead of

the time required to dissolve a given copper percentage. The latter would eliminate error due to the variation of rate with %Cu dissolved. The slope gives a value of 0.82 ± 0.09 kcals for the activation energy of the first reaction-half. This is of the same order as the activation energy for diffusion of copper ions in the Cu_2S lattice[94], indicating that the diffusion of copper ions in the lattice is the rate-controlling step of the first reaction-half.

For the second reaction-half it was possible to measure the rates of dissolution at different temperatures when a given copper percentage had been dissolved. However, it was innacurate to measure the tangent of each curve at a particular value of %Cu dissolved and the rate of dissolution was determined over a small range of %Cu dissolved, (Appendix 2). The Arrhenius plot (fig. 75) shows the activation energy to increase from 24.2 to 29.2 kcals over the range 50 to 90% of the copper dissolved, clearly indicating a chemically controlled process. The increase in the activation energy is associated with the change from the chemical process accompanying the removal of copper during the CuS range of non-stoichiometry, to the chemical transformation of $Cu_{0.8}S$ to elemental sulphur.

The difference in the rates of the first and second reaction-halves is indicative of the difference in the

structures of Cu_2S, $Cu_{1.8}S$, CuS and sulphur, (Sections 1.2 and 1.3). The Cu_2S and $Cu_{1.8}S$ structures are very open, so much so that in the Cu_2S II phase which is stable between 110 and 475°C, the copper atoms are in a state of constant mobility within the sulphur lattice. The speed of the first transformation shows the ease of interstitial copper diffusion, even in the lower temperature Cu_2S III phase. By comparison, the CuS structure is very ordered and compact, and diffusion more difficult. It would also be more difficult to remove copper chemically from the ordered CuS phase.

The charge neutrality of the copper sulphide structure must be maintained as it loses copper. As copper atoms are removed in the first reaction-half, some of the cuprous ions of the Cu_2S structure are easily oxidised to the cupric state and the charge neutrality is maintained. In the second reaction-half copper atoms are removed from the CuS structure during the range of non-stoichiometry CuS to $Cu_{0.8}S$, but the charge neutrality can no longer be maintained by oxidation of the copper atoms in the copper sulphide structure since there is no known Cu^{3+} ion. The charge neutrality must therefore be maintained by the more difficult process of removal of electrons from the sulphide ion lattice.

Since X-ray powder photographs (Section 3.3) show that sulphur is not formed until the CuS structure is reduced to $Cu_{0.8}S$, the electrons in the sulphide ion planes of the CuS structure must be shared, at least within the individual sulphide ion planes. A limited deficiency of the electrons in these sulphur atom planes is tolerated without the deficiency of electrons becoming localised which would result in the formation of elemental sulphur. When the sulphide ion planes no longer tolerate this deficiency, the $Cu_{0.8}S$ of the CuS phase is transformed to elemental sulphur.

The arrangement of sulphur atoms in the orthorhombic sulphur formed as the end product of the leach is completely different to the arrangement of sulphur atoms in the CuS lattice. Orthorhombic sulphur comprises ring molecules of 8 atoms; the sulphur atoms in the intermediate CuS phase are in hexagonal double-layers. There is no available gradual transformation from one arrangement to the other, and the direct transformation is predicted.

3.1.2 Particle Size

The rate of the first reaction-half is greatly increased by a reduction in particle size, fig. 33.

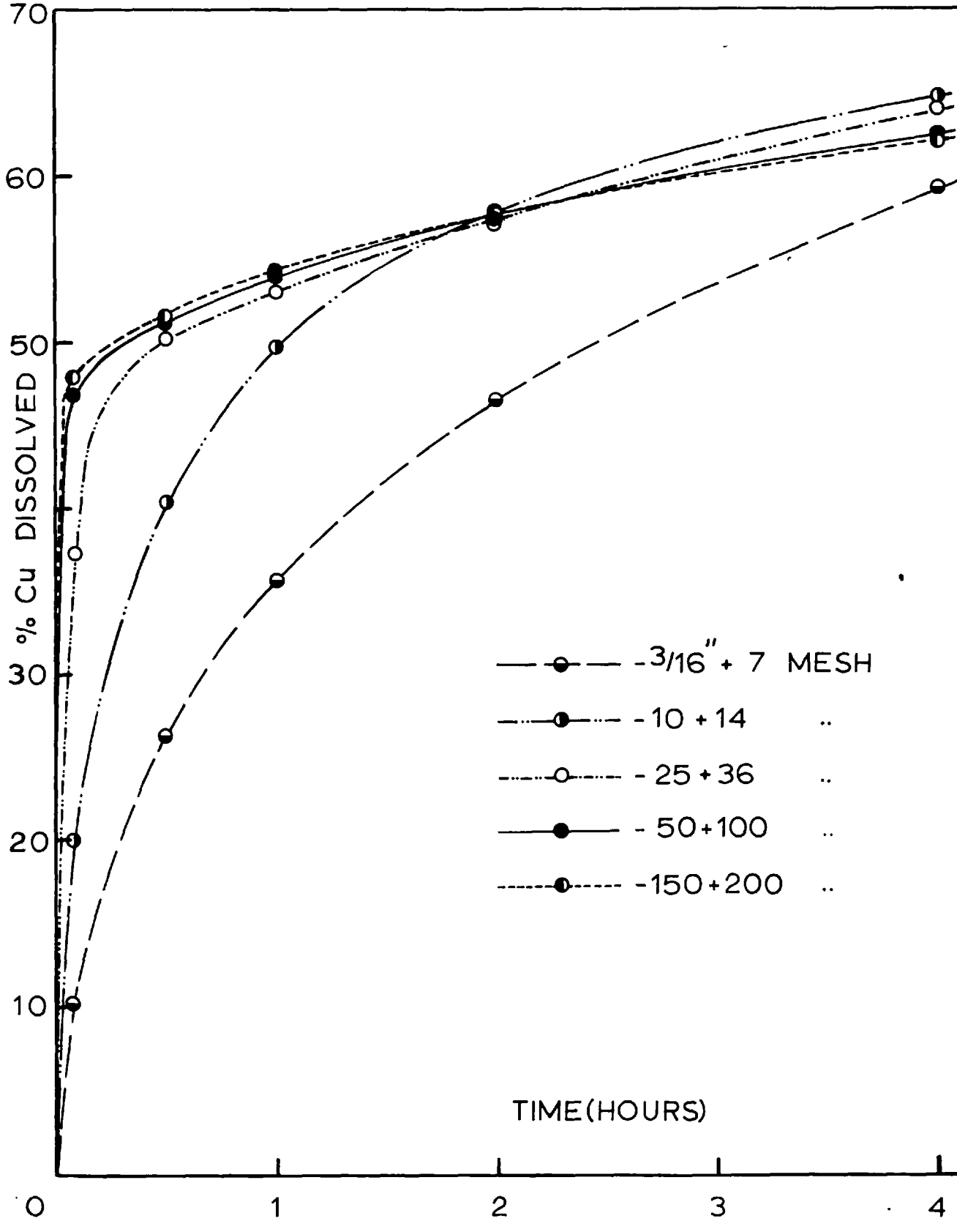


FIG.33 EFFECT OF PARTICLE SIZE ON THE RATE OF LEACHING CHALCOCITE.

This is to be expected if the rate-controlling step is the diffusion of copper atoms in the sulphide lattice. A reduction in particle size reduces the diffusion distances and the rate of dissolution therefore increases.

The rate of the second reaction-half does not vary significantly with particle size. The rate decreases slightly as the size decreases and this decrease is most likely due to a flotation of the particles in the turbulently stirred bath of low pulp density. Flotation results (Appendix 3) showed the chalcocite and leach residues to have strong tendencies to float, and the floatability is greatly increased as the size is decreased.

It is difficult to estimate the depressive effect of flotation of the particles on the rate of the second reaction-half. The effect may be so severe that the rate of the second reaction-half would otherwise increase with a decrease in the size of the particles.

The photographs of the chalcocite surface after leaching as a cube or disc, showed the structure to be extremely porous, figs.39 to46. Assuming the original outline of the chalcocite is maintained throughout the leach, the densities of Cu_2S and CuS, 5.6 and 4.6 g/cc[89] respectively, indicate a 25% voidage

in the artifically produced covellite. The density of sulphur, 2.1 g/cc., results in a further increase of 17% in total voidage during the transformation from CuS to sulphur.

The only mechanism whereby the reaction rate would not be expected to increase significantly as the particle size decreased is attack in pores. Since the inter-lamella distance of the porous residue structure is constant, the area of liquid-solid interface remains constant regardless of the size of a given weight of sample. The assumption that attack in pores presents the same area of attack and results in size having an insignificant effect on the rate, is true if, i) there is attack actually in the pores, ii) the rate-controlling step is the chemical process accompanying the removal of copper atoms from the CuS structure or by the rate of the transformation of $Cu_{0.8}S$ to sulphur, and iii) the rate is not controlled by the diffusion of copper ions in the solid to the lamella-liquid surface of the pores or by the availability of ferric ions in the pores, i.e. by the bulk concentration of ferric ions and rate of diffusion of the ferric ions in the pores.

The contraction of the Cu_2S structure as it loses copper is probably by a contraction of the distance

between the sulphur basal planes of the pseudo-hexagonal structure, resulting in the formation of pores in the CuS phase, parallel to the basal planes of the hexagonal CuS structure. Electron probe results (Section 3.4) showed concentration gradients across the breadth of the lamellae (fig.72), indicating diffusion of copper atoms across the lamellae towards the pore surface, and that chemical attack was evident in the pores of the structure. The results also showed a marked decrease in the copper concentration gradient along the length of a lamella of continuous solid towards the bulk solution (fig.73), indicating that a proportion of the copper diffusion was along the length of the lamellae. This suggests that chemical attack was also evident at the end of the lamellae. One would expect chemical attack to be easier at the end of the lamellae, since the copper atoms would be removed from the CuS structure more easily from between the basal plan than across it.

3.1.3 Stirring Speed

The rate of leaching was studied at 250, 540, 900 and 1500 rpm, fig. 34.

Above 540 rpm, the rate was unaffected by the

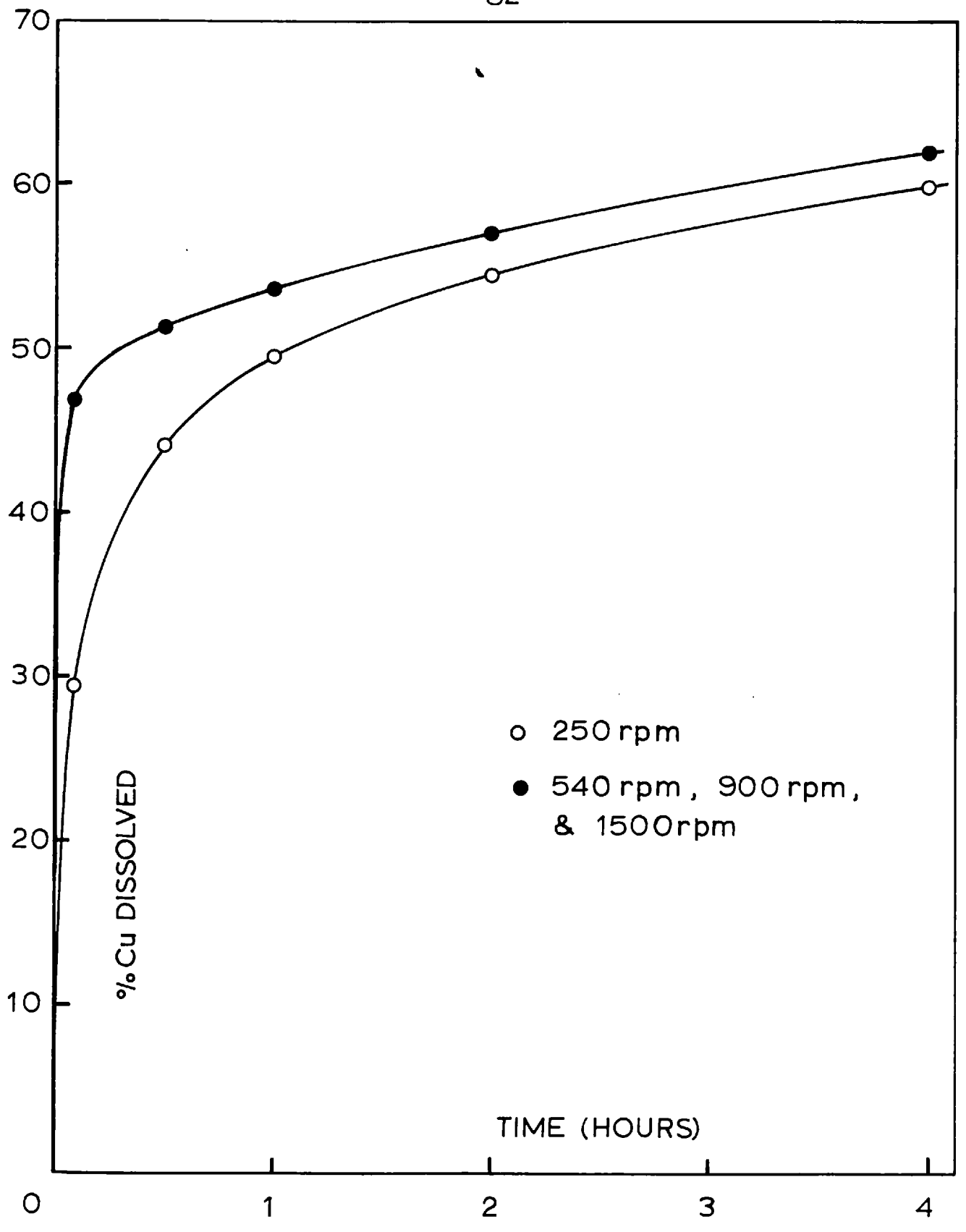


FIG.34 EFFECT OF STIRRING SPEED ON THE RATE OF LEACHING CHALCOCITE.

stirring speed. It will be shown in Section 3.1.4 that the Fe^{3+} oxidant concentration had no effect on the rate of the first reaction-half, and it has been shown that the rate of the first half of the reaction is dependent on the particle size, i.e. the diffusion distances. These factors indicate that the rate-controlling step of the first reaction-half is not the hydrodynamic transfer of oxidant to the mineral surface but diffusion of copper atoms in the sulphide lattice. This was suggested by the activation energy value of the first reaction-half in Section 3.1.1.

The stirring speed also had no effect on the rate of the second reaction-half. Unlike the first reaction-half, the ferric ion concentration does have an effect on the rate of the second reaction-half but the particle size has no effect. Thus the rate-controlling step is not by copper diffusion in the CuS lattice. This adds further evidence to support the theory that the rate-controlling step is a chemical process.

At 250 rpm, the rate of the first reaction-half decreased and the stirring speed became rate-controlling. Insufficiently high stirring rates produced poor transference of oxidant to the sulphide surface and also did not maintain all the particles in suspension,

resulting in a small heap of particles collecting under the impeller.

3.1.4 Ferric Ion Concentration

The rate of the first reaction-half is independent of the ferric ion concentration (fig. 35). This shows that the rate-controlling step is not a chemical process and the evidence presented in earlier sections proves it to be the diffusion of copper in the sulphide lattice.

The rate of the second reaction-half is proportional to the ferric ion concentration over the range of concentration studied. This, together with a) the high activation energy of the second reaction-half and b) the non dependence of the rate of the second reaction-half on the particle size and the stirring speed, shows conclusively that the rate-controlling step of the second reaction-half is a chemical process. This is believed to be the oxidation of the sulphide ions during the removal of copper atoms from the CuS lattice, followed by the chemical transformation of $Cu_{0.8}S$ to sulphur.

An increase in the amount of elemental sulphur present in the residue particles decreased the rate of dissolution of copper. This is due to a decrease

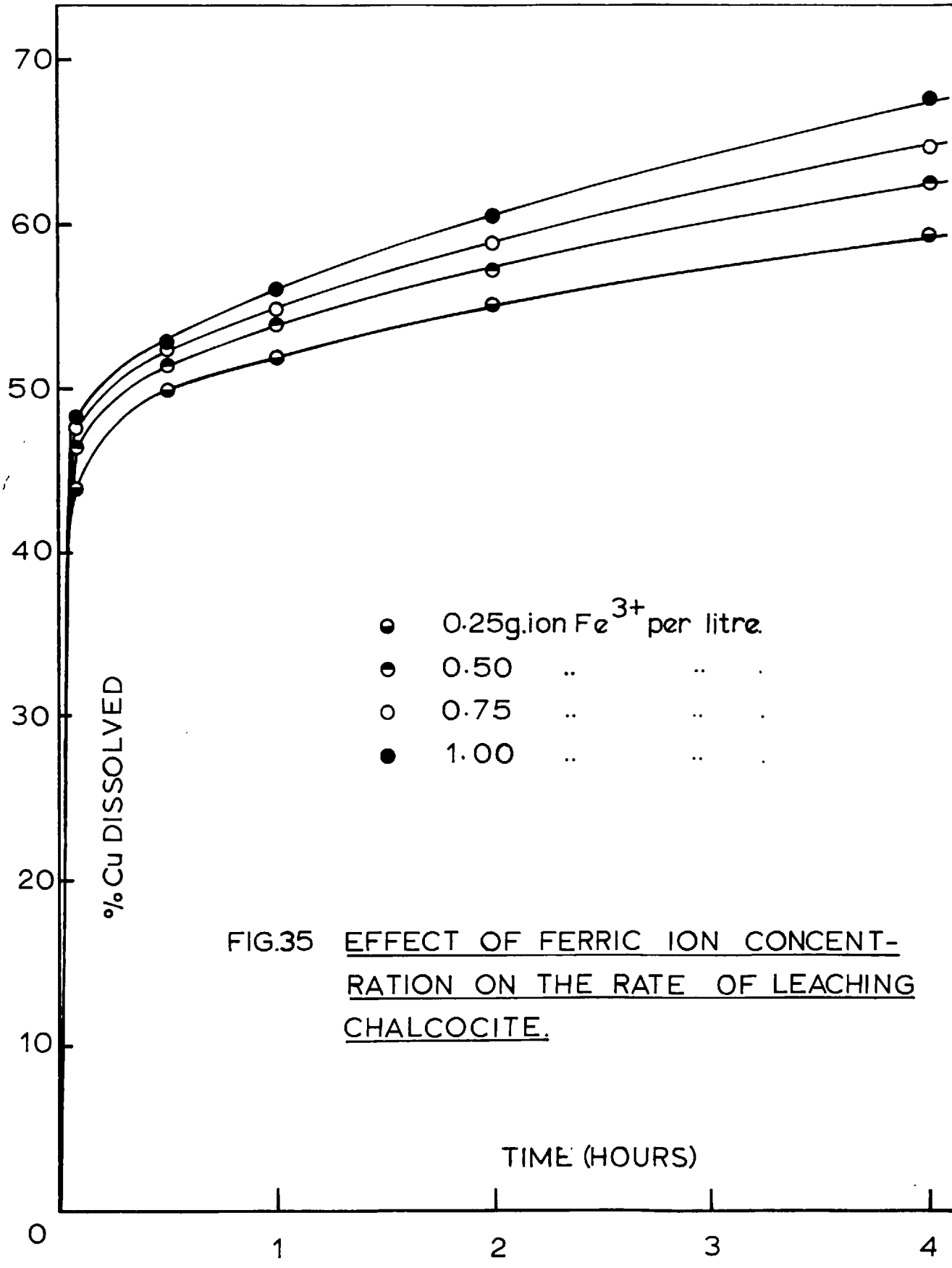


FIG.35 EFFECT OF FERRIC ION CONCENTRATION ON THE RATE OF LEACHING CHALCOCITE.

in the area of $Cu_{0.8}S$ surface in contact with the aqueous solution of the oxidant. The sulphur formed in the pores is porous so that the reaction is not stopped completely, and further attack is continued by diffusion of ferric ions in the pores of the elemental sulphur. Thus, although the rate-controlling step for the dissolution of copper from a residue of composition Cu_xS, where $0.8 > x > 0$, is the chemical transformation of $Cu_{0.8}S$ to elemental sulphur, the actual rate of removal of copper depends on the area of $Cu_{0.8}S$ surface in contact with the oxidant solution, i.e. the amount of sulphur present in the porous residue structure.

It is believed that copper ions do not diffuse through the elemental sulphur. If this occurred it would be evident in the X-ray powder photographs of the leach residues.

3.1.5 Ferrous Ion Concentration

Leaching 2.5g of Cu_2S in acidified 1N $FeCl_2$, it was found that 25% of the copper was removed (fig. 36). Assuming that the leach reaction for the first half is given by

$$Cu_2S + 2FeCl_3 = CuS + CuCl_2 + 2FeCl_2$$

approximately 0.016 moles of Fe^{3+} ion are required to

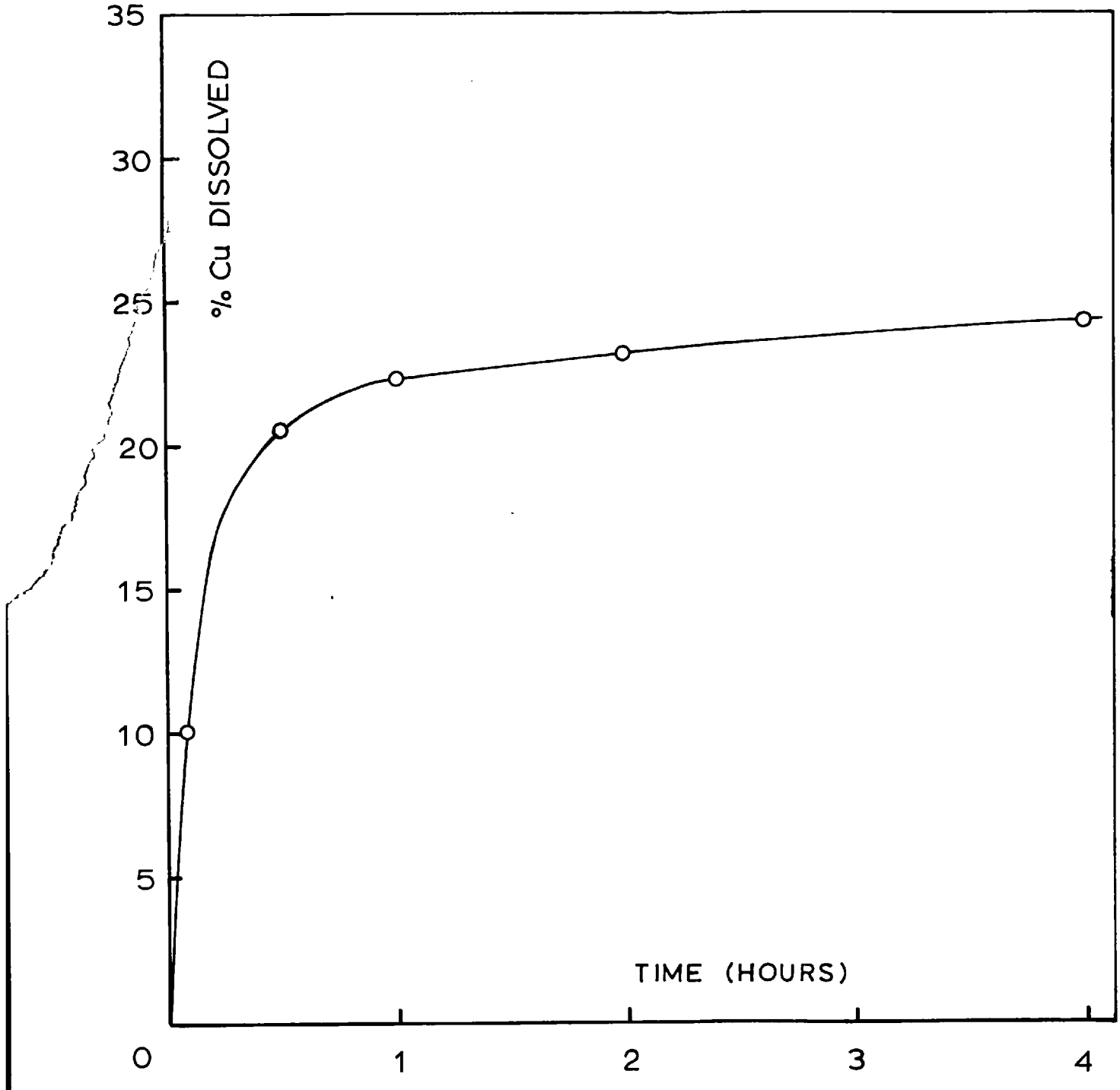


FIG.36 RATE OF LEACHING CHALCOCITE IN ACIDIFIED 1 M $FeCl_2$ AQ.

remove 25% of the copper from 2.5g Cu_2S. This quantity of ferric ion was present in the 1 mole of G.P.R. ferrous chloride which could contain up to 2% ferric ion impurity. Once the ferric ion impurity had oxidised copper ions and had been transformed completely to ferrous ion, the reaction stopped since ferrous ions can have no oxidant properties. This explains why only 25% of the copper was removed when 50% is removed so easily.

3.1.6. Ferrous Ion in the presence of ferric Ion

Ferrous ion, in the presence of a substantial amount of ferric ion, has the same effect as ferric ion (fig. 37), i.e. it has little effect on the first half of the reaction but the rate of the second half is increased.

This behaviour suggests an easy exchange of electrons between the ferrous and ferric ions in solution. The limited amount of literature available on the subject (Section 1.4.8) verifies that this exchange is possible and in chloride solutions it probably takes place rapidly.

An increase in the ferrous ion concentration has a slightly greater effect on the rate of the second

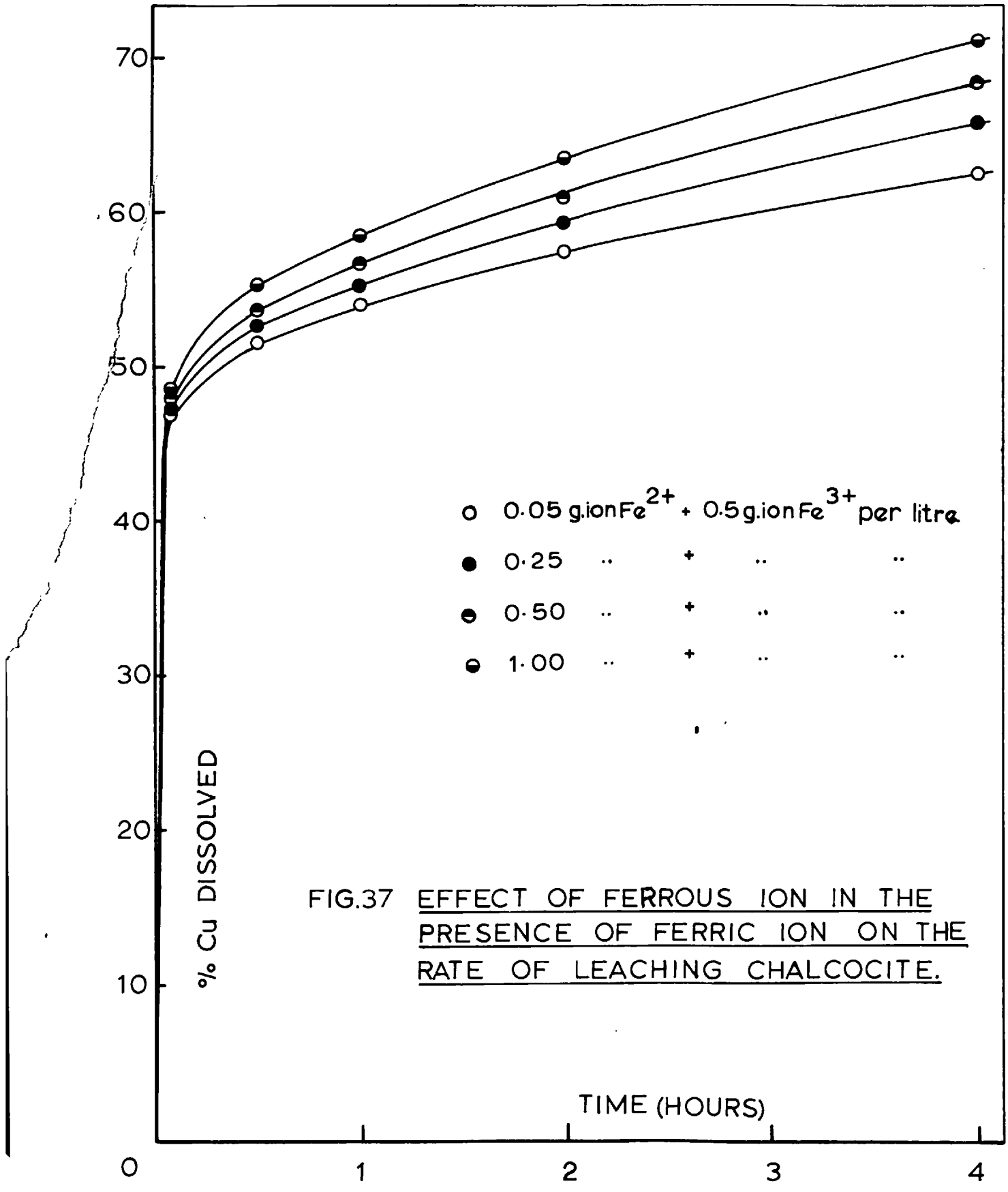


FIG.37 EFFECT OF FERROUS ION IN THE PRESENCE OF FERRIC ION ON THE RATE OF LEACHING CHALCOCITE.

reaction-half than a corresponding increase in the ferric ion concentration. This is probably due to a ferrous-ferric chloride solution being less dense than a ferric chloride solution of the same total iron content, (Appendix 3), i.e. flotation of residue particles in the ferrous-ferric chloride solution would be expected to be less than in a ferric chloride solution of the same iron content.

3.1.7 Acid Concentration

Acid concentration had no effect on the reaction (Appendix 1). Severe hydrolysis of the ferric ion would probably slow the leaching reaction. However, there was sufficient acid present to prevent severe hydrolysis of the ferric ion. In a solution containing 0.5 g.ion Fe^{3+} and 5 mls of cHCl per litre, the fraction of ferric ion that is hydrolysed is approximately 5% of the total ferric ion concentration.

The increase in chloride ion concentration due to the increasing acid concentration results in an increase in the chloride complexing of the ferric ion over the range of acid concentration studied. A ferric chloride solution with 0.5 g.ion Fe^{3+} and 5 mls cHCl per litre contains approximately 8% Fe^{3+}, 16% $FeCl^{2+}$, 52% $FeCl_2^+$

and 24% $FeCl_3$. A ferric chloride solution with 0.5 g.ion Fe^{3+}, and 80 mls cHCl per litre contains approximately 5% Fe^{3+}, 10% $FeCl^{2+}$, 58% $FeCl_2^+$ and 28% $FeCl_3$. This slight increase in the Fe^{3+} complexing produces no detectable change in the rate of the reaction, suggesting that it is equally as easy for the following reactions to take place.

$$4Fe^{3+} + Cu_2S = 4Fe^{2+} + 2Cu^{2+} + S^o$$
$$4FeCl^{2+} + Cu_2S = 4Fe^{2+} + 4Cl^- + 2Cu^{2+} + S^o$$
$$4FeCl_2^+ + Cu_2S = 4Fe^{2+} + 8Cl^- + 2Cu^{2+} + S^o$$
$$4FeCl_3 + Cu_2S = 4Fe^{2+} + 12Cl^- + 2Cu^{2+} + S^o$$

3.1.8 Sample Weight

The rate of reaction was not significantly affected by increasing the sample weight from 2.5 to 5.0 grams, (fig. 38). The slight decrease in the rates of both halves was probably due to particles collecting at the bottom of the bath, the same as the effect experienced with the low stirring speed of 250 rpm.

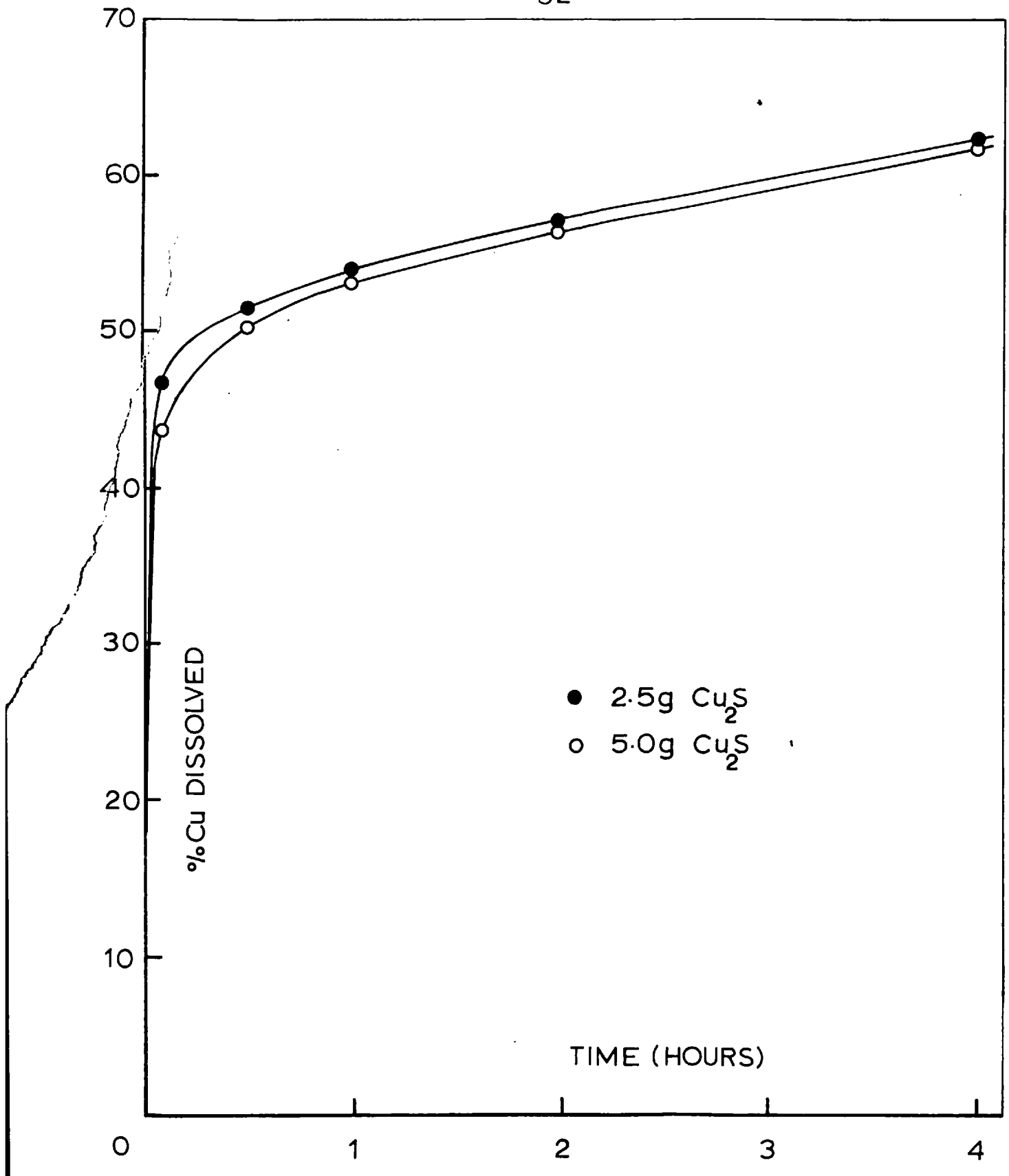


FIG.38 EFFECT OF SAMPLE WEIGHT ON THE RATE OF LEACHING CHALCOCITE.

3.2 MICROSCOPIC EXAMINATION OF LEACHED CHALCOCITE CUBES

In order to study microscopically the phases that are present in the leach from Cu_2S to sulphur, cubes of chalcocite were ground from the massive recrystallised Cu_2S and leached under conditions such that the microstructures would show all phases between Cu_2S and sulphur.

The cubes were polished and enclosed in a platinum wire cage. The cage was suspended in acidified aqueous ferric chloride, (0.5 gion. Fe^{3+} and 20 ml. cHCl per litre), and cubes were leached for 24 hours at 40 and 60°C, and 60 hours at 60°C. The leach solution was agitated by the stirrer rotating at 250 rpm which ensured good transference of Fe^{3+} oxidant to the cube surface without the aeration and turbulence associated with highly stirred solutions.

The leached cubes were sectionalised, polished, and examined microscopically.

(a) 24 hours at 40°C

The dimensions of the cube were 10 x 9 x 7 mm. After leaching, the cube was extremely porous (fig. 39) as predicted from the density considerations, (page 79).



Fig. 39 The unpolished surface of the chalcocite cube leached for 24 hrs. at 40°C. (Magnification x23).

Particulate chalcocite (-50 + 100 mesh) leached in the X-ray powder photograph studies (Section 3.3, Appendix 7), gave a residue with 82.2% of the copper removed after leaching for 24 hrs. at 40°C. Electron probe results (Section 3.4) and X-ray powder photograph studies.(Section 3.3), show that sulphur is formed when

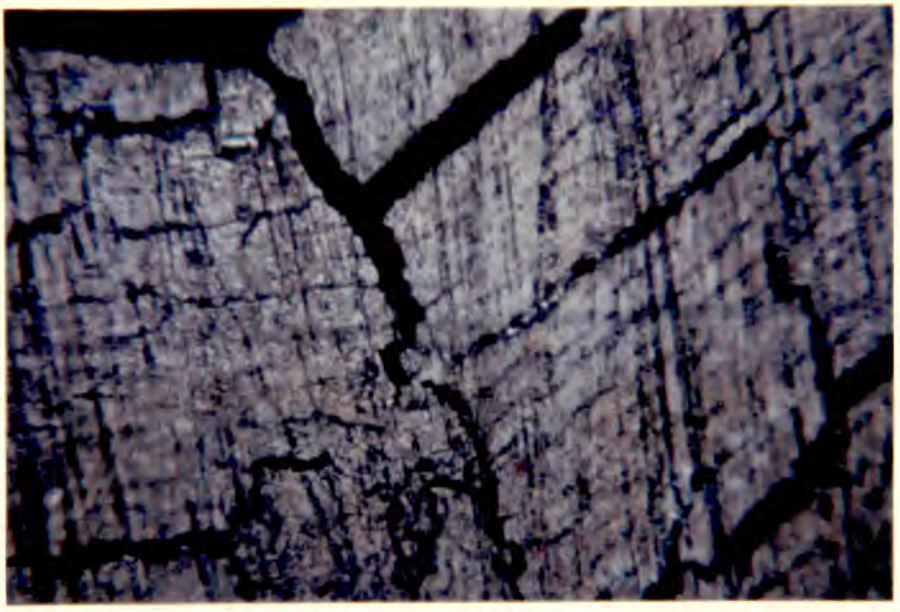


Fig. 40

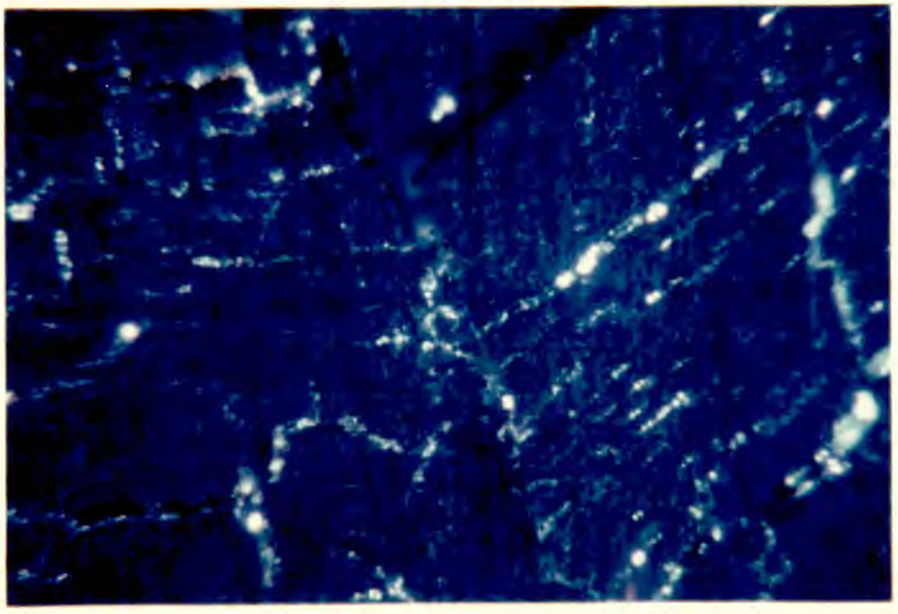


Fig. 41

Figs. 40 & 41 The unpolished cube surface showing the presence of sulphur in the pores of the structure. (Polarised light, magnification x250)

60% of the copper is removed. Thus the surface of the cube should show the presence of sulphur. The sulphur is evident from the examination of the unpolished leached cube surface under polarised light (figs. 40 and 41). The copper sulphide of composition $Cu_{0.8}S$ is seen to transform to sulphur in the pores of the structure.

The cube was sectionalised along its length and polished on carborundum papers and diamond cloths, fig. 42. Because of the porous structure, the leach residue material was extremely fragile and crumbled easily. Fragments were torn from the structure despite the great care taken in the polishing procedure.

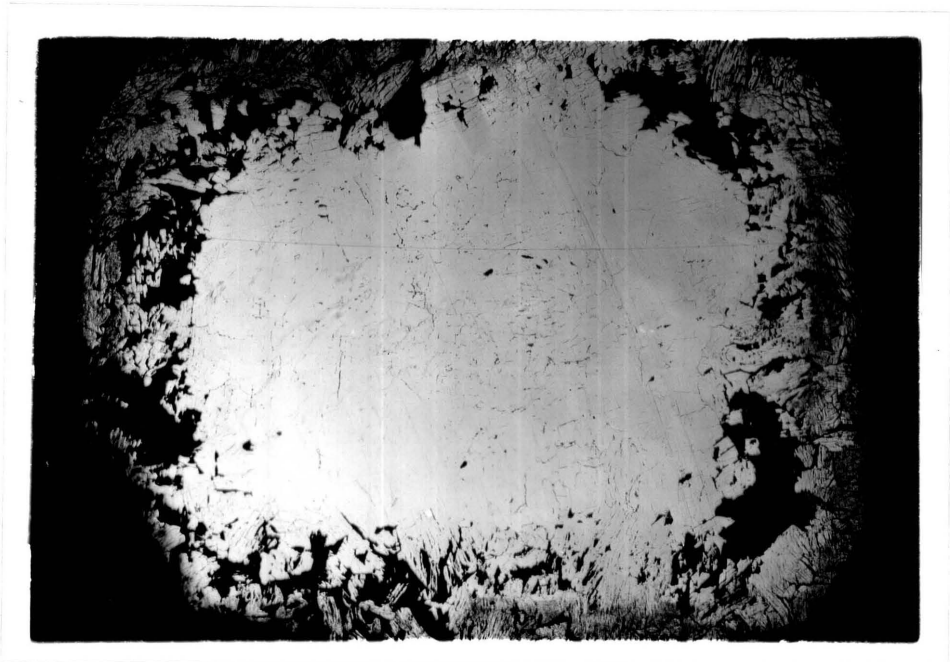


Fig. 42 Polished section of the cube leached for 24 hrs at 40°C (Magnification x10.7)



Fig. 43

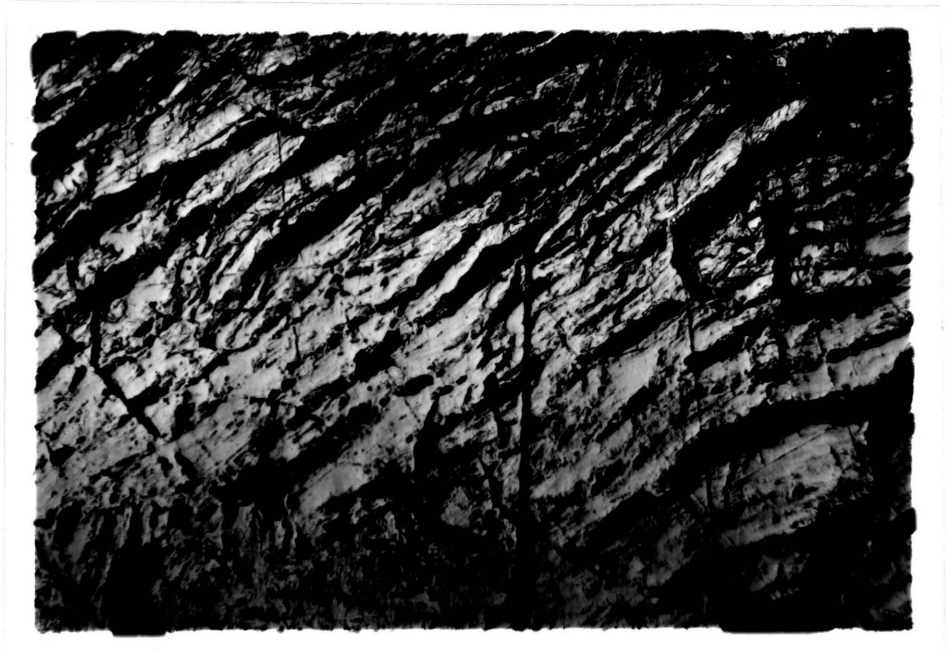


Fig. 44

Figs. 43 and 44. The porous structure and edge of the polished cube section. (Magnification x100)

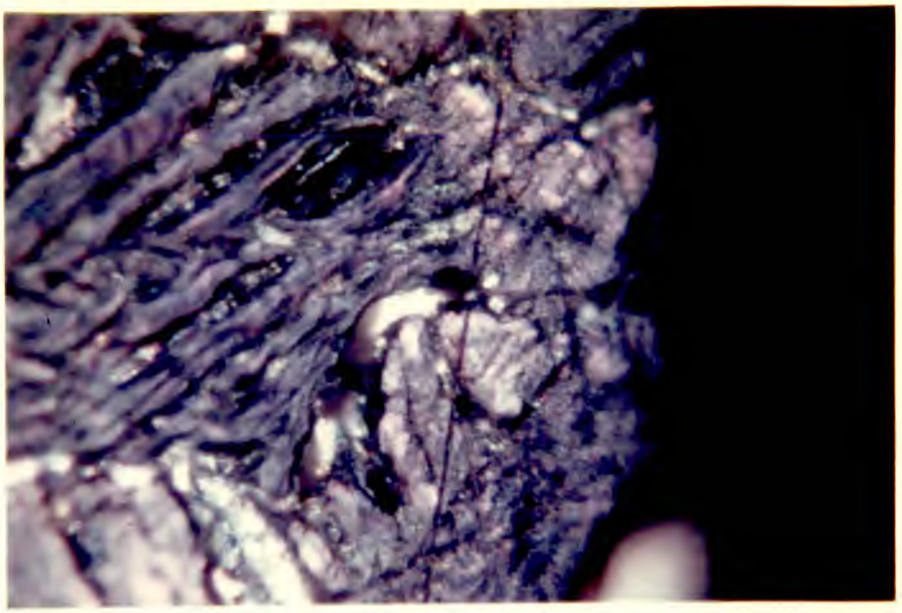


Fig. 45 Sulphur in the porous residue at the cube edge.
(Polarised light, magnification x250)

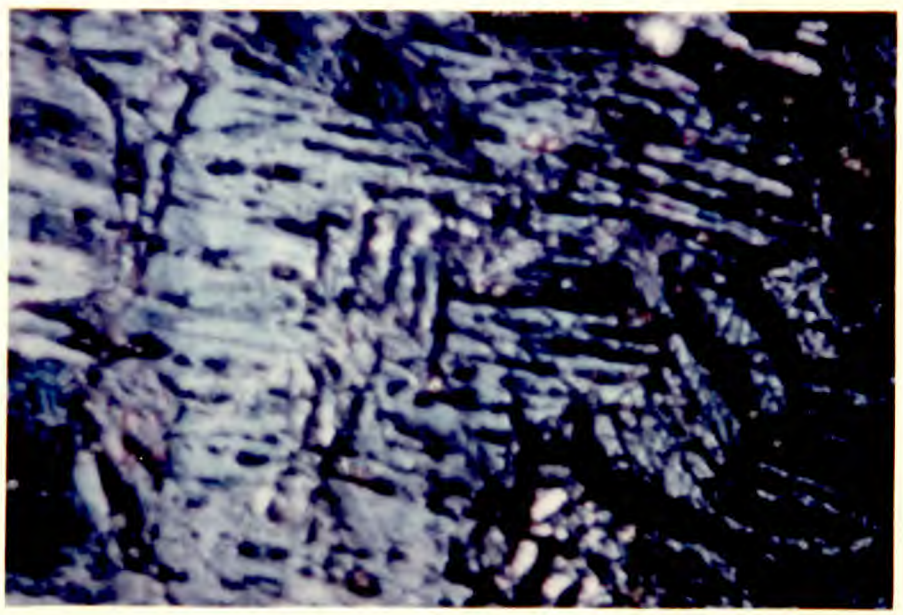


Fig. 46 The decrease of structural porosity towards the centre of the specimen.
(Polarised light, magnification x100)

The edge region of the cube section showed a very porous structure, figs 43 to 46. This region was badly polished due to bevelling of the specimen edges during the polishing procedure and the resultant photographs were not very satisfactory. However, they did show that the pores of the unleached surface were in preferred crystallographic directions and that the orientation of the individual crystal grains determined the angle of inclination of the pores to the cube surface.

The porosity was extensive at the cube edge, corresponding to the $Cu_{0.8}S$ - sulphur residue. The porosity decreased through the CuS phase to the unleached Cu_2S phase in the centre of the cube which was compact.

The material at the cube edge displayed anisotropic properties, changing from dark blue to light green in colour as the analyser of the polarised light microscope was rotated. The sulphur was highlighted in the dark blue field, figs. 45 and 46, and like the photographs of the unpolished leach surface, figs. 40 and 41, the $Cu_{0.8}S$ is seen to transform to elemental sulphur in the pores of the structure.

Proceeding from the edge towards the centre of the cube, the residue showed the complete anisotropic colour sequence of covellite, figs. 47 to 51. The colours are, in sequence, cream, light blue, dark blue, bright crimson,

Covellite Anisotropy

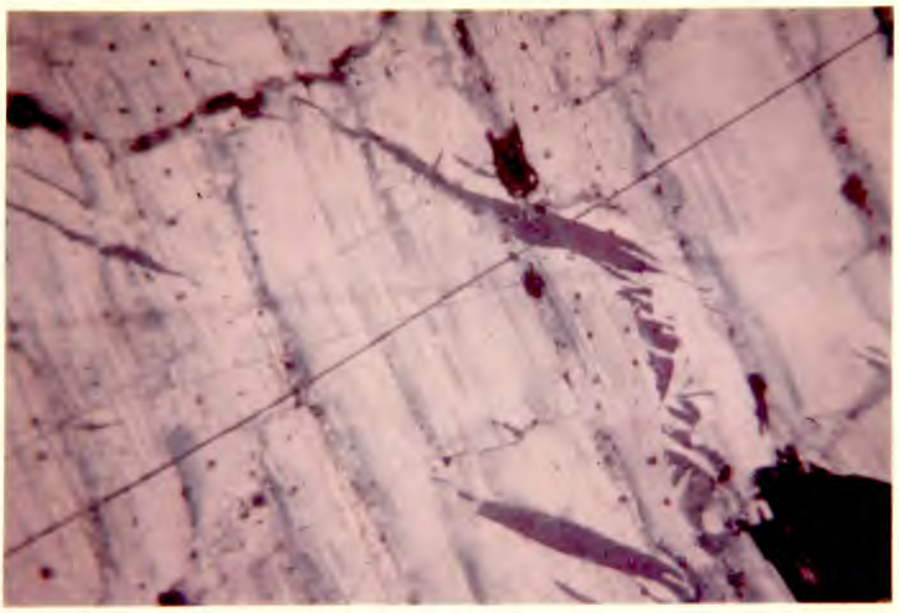


Fig. 47

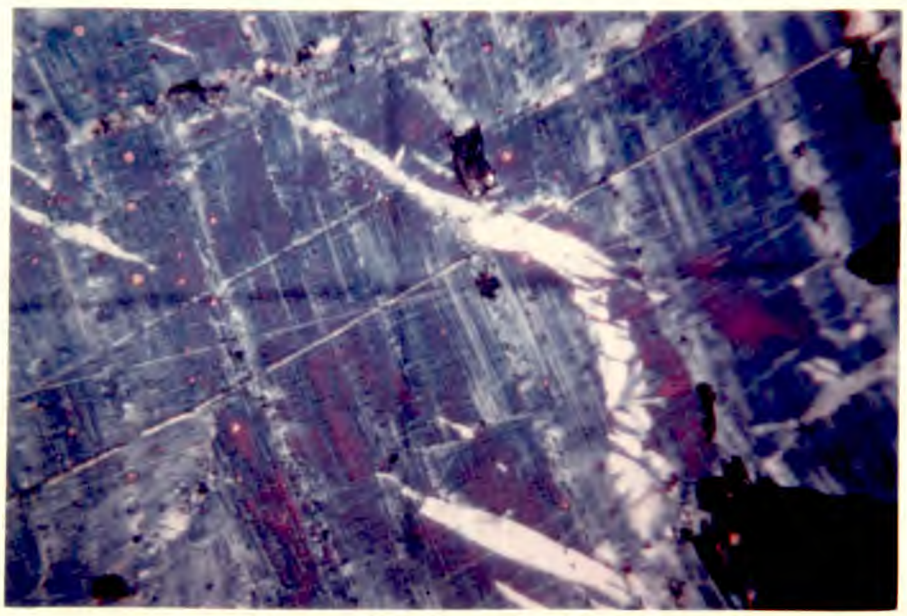


Fig. 48

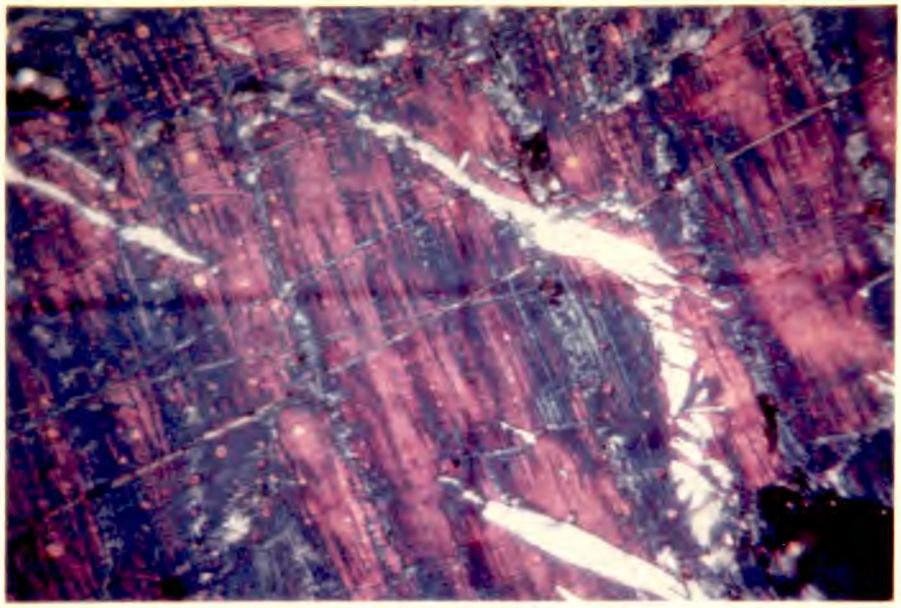


Fig. 49

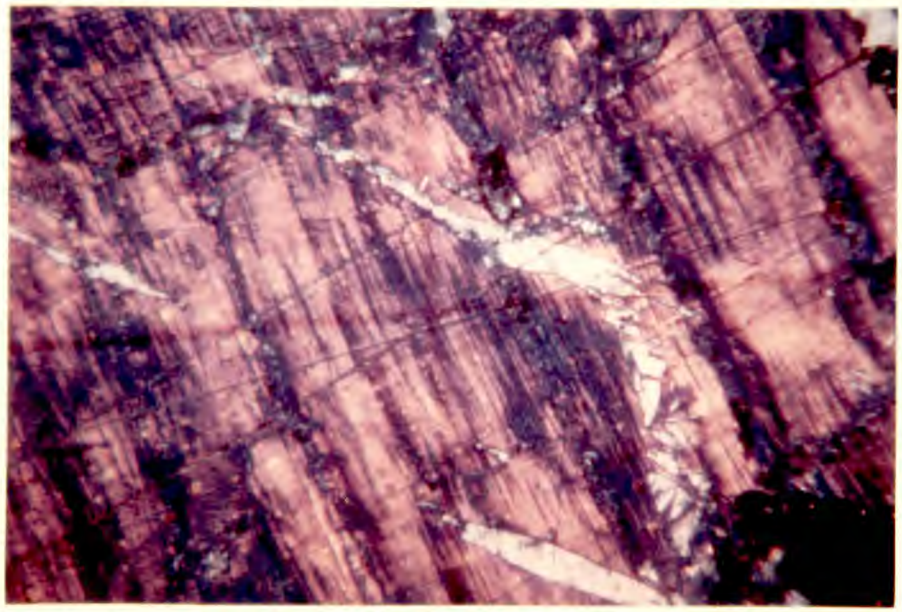


Fig. 50

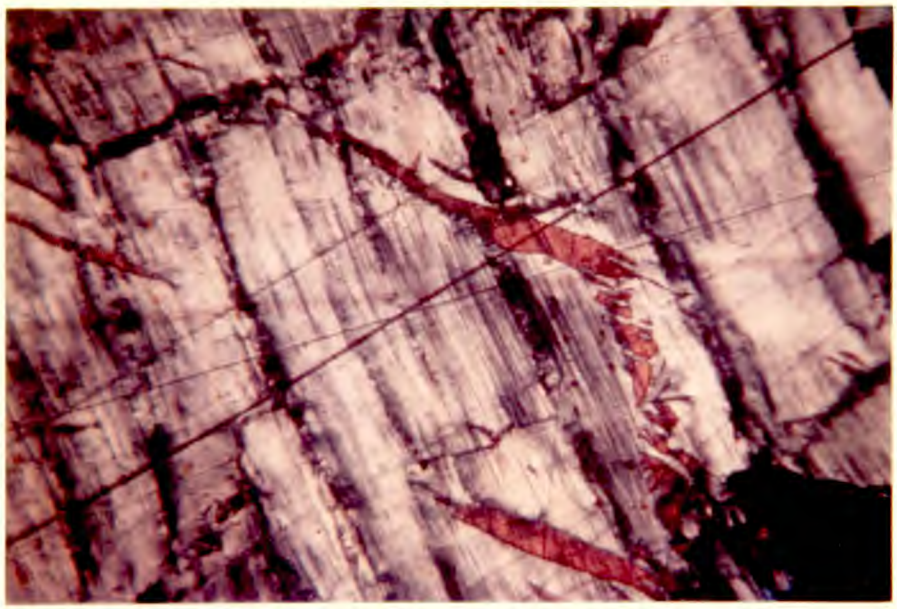


Fig. 51

Figs 47 to 51 The colour sequence of covellite anisotropy, shown in the microstructure of a sectionalised cube leached for 20 hrs at 40°C. (Polarised light, magnification x250)

orange, returning to cream. This colour sequence occurs twice for every rotation of the analyser.

Twinning, a common crystal form of chalcocite, was evident in the photographs of covellite anisotropy. Crystals of different orientation are contrasted by difference in colour.

The anistropic colours of covellite gradually disappeared as one proceeded towards the cube centre and the Cu_2S structure. Figs. 52 and 53 show the transition region between Cu_2S and CuS. The top of the field shown in fig. 52 was Cu_2S; the lower half of the picture showed the removal of copper from the structure along preferred crystallographic planes. The blue phase that was formed by removal of copper from the Cu_2S became darker as more copper was removed. This blue phase is probably the $Cu_{1.8}S$ phase found in the X-ray powder photograph study of the leach residue (Section 3.3). Proceeding towards the cube edge, the blue phase gradually transformed to covellite.

Chalcocite exhibits faint anisotropy, figs. 54 and 55, the colours being light blue and cream. The prismatic twinning of chalcocite is again evident in the microstructure. A region of copper removal is seen in the lower right hand corner of the photographs.

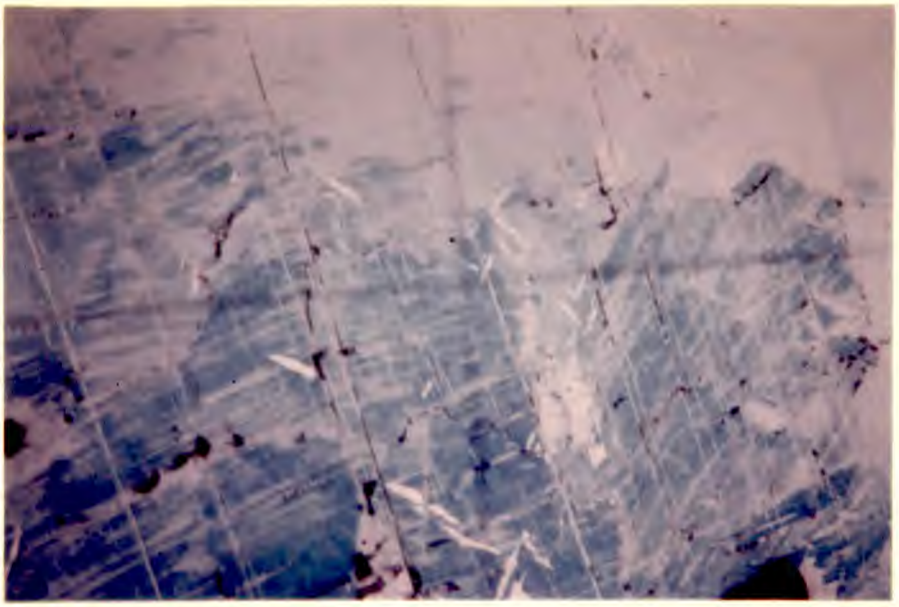


Fig. 52 Transition region between Cu_2S and CuS.
(polarised light, magnification x250)

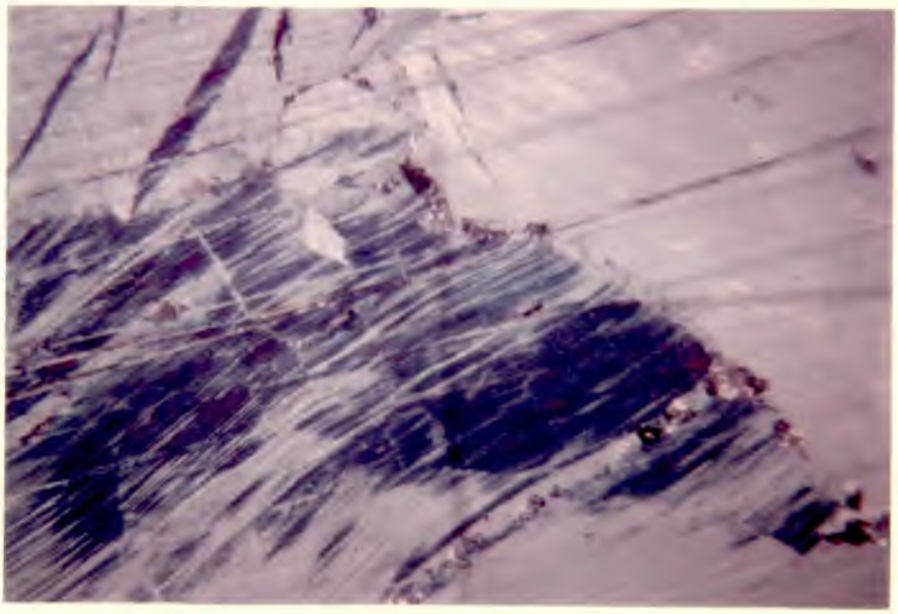


Fig. 53 Diffusion along preferred crystallographic planes.
(polarised light, mangification x500)

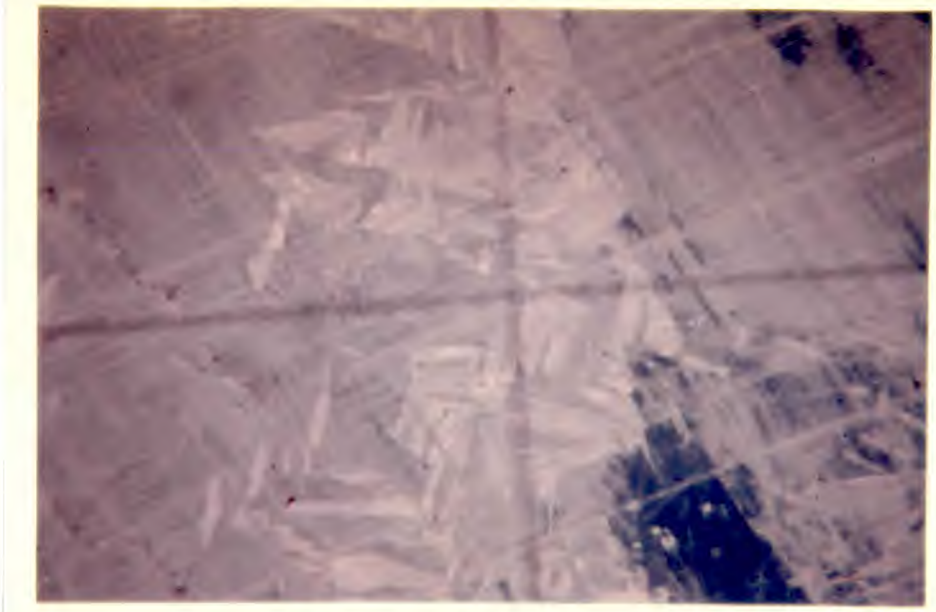


Fig. 54



Fig. 55

Figs. 54 and 55 Anisotropy of Cu_2S.
(polarised light, magnification x250)

(b) 24 hours at 60°C

The dimensions of the cube were 9 x 6 x 6 mm. The polished surface of the sectionalised cube, fig. 56, showed the formation of a thin sulphur coating. By comparison, particulate chalcocite (-50 + 100 mesh) is leached to elemental sulphur in 24 hrs., (Appendix 7).

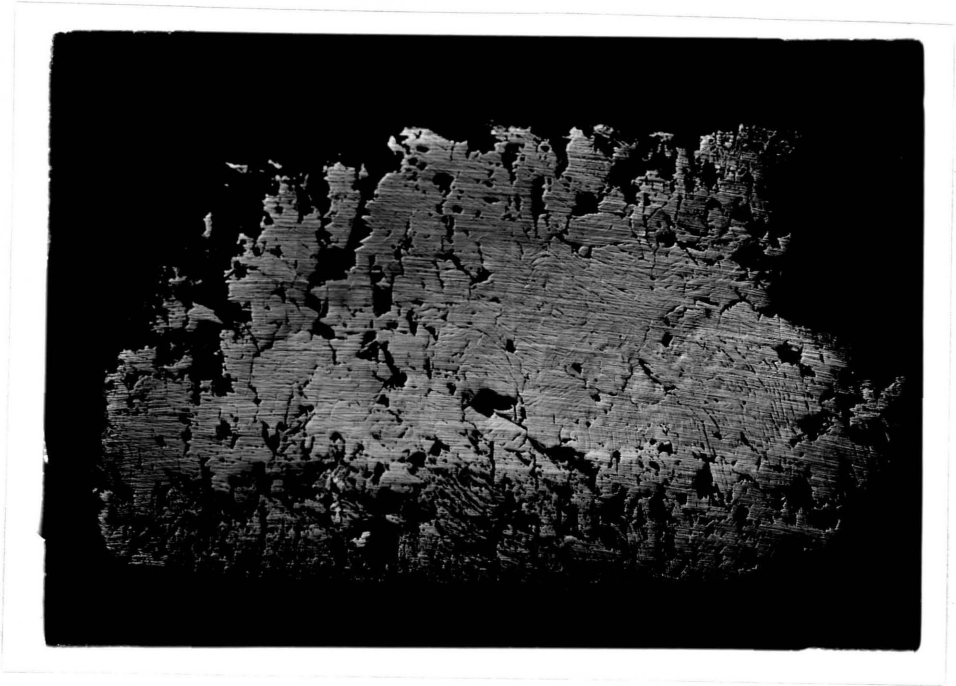


Fig. 56 Polished surface of the sectionalised cube leached for 24 hrs at 60°C (magnification x10.7)

(c) 60 hours at 60°C

The dimensions of the cube were 9 x 6 x 6 mm. The polished surface of this sectionalised cube was

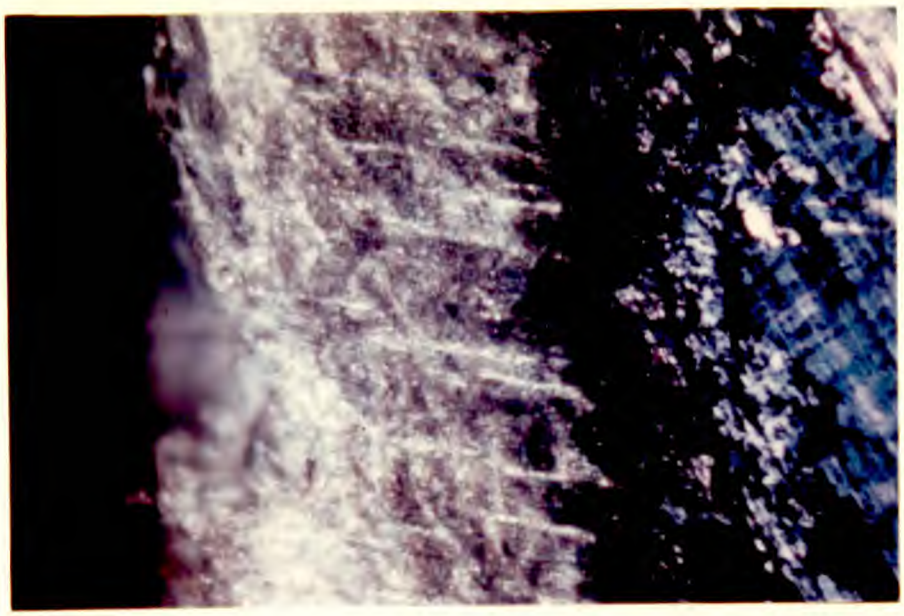


Fig. 57 The sulphur coating around the cube leached for 60 hrs at 60°C.
(polarised light, magnification x100)

similar to that leached for 24 hours at 60°C but the sulphur coating had grown in thickness. The sulphur coating is best illustrated in colour and under polarised light, fig. 57.

The sulphur is formed by chemical attack in the pores of the structure and therefore along preferred crystallographic planes, figs. 58 and 59. The sulphur formed in the pores is itself porous and further reaction occurs by diffusion of Fe^{3+} oxidant along these newly created pores.

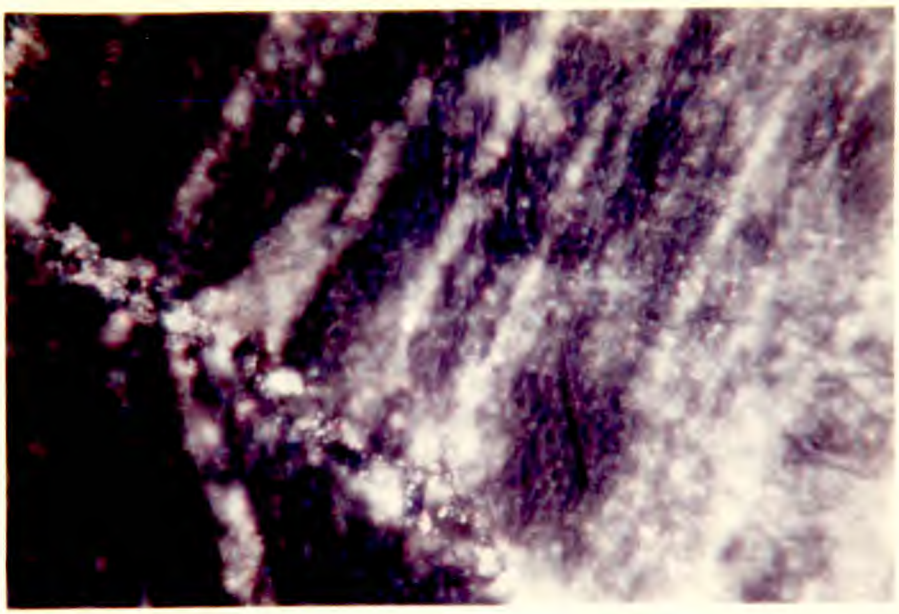


Fig. 58

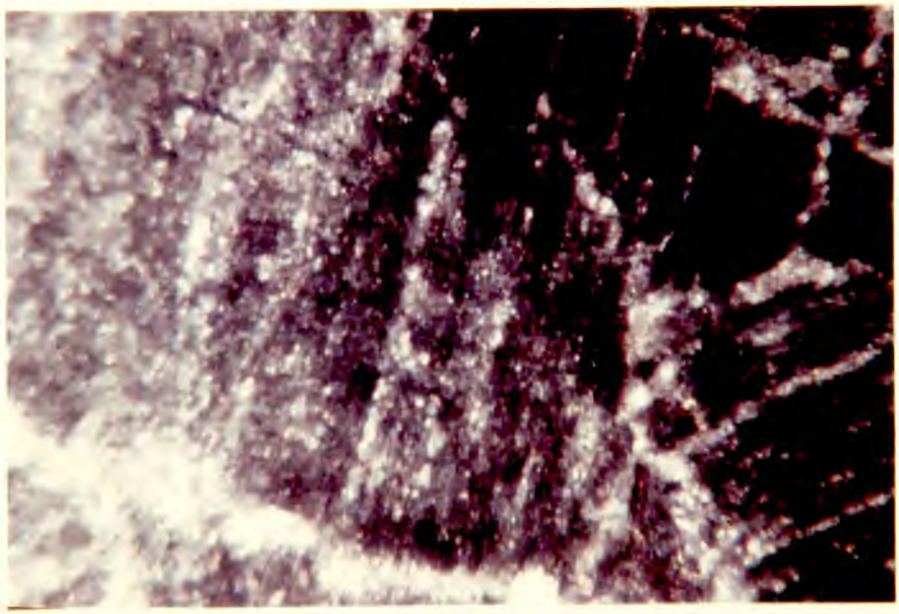


Fig. 59

Figs. 58 & 59 Sulphur in the pores of the copper sulphide ($Cu_{0.8}S$) structure.
(Polarised light, magnification x250)

3.3 X-RAY POWDER DIFFRACTION STUDY OF THE LEACH RESIDUES

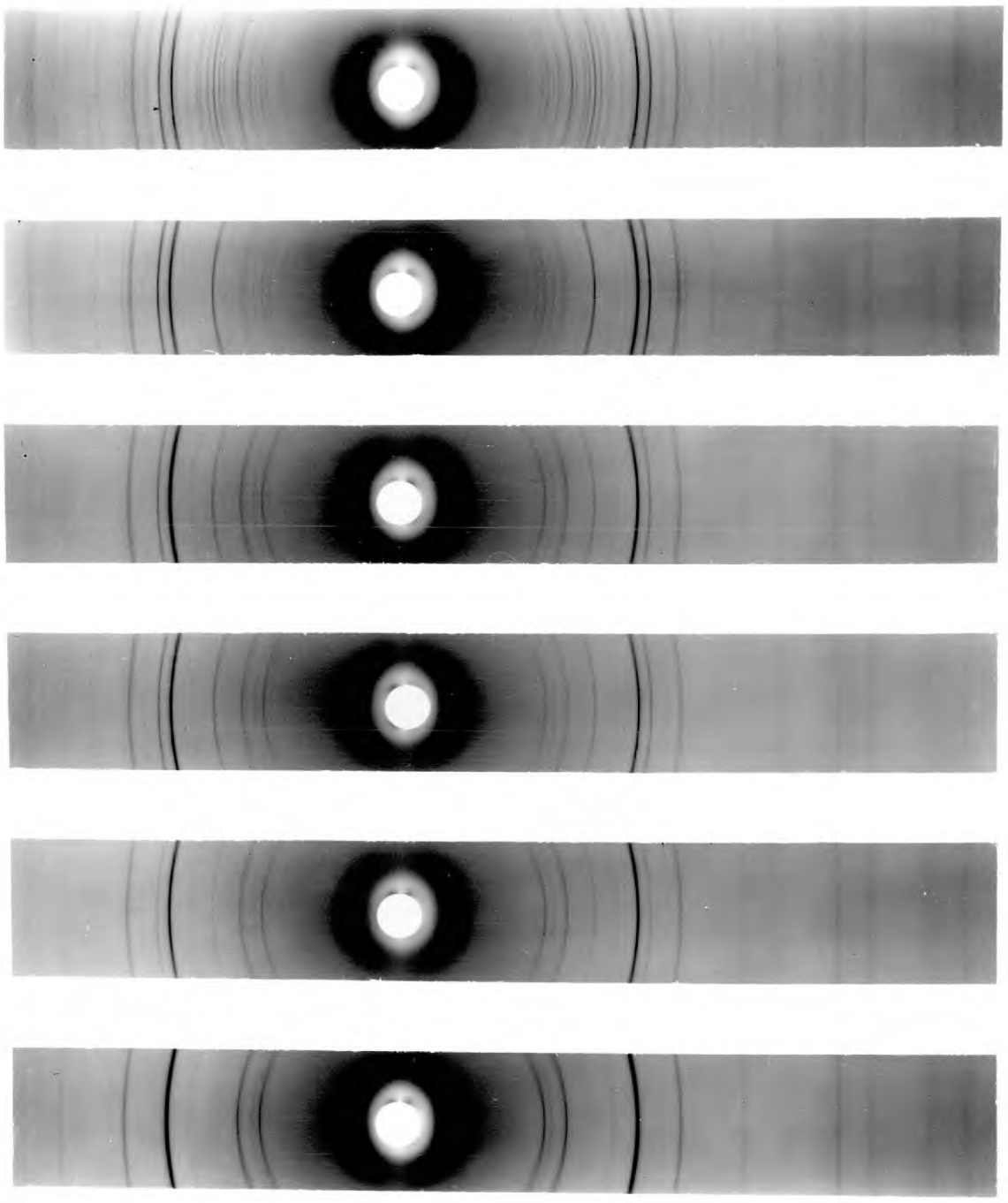
Residues covering the range of the leach reaction from Cu_2S to sulphur were obtained by leaching chalcocite under different conditions.

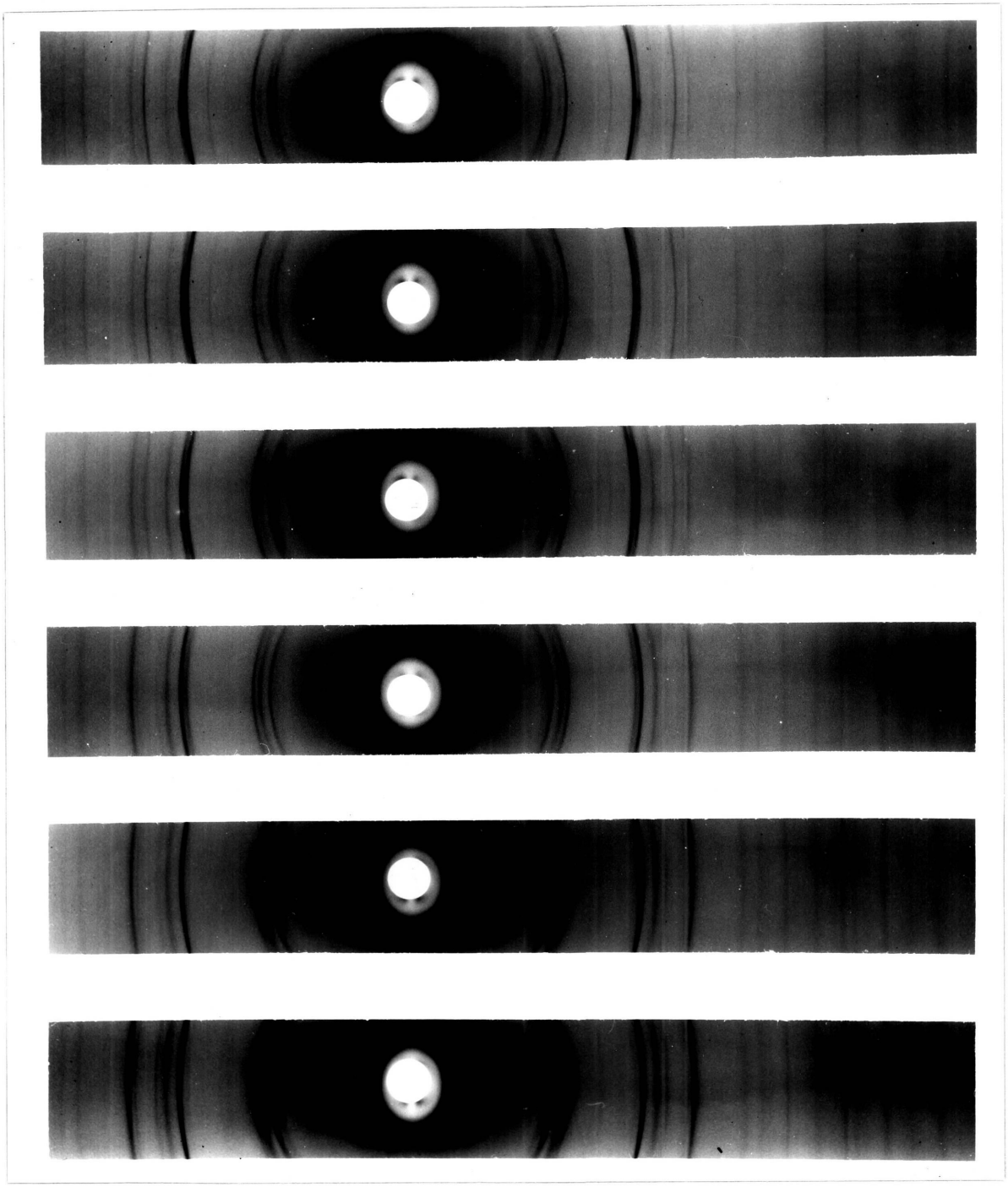
For the first reaction-half, chalcocite was leached for 1 hour in acidified ferric chloride solution of variable concentration. Experimental conditions and results are given in Appendix 5(a). X-ray powder photographs of the residues in the range Cu_2S to CuS are shown in fig. 60. The X-ray diffraction data calculated from measurement of the photographs is shown graphically in fig. 64, and is tabulated in Appendix 7(a).

For the second reaction-half, chalcocite was leached under set experimental conditions for different lengths of time to remove the required amounts of copper. Experimental conditions and results are shown in Appendix 5(b). X-ray powder photographs of the residues in the range CuS to S are shown in figs. 61, 62 and 63. The X-ray diffraction data has been tabulated in Appendix 7(b), and the data for the residues leached at 60°C is shown graphically in fig. 64.

Fig. 60 X-ray Powder Photographs of the residues

a) First reaction-half



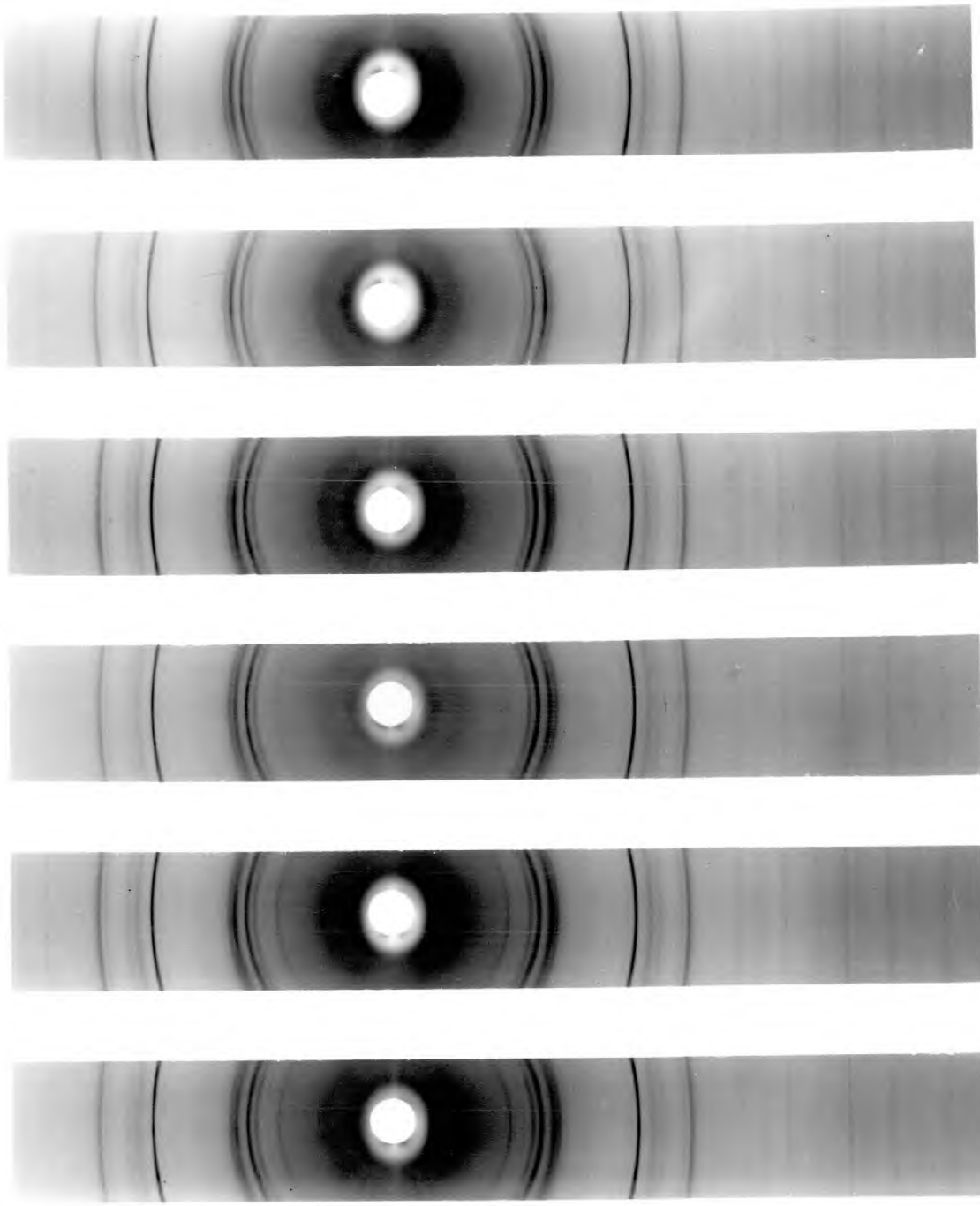


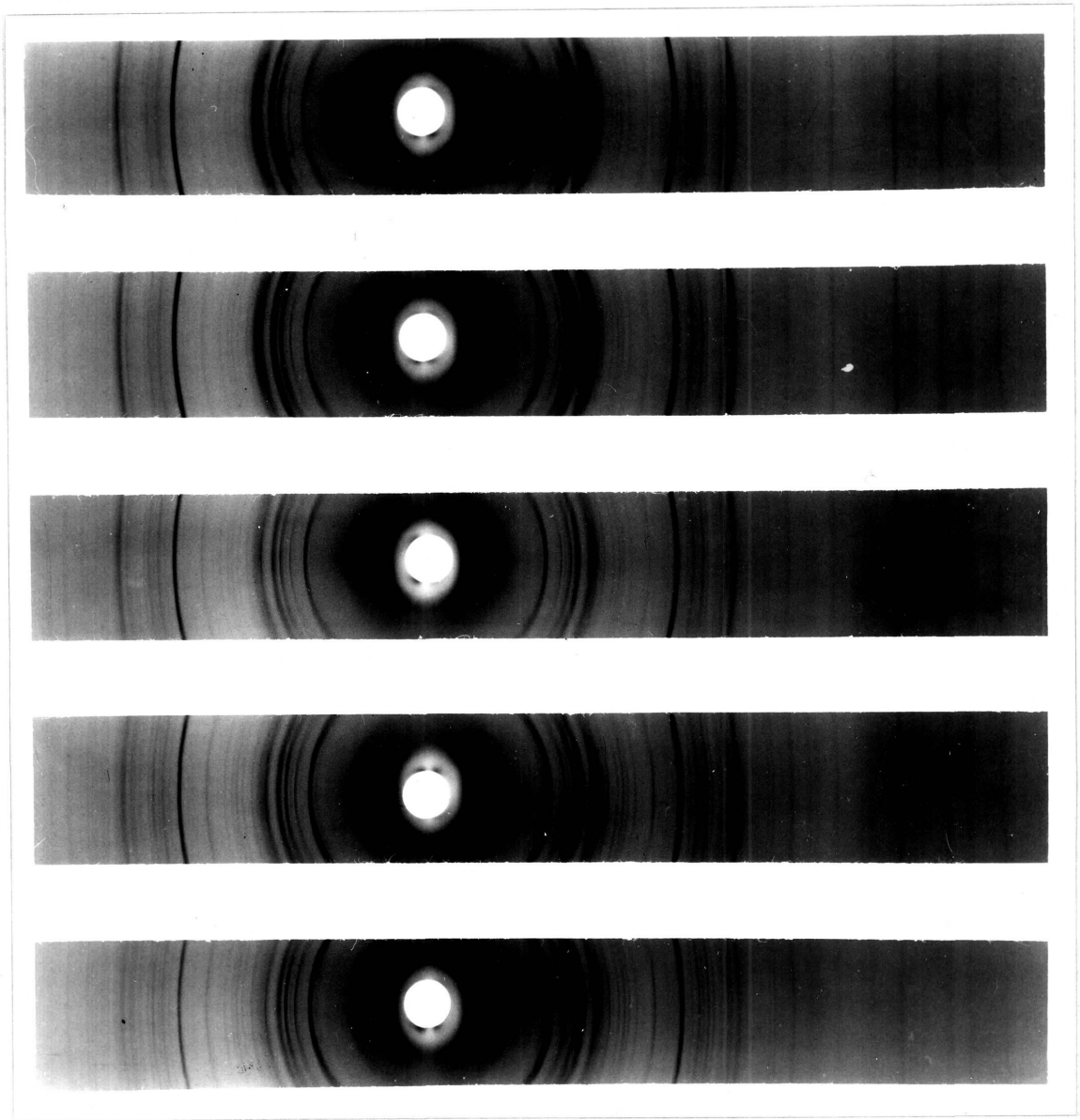
Film 1	Cu_2S	Film 7	20.7 %Cu dissolved
2	7.28 %Cu dissolved	8	23.4
3	8.83	9	27.0
4	10.0	10	34.7
5	11.2	11	41.2
6	13.6	12	47.9

Fig. 61 X-ray Powder Photographs of the Residues

b) Second reaction-half

40°C





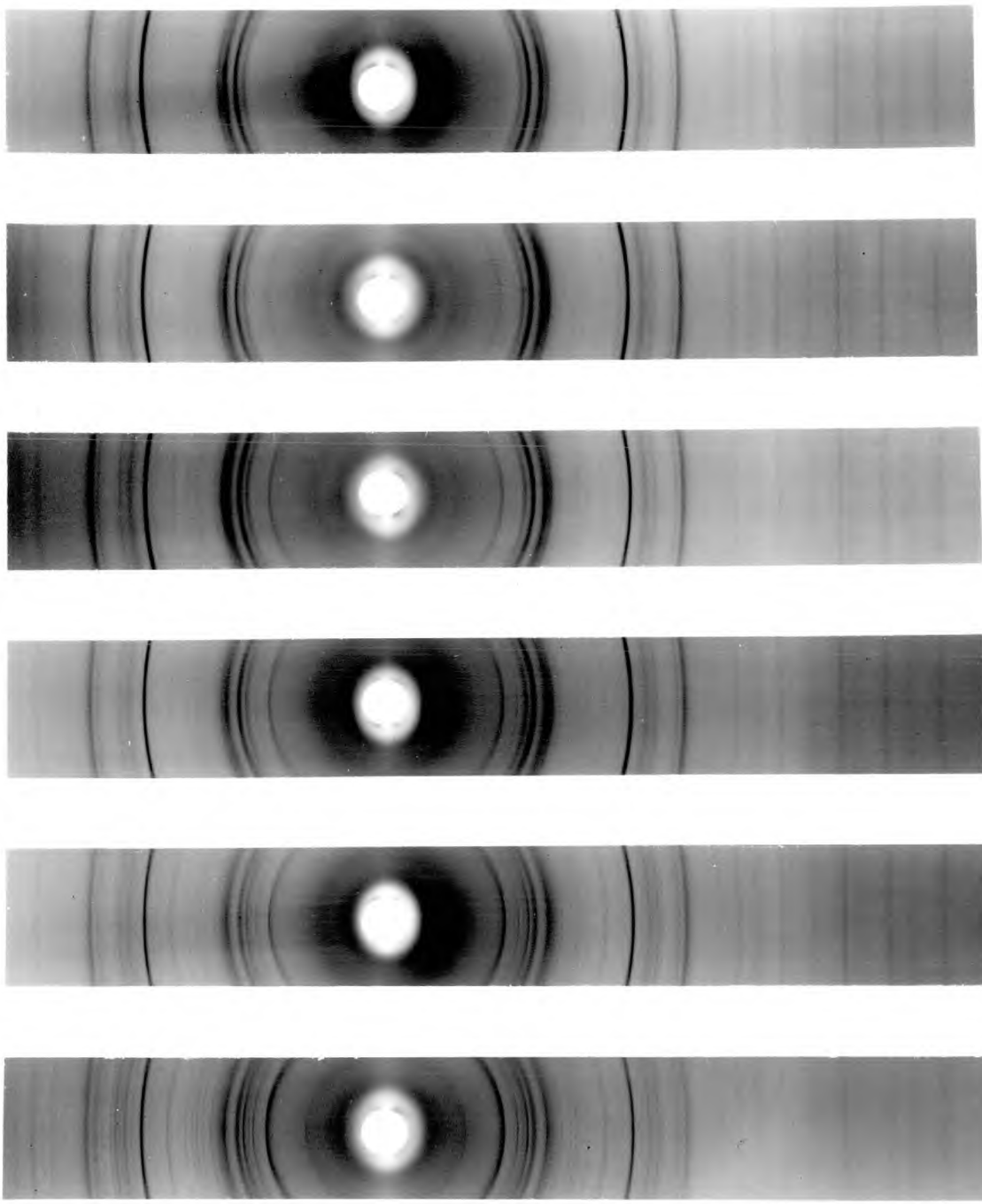
Film	13	46.7 %Cu dissolved	Film	19	79.0 %Cu dissolved
	14	52.4		20	82.2
	15	58.4		21	86.0
	16	65.1		22	88.6
	17	70.2		23	91.7
	18	74.2			

Fig. 62 X-ray Powder Photographs of the Residues

b) Second reaction-half

60°C

Film



24

25

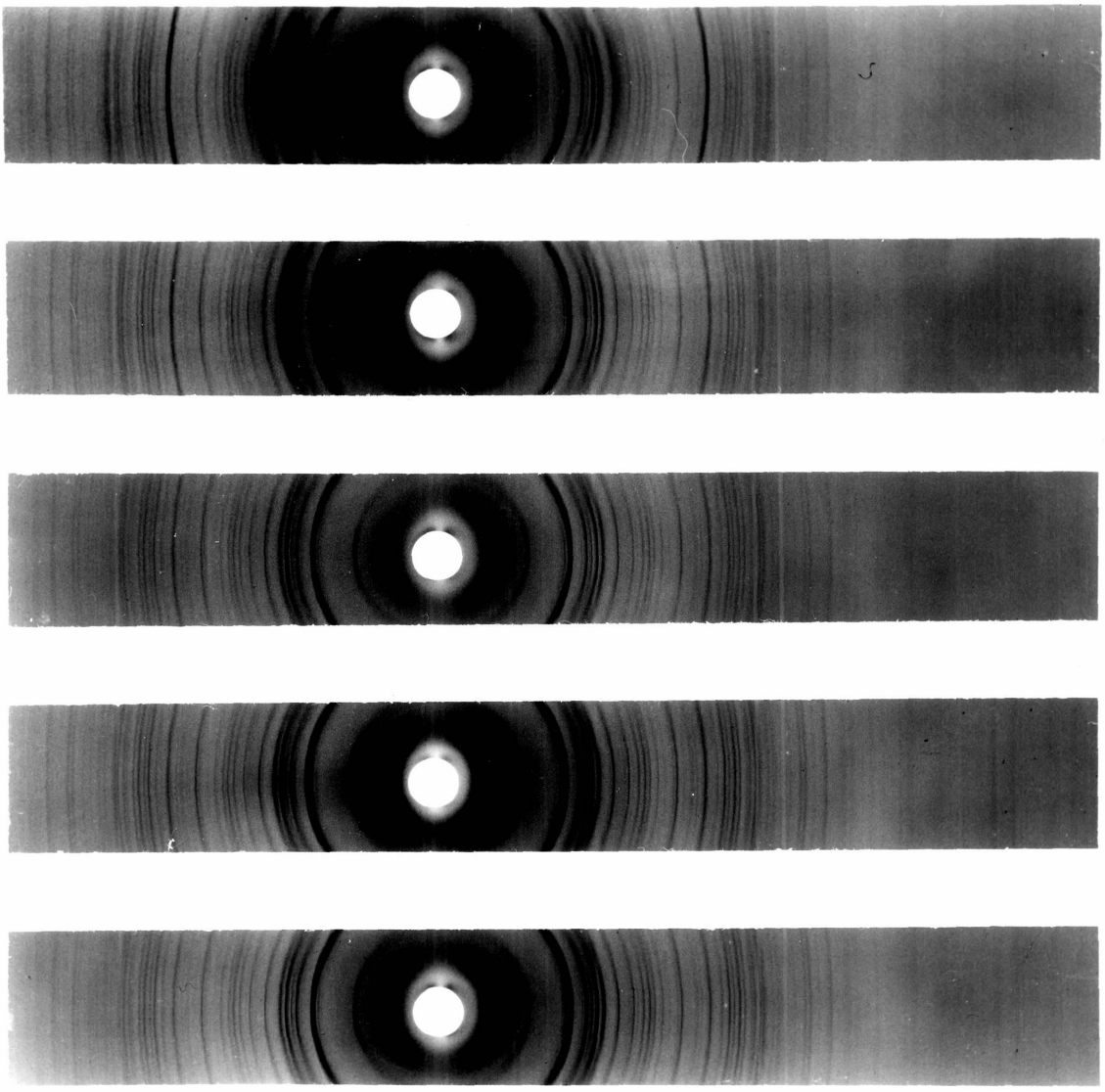
26

27

28

29

Film



30

31

32

33

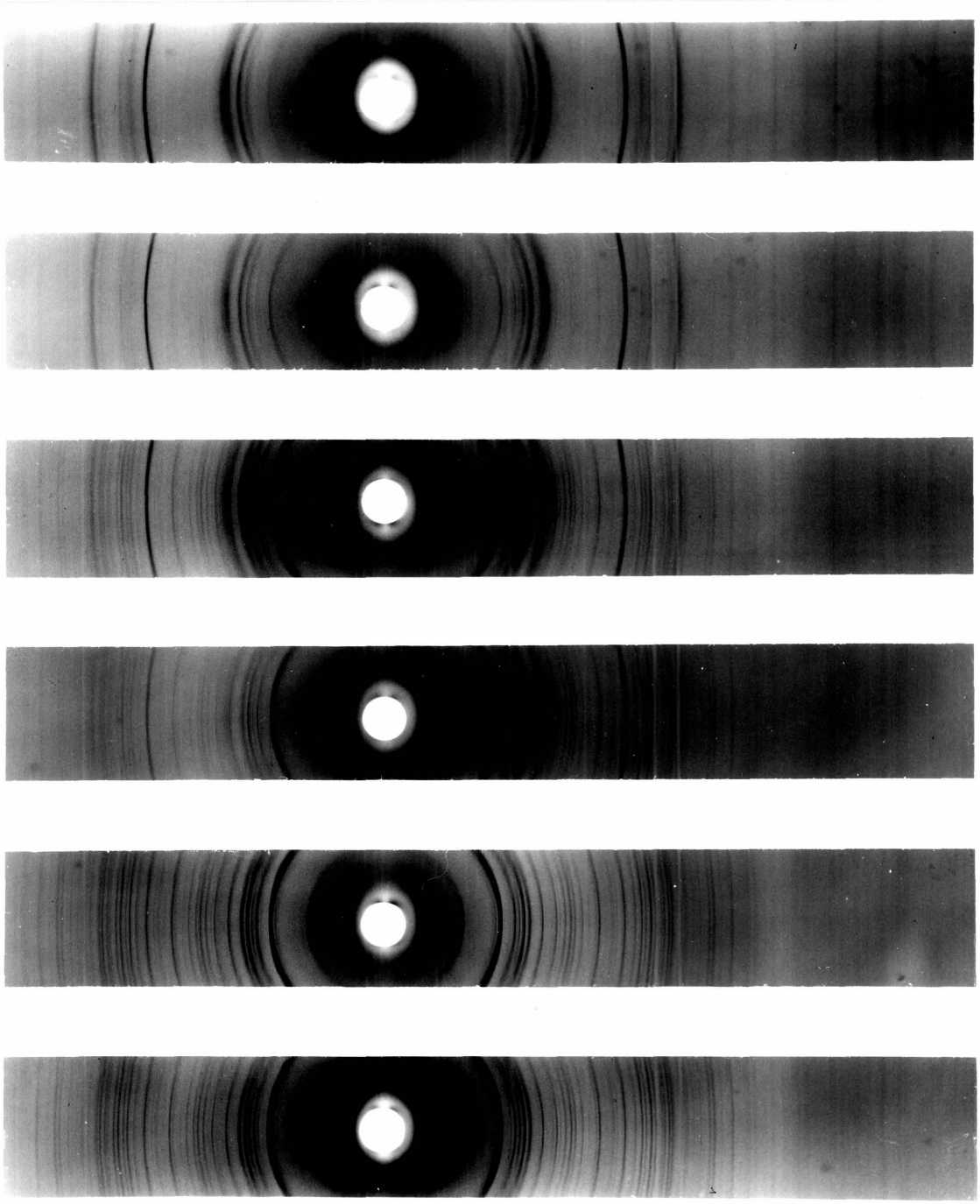
34

Film	24	51.3 %Cu dissolved	Film	30	89.7 %Cu dissolved
	25	60.5		31	94.1
	26	67.1		32	96.3
	27	74.2		33	97.6
	28	82.0		34	99.2
	29	86.4			

Fig. 63 X-ray Powder Photographs of the Residues

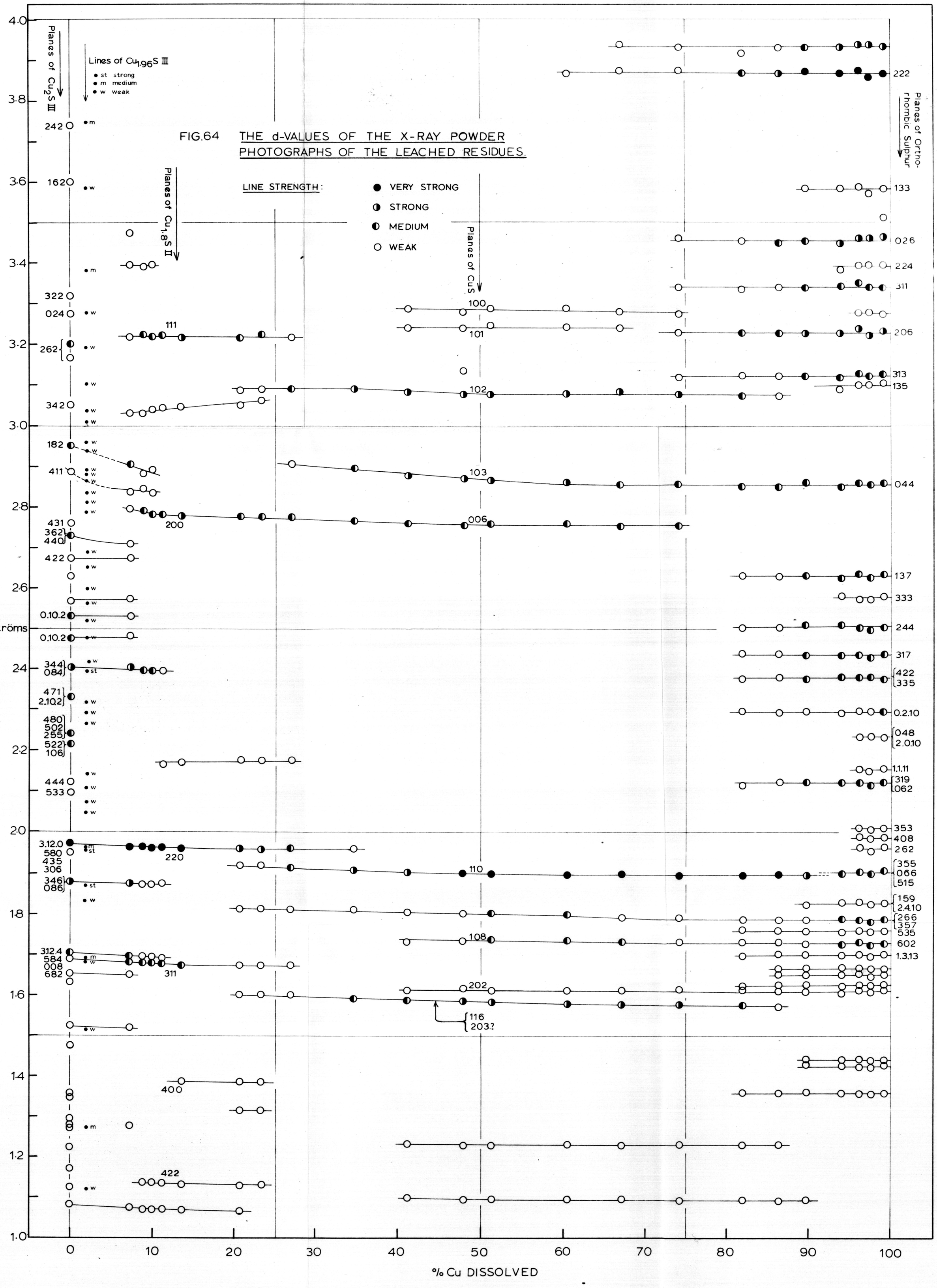
b) Second reaction-half

80°C



Film 35	64.7 %Cu dissolved		Film 38	96.8 %Cu dissolved	
36	76.5		39	99.6	
37	89.2		40	100.0	

FIG.64 THE d-VALUES OF THE X-RAY POWDER PHOTOGRAPHS OF THE LEACHED RESIDUES.



3.3.1 The First Reaction-Half

The d-values of the Cu_2S lines are in excellent agreement with those of Djurle[18] for the A-centred orthorhombic low temperature Cu_2S III phase, Section 1.2.1.

The lines of the residue representing the composition CuS were in satisfactory agreement with those given in the literature[90] for hexagonal CuS, Section 1.2.2. The discrepancies at high d-values are most likely due to the residue CuS phase being slightly deformed and not having the exact cell dimensions of the equilibrium phase.

The d-values of the lines of the residue of $Cu_{1.80}S$ are in good agreement with those of Djurle[18] in Appendix 6 for the low temperature $Cu_{1.8}S$ II phase. Djurle found that this low temperature phase has a range of non-stoichiometry that extended surely from $Cu_{1.80}S$ to $Cu_{1.73}S$, and possibly from $Cu_{1.82}S$ to $Cu_{1.70}S$, the uncertainity being due to possible errors in his measurements. The lines of the residues in the range $Cu_{1.82}S$ - $Cu_{1.70}S$ are in good agreement with those of Djurle for the $Cu_{1.8}S$ II phase over the same range of composition. The residue lines show the same regular displacements in the d-values for the various compositions. This indicates that the residue phase in this range has the same structure as Djurle's $Cu_{1.8}S$ II

phase and shows the same range of non-stoichiometry. The regular displacements in the residue lines extend below $Cu_{1.70}S$ and from fig. 64 it can be seen that the range of non-stoichiometry extends as low as $Cu_{1.50}S$. This extension of the non-stoichiometry is of a non-equilibrium nature and produced artificially by the copper diffusion.

Around the composition $Cu_{1.50}S$, the $Cu_{1.80}S$ II phase transforms to the CuS phase. The regular displacements in the lines of the CuS phase indicate that a range of non-stoichiometry exists in the CuS phase in the range $Cu_{1.50}S$ to CuS.

The strongest lines of Cu_2S III and the $Cu_{1.80}S$ II phase correspond reasonably well. This indicates that the $Cu_{1.8}S$ II phase may be directly derived from the Cu_2S III phase by removal of copper atoms from the latter phase by diffusion. This indication is further supported by the theory of Djurle (Section 1.3) that there is a range of continuity in high temperature phases of Cu_2S I, $Cu_{1.96}S$ I and $Cu_{1.8}S$ I. However the weaker lines of the Cu_2S III and the $Cu_{1.8}S$ II phases either do not correspond well or do not correspond at all. This suggests that there may in fact be a phase change between Cu_2S to $Cu_{1.8}S$ and that there is only marked similarity between the two structures.

There is no residue of composition $Cu_{1.96}S$ and the possibility of this phase being an intermediary between Cu_2S III and $Cu_{1.8}S$ II cannot be dismissed. However, the d-values of the low temperature $Cu_{1.96}S$ III phase, which are given in Appendix 6 and plotted in fig. 64, do not suggest this to be the case. Referring to fig.64 the arguments behind this suggestion are:

i) There is no trace of the medium intensity line of $Cu_{1.96}S$ III at 3.748Å in the residue photographs.

ii) The medium line of $Cu_{1.96}S$ III at 3.381Å does not correspond to any in the residue photographs.

iii) There is no medium intensity line in the lines of $Cu_{1.96}S$ III at around 2.90Å.

iv) The weak intensity lines of $Cu_{1.96}S$ III in the region d = 2.4 - 2.7Å do not correspond with those of the Cu_2S III and residue photographs.

v) The strong intensity line of $Cu_{1.96}S$ III at 2.389Å does not coincide very well with that of Cu_2S III and the residues.

vi) The two lines of $Cu_{1.96}S$ III at 1.963 and 1.957Å are medium and strong. The nearest line of the Cu_2S III and residues is at 1.97Å

and is strong. Assuming that the Cu_2S III and residue line at 1.97Å is the unresolved $Cu_{1.96}S$ III doublet, one would expect the $Cu_{1.96}S$ III line to be of a greater d-value.

vii) The very strong line of $Cu_{1.96}S$ III is at 1.870Å. The strong line of the Cu_2S III and residues is slightly higher at 1.875 - 1.880Å.

viii) The medium and weak lines of $Cu_{1.96}S$ III at 1.690Å and 1.680Å respectively are lower than the values of the two Cu_2S III and residue lines.

ix) There is no $Cu_{1.96}S$ III line at about 1.650Å, whereas both the Cu_2S III and the residue with 7.2% Cu dissolved show a weak line of this d-value.

The d-lines of $Cu_{1.96}S$ II, given in Appendix 6, do not agree with the d-lines of Cu_2S III or of the residues. Thus the $Cu_{1.96}S$ phase is almost certainly not present in the first reaction-half.

A review of the phases and phase changes indicated by the X-ray powder diffraction data is as follows. Either i) the Cu_2S III phase loses copper by atomic diffusion in the lattice and this copper diffusion proceeds until an apparent limit of Cu_2S non-stoichiometry is reached at about $Cu_{1.85}S$, when the Cu_2S phase transforms to the

$Cu_{1.8}S$ phase, or ii) the Cu_2S III is transformed continually via non-stoichiometry to $Cu_{1.8}S$ II by removal of copper atoms by diffusion. Further copper diffusion in the $Cu_{1.8}S$ II phase reduces the $Cu_{1.85}S$ to approximately $Cu_{1.5}S$, as indicated by the range of non-stoichiometry of $Cu_{1.8}S$ II. The $Cu_{1.5}S$ of the $Cu_{1.8}S$ II phase is then transformed to the CuS phase. Copper diffusion continues in this phase until stoichiometric CuS results.

The phase changes must be related to the structural changes that occur.

The Cu_2S III phase has an A-centred orthorhombic cell (Section 1.2.1). Although the exact structure is unknown, the substructure - superstructure relationship that exists between the intermediate hexagonal Cu_2S II phase and the low temperature orthorhombic Cu_2S III phase indicates that the Cu_2S III phase is pseudo-hexagonal, probably characterised by sulphur atoms in a hexagonal close packed array with copper atoms in tetragonal and trigonal sites as found in the Cu_2S II phase.

The structure of the $Cu_{1.80}S$ phase is unsolved (Section 1.3). The strong d-lines suggest a face-centred cubic basic lattice, but the displacement of

most of the other d-lines show that the real lattice cannot be cubic.

The CuS structure has been determined[5]. It is hexagonal and described in Section 1.2.2.

Although the structures of Cu_2S III and $Cu_{1.8}S$ II are unknown, the speed with which the first reaction-half proceeds suggests that i) the Cu_2S III, $Cu_{1.8}S$ II and CuS phases are very similar since they must be easily derived from each other, and ii) they all have a hexagonal or pseudo-hexagonal structure.

3.3.2 The Second Reaction-Half

The regular displacements of the d-lines of CuS in fig. 64 suggest that there is non-stoichiometry in the CuS phase between CuS and approximately $Cu_{0.8}S$. The d-lines indicate that the $Cu_{0.8}S$ residue is transformed into orthorhombic sulphur.

In the residues leached at 60°C the strongest intensity line of sulphur at 3.87Å begins to appear in residues of composition CuS but this may be attributed to the inhomogeneity of the leached particles. The surface of the particles will be at a further stage of transformation than the centre of the particles, despite the small size of the Cu_2S particles selected to

minimise this effect. This is illustrated by the effect of the temperature of the leach on the amount of copper that is dissolved before the strong line of sulphur appears. The higher the temperature, the faster the rate of the second reaction-half, the greater the difference between the surface and the bulk of the particles, and the sooner the sulphur strong line appears. The sulphur strong line appears in the particles leached at 60°C sooner than those leached at 40°C (cf figs. 62 and 63). In the residues leached at 40°C, the strong line of sulphur appears in residues of composition $Cu_{0.8}S$.

The straight transformation from $Cu_{0.8}S$ to sulphur is to be expected since it cannot be expected that the hexagonal sulphur atom arrangement in CuS, Section 1.2.2 is easily transformed to the 8-numbered ring sulphur atom arrangement in orthorhombic sulphur, Section 1.2.3. Thus when the limit of CuS non-stoichiometry is reached, the CuS phase is transformed directly to sulphur.

3.4 ELECTRON PROBE WORK

A JEOL electron probe microanalyser was used to determine the composition of the phases formed in the leaching process, and to investigate any non-stoichiometry in the same phases.

3.4.1 Theory of the Electron Probe Microanalyser

The basic construction of the probe is shown in fig. 65. The beam from the electron gun is directed onto the specimen. Of the electrons reaching the specimen, a proportion are reflected, and the remainder penetrate the specimen. Of those that penetrate the specimen, some are reflected out of structure, taking with them secondary electrons which are torn from the outer shells of atoms in the specimen. This leaves the specimen with a nett positive charge. However, this positive charge is swamped by the negative charge of those electrons penetrating the specimen and which are absorbed. If this negative electric charge is not conducted away, the specimen is heated excessively. Thus the surface is coated with a conducting coating, e.g. carbon, aluminium.

The electrons penetrating the specimen excite the atoms in the specimen, causing emission of the characteristic X-ray radiation of each element present.

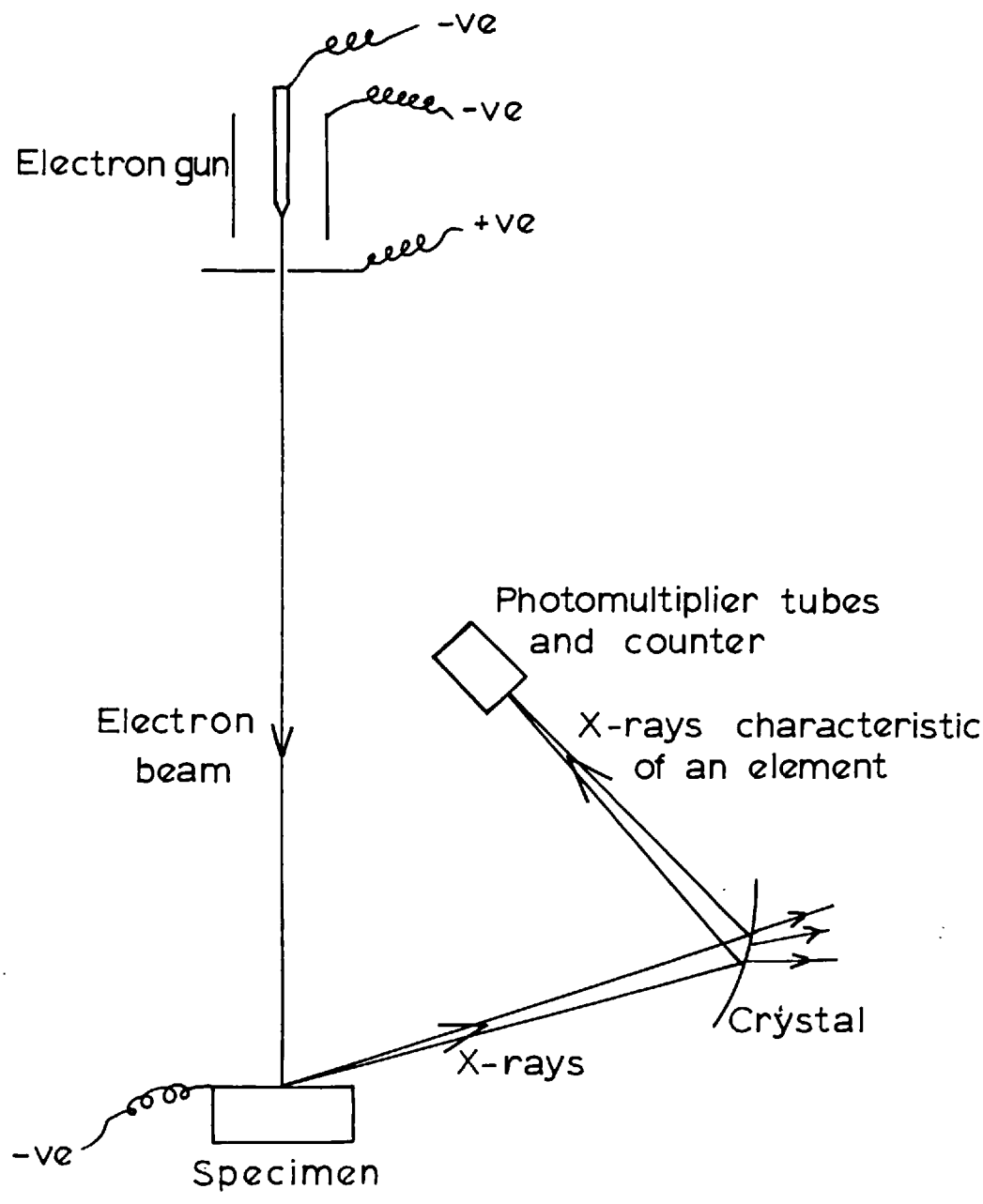


FIG.65 BASIC CONSTRUCTION OF THE ELECTRON PROBE MICROANALSER

The characteristic radiation wavelength of each element is different, the wavelength λ being related to the atomic weight W of the element for a given K or L series by

$$\log \frac{\lambda}{\rho} = k \log W$$

where k is a constant and ρ the density of the element.

For a given beam intensity, the intensity of the X-ray radiation emitted from the surface is dependent on the weight percentage present of the particular element measured. This is the basis of electron probe microanalysis.

Increasing the beam intensity increases the excitation and X-ray emission. The intensity of X-ray emission is proportional to the number of electrons absorbed in the specimen, i.e. the current conducted from the specimen.

The X-rays emitted from the surface at a defined angle strike an optical crystal. When the crystal is at a certain angle to the X-ray beam, the characteristic X-rays of a particular wavelength, i.e. particular element, will be reflected. The intensity of these reflected X-rays is measured by photomultiplier tubes and a pulse counter (fig. 65).

The surface of the crystal is curved to focus the beam into the photomultiplier tubes and pulse counter,

(fig. 65). A slit in front of the analyser reduces the size of the cone of entering X-rays and so increases the resolution of the examined surface. The more intense the X-ray beam emitted, the greater the resolution that can be obtained. It can be as low as 1 or 2 microns.

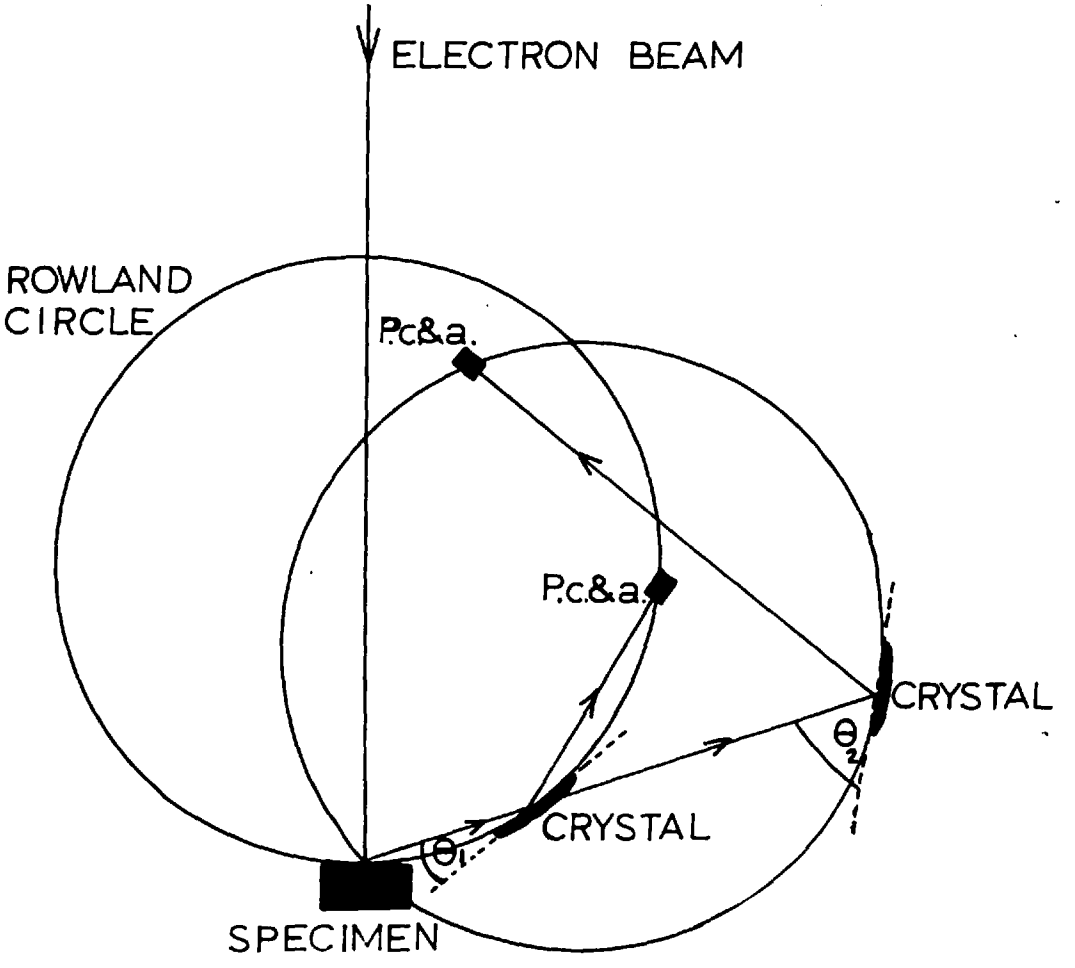
When the crystal is moved to a different angle, it must remain at the same angle to the specimen since the intensity of the emitted X-rays is dependent on the angle of take-off from the surface, i.e.

$$I_\theta = I_o \text{ Cos } \theta$$

This dictates the geometric relationship between the specimen, crystal, and analyser. They must all lie on the circle shown in fig. 66, known as the Rowland circle. As different crystal angles are required to reflect the characteristic wavelength X-rays of different elements, all three move along a trajectory determined by the movement of the Rowland circle.

3.4.2 Experimental Procedure

The most satisfactory method of examining the phases present in the whole range of the leach from Cu_2S to sulphur was to leach uni-directionally a crystal of chalcocite, ensuring that the leached surface was sulphur and the material furthest away from the



Crystal reflecting characteristic x-rays of element A at θ_1
" " " " " " B " θ_2

FIG.66 GEOMETRICS OF THE PROBE

leaching solution remained as chalcocite. It was desirable that the uni-directional leach was even over surface and into the body of the chalcocite crystal. These conditions are present in the leaching of a rotating disc.

A chalcocite disc 1" in diameter and approximately $\frac{1}{2}$" in length was ground from recrystallised massive Cu_2S. The disc was cast in Araldite to protect all but one of the circular faces from attack by the leach solution (fig. 67). A glass shaft was centrally attached to the Araldite. The disc and glass shaft were connected to the motor of the leaching apparatus (Section 2.3) with rubber tubing. The disc was leached for 20 hrs at 80°C, using a shaft speed of 1500 rpm. Photographs of the surface of a leached disc (fig. 68) showed that the leach residue maintained the outline of the original chalcocite, and that the material was extremely porous. The leached disc was sectionalised in the direction of attack, i.e. perpendicular to the surface, and polished on carborundum papers and diamond cloths (fig. 69). The polished surface was coated with a thin carbon film to conduct away the specimen current during the probe analysis.

Calibration curves of counts per minute vs. weight%

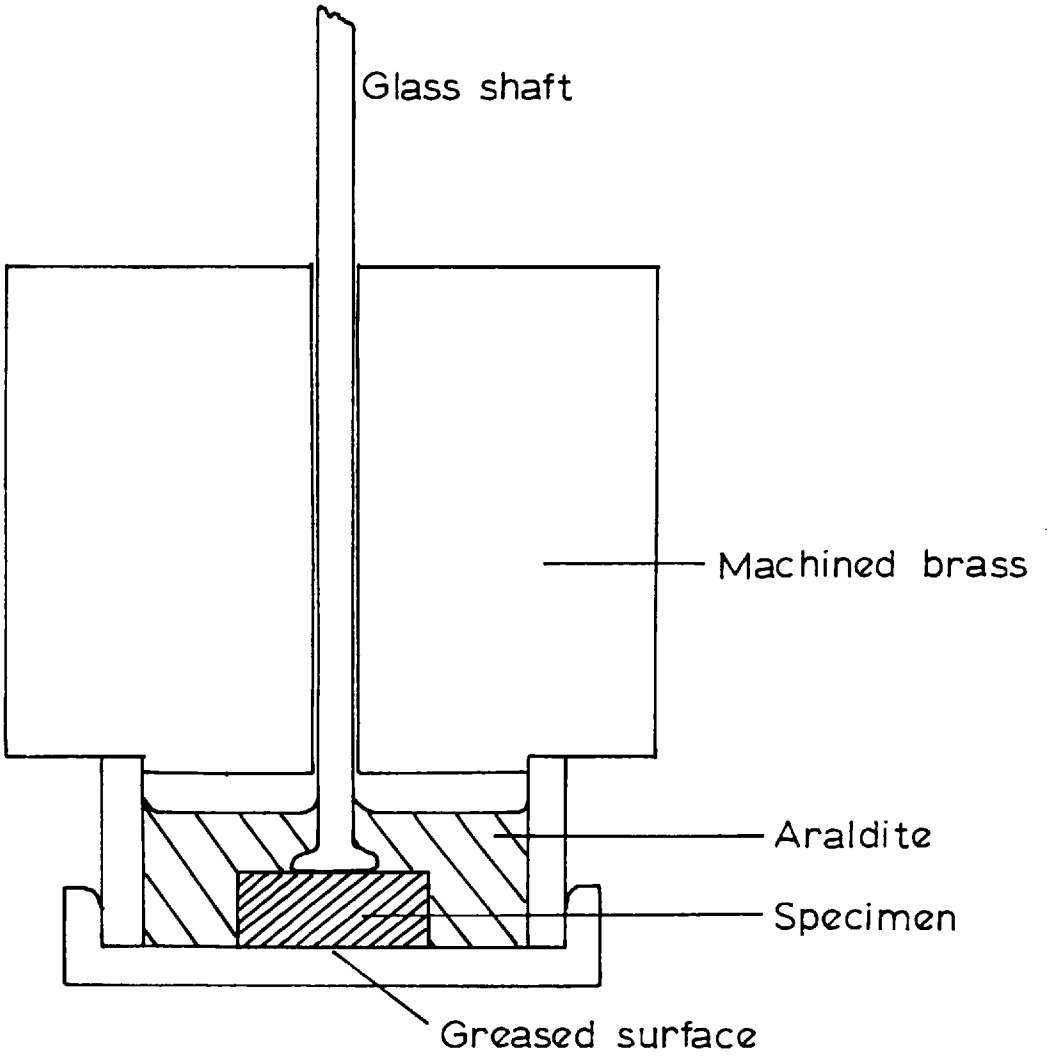


FIG. 67 CHALCOCITE DISC MOUNTING

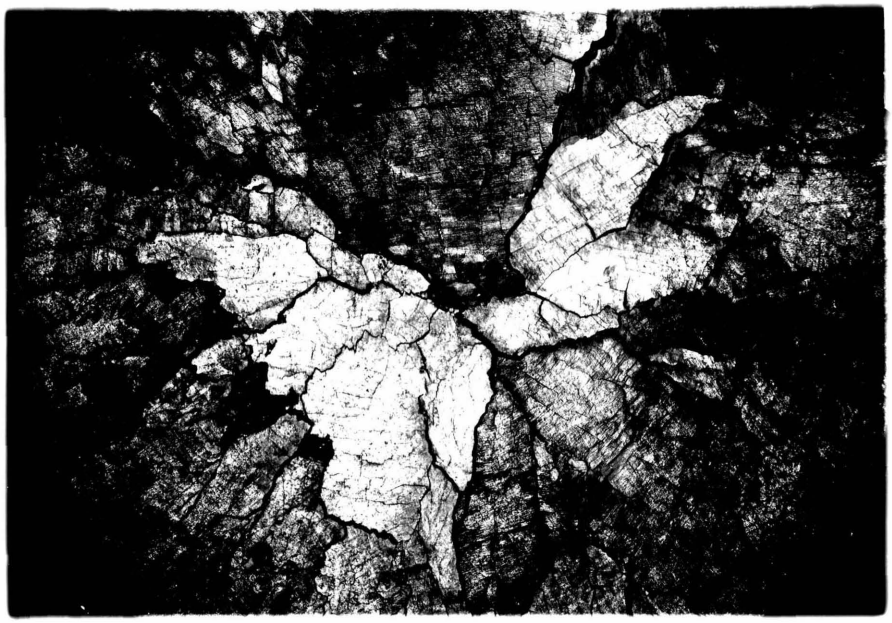


Fig. 68 Surface of the leached disc. (Magnification x4.5)

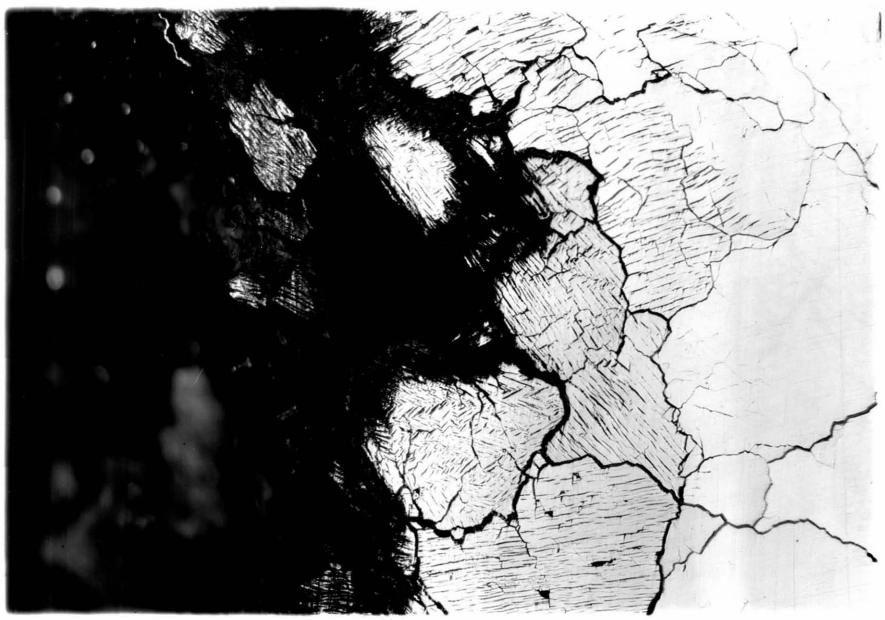


Fig. 69 Microstructure of the sectioned disc. (Magnification x10.7)

copper and sulphur were constructed (Appendix 8). This obviated lengthy calculations due to adsorption and fluorescence corrections. The 100% Cu point was the count from spectrographically pure copper rod and the 79.86% Cu point was the count from the recrystallised Cu_2S. Mean point counts on leach residues in the range Cu_2S - CuS were taken, the copper content being between 79-86 and 66.6 Wt%.

3.4.3 Results and Discussion

Point counts across a large crystal of the recrystallised Cu_2S showed perfect uniformity of composition.

Copper and sulphur scans across the disc leached for 20 hrs at 80°C and 1500 rpm are shown in figs. 70 and 71. The copper and sulphur scans were parallel and perpendicular to the surface. The distance between the two scans was approximately 200μ. The copper scan shows a gradual copper gradient from 80 to approximately 65 wt% Cu, corresponding to the change from Cu_2S to CuS. This indicates that there is non-stoichiometry in the phase or phases existing between Cu_2S and CuS. This is verified by the X-ray powder photographs of the residues in Section 3.3. It also indicates that there is a

FIG.70 ELECTRON PROBE SCAN FOR COPPER ACROSS A SECTION OF A LEACHED DISC OF CHALCOCITE (20hrs, 80°C, 1500rpm.)

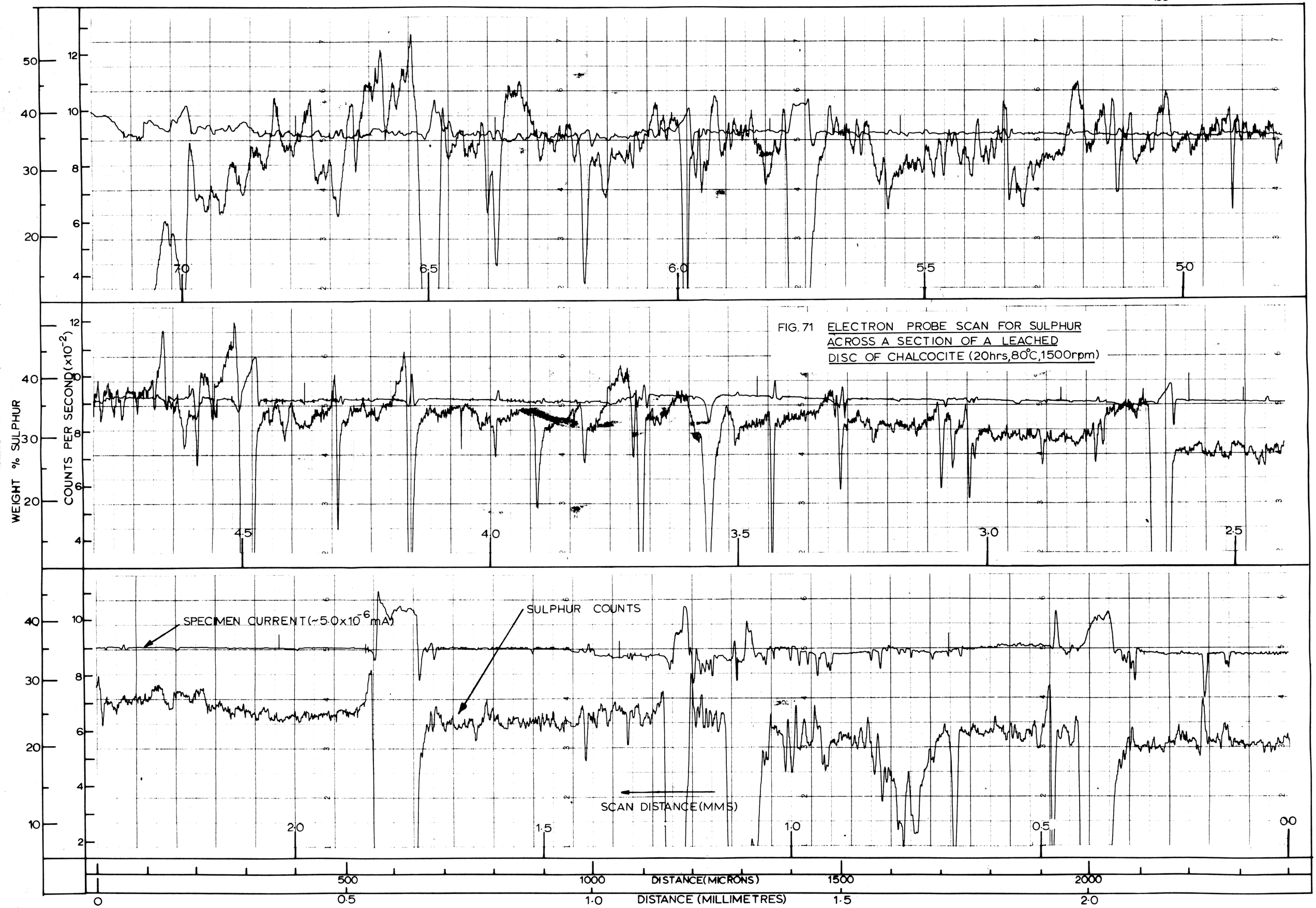


FIG. 71 ELECTRON PROBE SCAN FOR SULPHUR ACROSS A SECTION OF A LEACHED DISC OF CHALCOCITE (20hrs, 80°C, 1500rpm)

smooth transition from one phase to another in the phase changes that are shown to occur in the range Cu_2S to CuS by the X-ray powder photograph studies, i.e. that material of composition Cu_xS of phase 1 transforms to material of composition Cu_xS of phase 2.

There is a possibility that there is a direct transformation from Cu_xS of phase 1 to Cu_yS of phase 2 and that material of the composition Cu_zS, where $x > z > y$, is an intimate mixture of Cu_xS and Cu_yS in the correct proportion on a microcrystalline scale. If the crystal size was appreciably smaller than the electron beam width of 1 micron, i.e. 10^{-4}cm or 1000Å, then the beam would not resolve the difference in copper content of the two phases Cu_xS and Cu_yS and would give the mean copper count from the crystals of the two phases under the beam, corresponding to the composition Cu_zS. For this to occur, the crystal size must be less than 10^{-5}cm. If the crystals were of this size, the X-ray powder photographs would show marked line broadening, which is not the case. Thus Cu_xS of phase 1 transforms to Cu_xS of phase 2.

In fig. 70, the sudden fall and rise in the copper counts and specimen current occurs at grain boundaries and defects. Although the scans show a reasonably

smooth copper gradient between Cu_2S and CuS, it is seen that the copper gradient is not so smooth across grain boundaries. This is due to differences in grain orientation. The copper atoms will diffuse along preferential planes and directions (fig. 70), and thus grains orientated with these planes perpendicular to the surface will be depleted of copper faster than those with these planes parallel to the surface.

The portion of the scan representing removal of copper from CuS (fig. 70) is rough and uneven due to the poor polishing properties of the leach product. The porous material, especially the sulphur, was easily crumbled and fragments were ripped from the surface despite great care taken in the polishing. The scan shown in fig. 70, does however show the general form of the copper gradient.

Removal of copper from CuS gives a steeper copper concentration gradient than that between Cu_2S and CuS. This would be expected from the fact that the first half of the copper is removed faster than the second half.

The copper concentration falls off sharply after a certain amount of copper has been removed from the CuS. This indicates that the CuS structure permits a

degree of non-stoichiometry and that the structure will tolerate the removal of copper until a specific limit is reached when the structure collapses. This limit corresponds to a residue containing 60 wt% Cu, i.e $Cu_{0.8}S$. Further removal of copper is by direct transformation of this limiting structure to crystalline orthorhombic sulphur and the copper going into solution.

This is in agreement with the X-ray powder photographs of residues over the range CuS - S. The photographs of residues leached at 40°C begin to show the strong line of sulphur when approximately 60% of the copper is removed from the Cu_2S. This represents a residue with 60 wt% Cu. Since the particles cannot be perfectly homogenous in the second reaction-half, especially if the Cu is removed quickly, the particles leached at higher temperatures will give X-ray photographs showing the sulphur strong lines when less than 60% of the copper is removed from Cu_2S. This is because of the significant increase in rate of the second reaction-half with the temperature causing the surface of a particle to be transformed to sulphur ahead of the bulk of the particle.

It is possible that the non-stoichiometry extends below $Cu_{0.8}S$ but that the material Cu_xS, where $x < 0.8$,

vapourised when hit by the beam. $Cu_{0.8}S$ corresponds to the lowest count rate of stable material; adjacent material vapourised as soon as it was hit by the beam. Such vapourisation is characteristic of light elements such as sulphur. It is very probable that the adjacent material was sulphur since the microstructure (x1200) was uniform from the adjacent material to the surface, known to be sulphur. Microscopically, there is a gradual change from steel grey chalcocite to the dark blue colour of covellite. The change from $Cu_{0.8}S$ was a distinct change from blue to the yellow-green of sulphur.

A scan across the breadth of lamellae of the porous structure is shown in fig. 72. The copper content is seen to be at a maximum in the centre of a lamella, decreasing towards the edge. A scan along the length of a lamella (fig. 73) showed the copper content to decrease as the scan proceeded towards the surface of the leached disc. This indicates that copper diffuses from (a) the solid copper sulphide into the pores of the structure, from whence it diffuses through the pores into the bulk of the leach solution, and (b) along the length of the lamellae of the porous sulphide structure towards the disc surface.

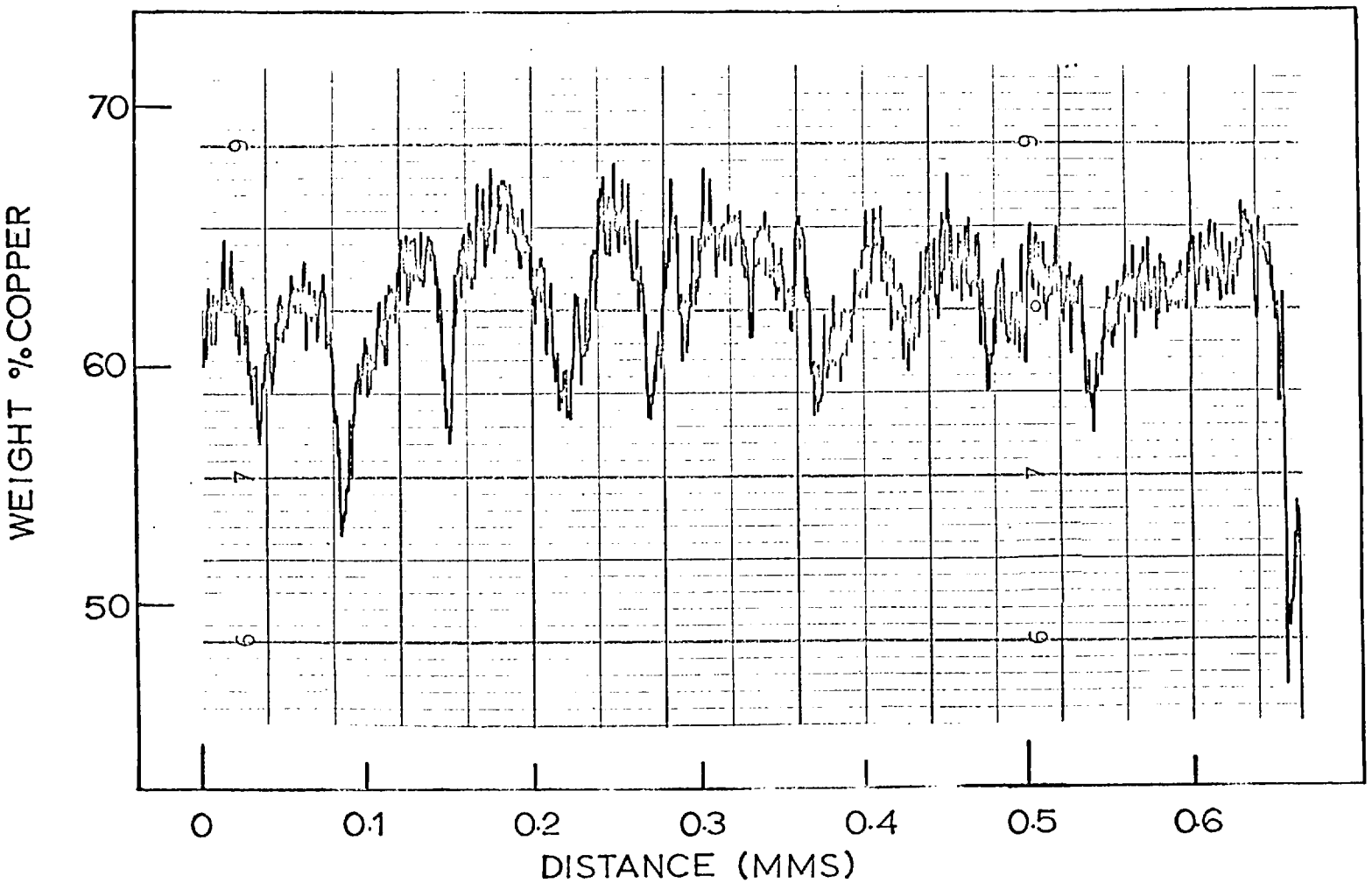


FIG.72 COPPER SCAN ACROSS THE BREADTH OF THE LAMELLAE OF THE POROUS RESIDUE

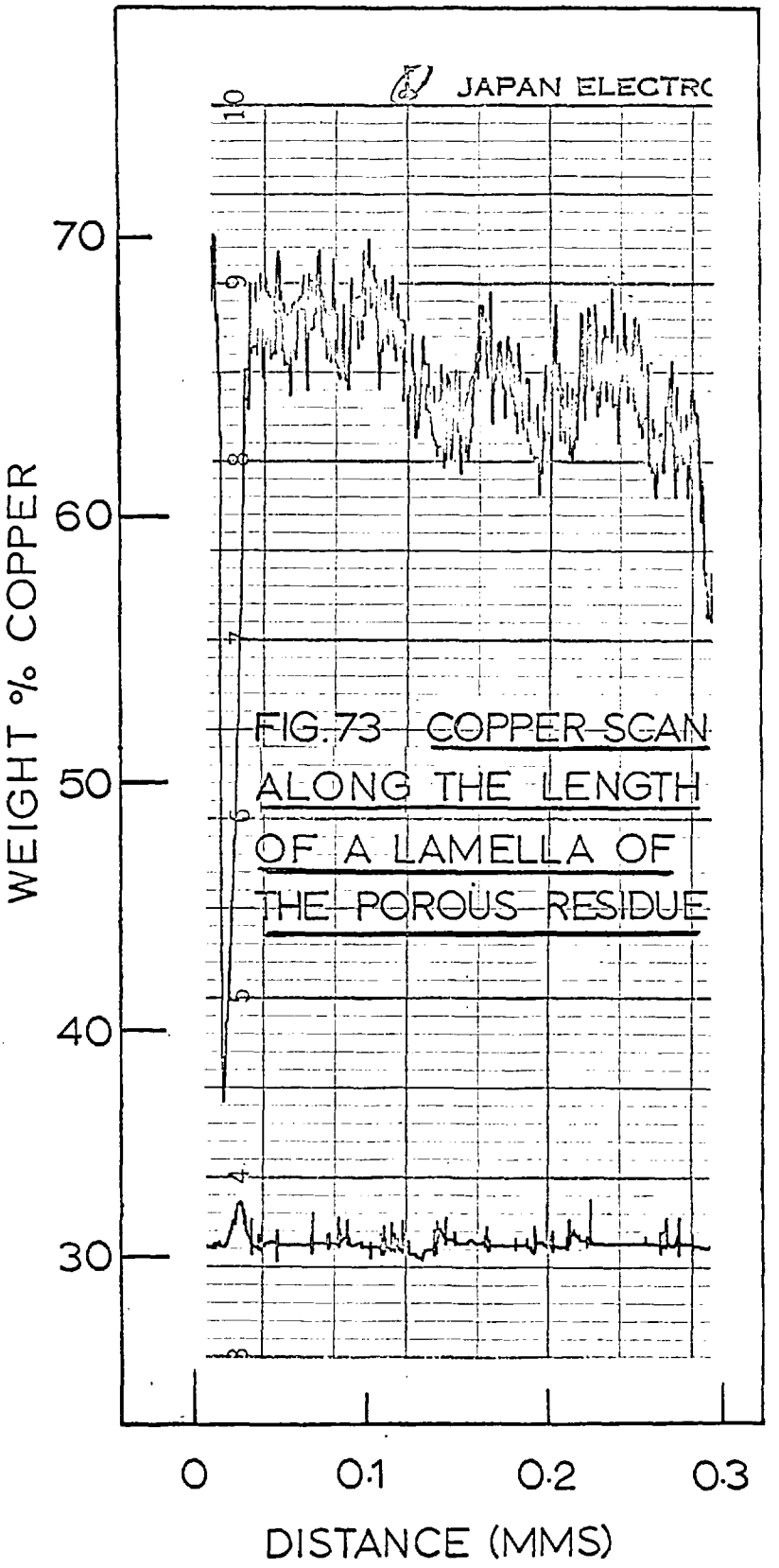


FIG. 73 COPPER SCAN ALONG THE LENGTH OF A LAMELLA OF THE POROUS RESIDUE

Therewere no detectable amounts of iron in the structure although in some pores and grain boundaries, a fraction of a percent was detected, originating from $FeCl_3$ solution residual in the porous structure.

SECTION 4

CONCLUSIONS

4.1. Summary of Results

The leaching of chalcocite proceeds in two distinct halves, represented by the reactions:

$$Cu_2S + 2Fe^{3+} = CuS + Cu^{2+} + 2Fe^{2+}$$

and $$CuS + 2Fe^{3+} = Cu^{2+} + S + 2Fe^{2+}$$

In the first reaction-half, chalcocite, Cu_2S, is rapidly transformed to covellite, CuS, via an intermediate phase digenite, $Cu_{1.8}S$. The copper is removed from the non-stoichiometric copper sulphide structures Cu_2S, $Cu_{1.8}S$ and CuS by diffusion of copper in the copper sulphide lattices. The mean activation energy determined for this diffusion is 0.82 ± 0.09 kcals. The artificially produced covellite is porous and maintains the original outline of the chalcocite.

X-ray powder photographs of the leach residues covering the first reaction-half, and electron-probe microanalyser scans over the section of a leached chalcocite disc, show that the Cu_2S exhibits non-stoichiometry, losing copper by diffusion in the Cu_2S lattice. The Cu_2S structure either transforms continually to the $Cu_{1.8}S$ structure or there is an easy change from the Cu_2S structure to the $Cu_{1.8}S$ structure

when the limit of Cu_2S non-stoichiometry is reached at a residue composition of $Cu_{1.85}S$. The non-stoichiometric $Cu_{1.8}S$ structure loses copper by diffusion until the residue composition reaches $Cu_{1.5}S$. An easy phase change then occurs and the $Cu_{1.5}S$ of the $Cu_{1.8}S$ phase structure is transformed to $Cu_{1.5}S$ of the CuS phase structure. The $Cu_{1.5}S$ of the CuS phases loses copper by diffusion until stoichiometric CuS is produced.

In the second reaction-half, covellite is transformed to $Cu_{0.8}S$, a non-stoichiometric copper sulphide of the CuS structure, by diffusion of copper and the removel of electrons from the sulphide ions in the CuS lattice. The apparent activation energy for the removal of electrons from the sulphide ions is approximately 24 kcals.

The $Cu_{0.8}S$ is transformed directly to elemental sulphur by further chemical reaction, the activation energy being approximately 25 kcals. This chemical attack occurs in the pores created during the first half of the reaction and during the transformation of CuS to $Cu_{0.8}S$.

The rate of the second reaction-half decreases as the amount of copper dissolved increases. This is due to the presence of sulphur in the pores which results

in a reduction in the area of $Cu_{0.8}S$ available for attack by the ferric solution.

Microscopic examination of leached chalcocite cubes illustrated the porosity of the residue phases, the existence of covellite by its anisotropic properties, and the porous attack mechanism of the transformation of $Cu_{0.8}S$ to sulphur.

4.2. Comparison of the Present Investigation with Previous Work

Sullivan[1] found that the rate of both halves of the leach increased with an increase in temperature. The rate of the second reaction-half was far more temperature sensitive than the first reaction-half. This is in agreement with the present work.

Sullivan found that the rate of the first half was increased by a decrease in particle size and that the rate of the second half was virtually independent of particle size. This is in agreement with the present work.

To explain the non-dependence of the rate of the second reaction-half on particle size, Sullivan believed that either chalcocite contained in its normal condition sufficient capilliary pores to permit ingress of solution, or that internal fractures are opened

during the crushing process. He thought the latter unlikely since the larger pieces received little crushing treatment, and presumed that chalcocite was naturally porous. This is quite untrue and it has been shown in this present work that pores are created in the chalcocite during its transformation to CuS. This phenomenum explains the dependence of the rate of the first reaction-half on particle size and the non-dependence of the second half.

Sullivan found that the concentration of ferric ion had no effect on the first reaction-half but that the rate of the second reaction-half was increased by increasing ferric ion concentration. Sullivan found no increase in the second reaction-half with a ferric ion concentration greater than 0.6 g.ion. Fe^{3+} per litre. The present work showed an increase in the rate using ferric concentrations up to 1.0 g.ion. Fe^{3+} per litre. It might be expected that in extremely concentrated viscous solutions, the rate would decrease due to increased difficulty of ferric ion diffusion into the pores of the residue structure.

Sullivan found that in dilute ferric sulphate solutions, high concentrations of ferrous ion retarded the rate of leaching. In these dilute solutions, the

diffusion of ferric oxidant in the aqueous phase is probably the rate-controlling step and by increasing the viscosity of the solution, i.e. by adding large quantities of ferrous sulphate, the rate of diffusion of the ferric ions in the aqueous phase will be retarded.

Sullivan believed that the artificially produced CuS was not the same as natural covellite since
a) the rate of dissolution of artificial covellite is faster than that of natural covellite and
b) the colour of natural covellite is a darker blue than the artificially produced material. The colour of the artificially produced covellite in the present work was a deep indigo-blue, the colour of covellite as classified by mineralogists[89]. The artificially produced covellite of this present work displayed the full anisotropic properties of natural covellite, and was shown by X-ray powder photograph studies to be synonymous with natural covellite. Sullivan's objection regarding the difference in the rate of leaching of natural and artificial covellite is explained by the porous nature of the artificial covellite, permitting ingress of solution into the bulk of the particle, compared with the compact natural form.

Sullivan found that the rate of dissolution of

natural covellite was increased by a decrease in particle size. This would be expected since there are no pores in natural covellite for ingress of solution and the reaction is at the mineral surface.

It is difficult to make a direct comparison of the present work with that of Warren[2], the experimental conditions being different. Warren used high temperatures (100-200°C) and oxygen gas (10-100 psi.) as the oxidant.

Warren found that chalcocite dissolved in two distinct stages. His rate of leaching for the first reaction-half was extremely slow compared with the present work. The first reaction-half was complete in 100 minutes at 100°C, using 40 psi O_2 and 30 g H_2SO_4/l, (fig. 6). This suggests that there was poor oxidant transfer to the particle surface, and that the rate-controlling step was either the diffusion of oxygen molecules in the solution or the rate of adsorbance of oxygen gas into the liquid.

The low value of the activation energy for the second stage of leaching, 1.8 kcals/mole, is as Warren suggests probably due to molten elemental sulphur coating the surface and making further reaction extremely difficult.

Increases in the oxygen pressure increased the rate of the first reaction-half, until at a critical point, 80 psi, the leach rate was independent of oxygen pressure. At this point, it is likely that the diffusion of copper atoms in the sulphide lattice became the rate-controlling step. The rate of the second reaction-half was increased by increases in the oxygen pressure over the whole range of pressure studied. Variation of the oxygen pressure produced exactly the same behaviour as variation of the ferric ion concentration in the present work.

It is difficult to understand why the activation energy that Warren obtained for the leaching of covellite was so different from the activation energy he obtained for the second half of the leach since the mechanism for copper removal should be basically the same.

SECTION 5

APPENDIXES

ACKNOWLEDGMENTS

REFERENCES

Appendix 1

Kinetic Results

The results given for each set of conditions are the mean of two leaching runs. The leach runs were extremely reproducible. The maximum error in the %Cu dissolved was an estimated $\pm$ 1%.

1. Temperature - The experimental conditions for the temperature variation were: Fe^{3+}/Fe^{2+} = 10, Fe^{3+} = 0.5g.ion.l^{-1}; 20ml. cHCl.l^{-1}; 2.50g.sample of -50 + 100 mesh Cu_2S; 900 rpm.

a) 22.5°C

The following is a specimen calculation.

The mean optical density gives the concentration of copper in the filtrate of the 100mls flask by dividing by the conversion factor of the Beers Law plot (1 gCu.l^{-1} = 3.42952'd' for 4cm cells).

Copper concentration in the filtrate = C_1

$$= \frac{\text{d mean}}{3.42952} \quad \text{gCu.l}^{-1}$$

The concentration of copper in the pipette is equal to the concentration of copper in the leach bath. Thus the concentration in the leach bath C_3, is given by :-

$$C_3 = C_1 \times \frac{\text{filtrate volume (ml)}}{\text{sampling pipette volume (ml)}}$$

$$= \frac{C_2}{\text{pipette}} \quad \text{Where } C_2 = C_1 \times \text{filtrate volume}$$

The weight of copper in the leach bath at the time of analysis, g_1, is given by $C_3 \times V_B$ where V_B is the volume of the leach bath at the time of analysis.

The weight of copper leached from the sulphide g_2, is g_1 plus copper removed in the analysis of previous aliquots. i.e.

$$g_{2(n)} = g_{1(n)} + \frac{5}{1000} \times g_{1(n-1)} + \frac{5}{1000} \times g_{1(n-2)} \text{ etc.}$$

where $g_{1(n-1)}$, $g_{1(n-2)}$, etc. is the concentration of copper present in the leach bath at the times of previous analyses. The subscript n denotes the nth aliquot to be analysed.

A final correction must be made for the copper added to the bath as impurities from the ferrous and ferric chlorides. The ferric chloride contained 0.0025 wt% Cu and the ferrous chloride 0.0005 wt% Cu as impurities. Thus the nett weight of copper leached from the sulphide, g_3, is g_2 less the weight of copper impurities W_i.

All three weights g_1, g_2 and g_3 are expressed in grams. The percentage of copper dissolved is the ratio of g_3 to the weight of copper in the Cu_2S sample.

The 22.5°C leach was performed with acidified 0.5 ions Fe^{3+}/0.05 Fe^{2+} chloride solution. At 22.5°C, the sampling pipette delivered 4.994 ml.

The filtrate volume = 100mls - effective precipitate volume.

The effective density of stoichiometrically precipitated $Fe(OH)_3$ is 0.4 $g.ml^{-1}$ (Section 2.4.5). The molecular weight of $Fe(OH)_3$ = 107

$\therefore$ Effective volume of the precipitate

$$= \frac{\text{no. of grams of } Fe(OH)_3}{0.4} \text{ mls.}$$

$$= \left[\frac{\text{pipette}}{1000} \times 0.55 \times 107\right] \Big/ 0.4$$

$$= \frac{4.994 \times 0.55 \times 107}{1000 \times 0.4}$$

$$= 0.73 \text{ mls.}$$

$\therefore$ Filtrate volume = 99.27 mls.

The correction for impurites:

1 mole of Analar $FeCl_3.6H_2O$ = 270.3 g.

1 mole of GPR $FeCl_2.4H_2O$ = 198.8 g.

$\therefore$ Impurities = 135.15 x 0.000025 + 9.94 x 0.000005 gCu

$\therefore$ W_i = <u>0.0034 g Cu</u>

sample time (mins)	5	30	60	120	240
d_1	0.152	0.171	0.173	0.175	0.180
d_2	0.150	0.170	0.172	0.175	0.179
d_{mean}	0.151	0.1705	0.1725	0.175	0.1795
$C_1 = \frac{d_{mean}}{3.42952}$	0.04403	0.4972	0.05030	0.05103	0.05234
$C_2 = C_1 \times V_{filtrate}$	4.371	4.936	4.993	5.066	5.196
$g_1 = C_3 \times V_B$	0.8752	0.9835	0.9898	0.9992	1.0196
$g_{2(n)} = g_{1(n)} + \frac{5}{1000} g_{1(n-1)}$	0.8752	0.9879	0.9991	1.0134	1.0388
$g_3 = g_2 - W_i$	0.8718	0.9845	0.9957	1.0100	1.0354
$\%Cu = \frac{g_3}{1.9963}$	43.67	49.32	49.88	50.59	51.87

b) 30°C

sample time	d mean	%Cu dissolved
5 mins	0.155	44.9
30	0.1705	49.4
60	0.1745	50.6
120	0.180	52.2
240	0.188	54.4

c) 40°C

sample time	d mean	%Cu dissolved
5 mins	0.161	46.9
30	0.177	51.5
60	0.186	54.1
120	0.197	57.3
240	0.215	62.4

d) 50°C

sample time	d mean	%Cu dissolved
5 mins	0.167	48.8
30	0.195	57.0
60	0.2145	62.8
120	0.238	69.5
240	0.2625	76.5

e) 60°C

sample time	d mean	%Cu dissolved
5 mins	0.177	52.0
30	0.229	67.3
60	0.2515	73.9
120	0.2815	82.6
240	0.306	89.7

f) 70°C

sample time	d mean	%Cu dissolved
5 mins	0.1945	57.5
15	0.240	70.9
30	0.2755	81.3
60	0.308	90.8
90	0.326	96.1
120	0.3305	98.3
240	0.336	98.9

g) 80°C

sample time	d mean	%Cu dissolved
5 mins	0.217	64.3
10	0.258	76.5
20	0.3005	89.0
30	0.327	96.7
60	0.336	99.3
120	0.337	99.6
240	0.3385	100.1

2. Particle Size

The experimental conditions for the variation of particle size were: Fe^{3+}/Fe^{2+} = 10, Fe^{3+} = 0.5 g.ion. l^{-1}; 20ml.cHCl.l^{-1} ; 2.50g sample of Cu_2S ; 40°C ; 900 rpm.

a) -3/16" + 7#

sample time	d mean	%Cu dissolved
5 mins	0.0355	10.2
30	0.091	26.3
60	0.1235	35.7
120	0.161	46.5
240	0.2055	59.2

b) -10 + 14#

sample time	d mean	%Cu dissolved
5 mins	0.069	20.0
30	0.1395	40.5
60	0.1715	49.7
120	0.199	57.6
240	0.2235	64.6

c) -25 + 36#

sample time	d mean	%Cu dissolved
5 mins	0.1285	37.4
30	0.173	50.3
60	0.1825	53.0
120	0.196	56.9
240	0.2205	63.9

d) -50 + 100 XX As for Table 1(c)

e) -150 + 200 XX

sample time	d mean	%Cu dissolved
5 mins	0.1645	47.9
30	0.178	51.8
60	0.1875	54.5
120	0.199	57.9
240	0.2135	62.0

3. Stirring Speed

Experimental conditions for the variation of stirring speed were: Fe^{3+}/Fe^{2+} = 10, Fe^{3+} = 0.5 g.ion.l^{-1} ; 20ml. cHCl.l^{-1} ; 2.5g sample of -50 + 100 mesh Cu_2S ; 40°C.

a) 250 rpm

sample time	d mean	%Cu dissolved
5 mins	0.1015	29.5
30	0.152	44.2
60	0.1705	49.5
120	0.1845	53.5
240	0.2065	59.8

b) 540 rpm

sample time	d mean	%Cu dissolved
5 mins	0.161	46.9
30	0.1765	51.3
60	0.1845	53.7
120	0.1965	57.1
240	0.214	62.1

c) 900 rpm as for Table 1(c)

d) 1500 rpm

sample time	d mean	%Cu dissolved
5 mins	0.1615	47.0
30	0.1765	51.3
60	0.184	53.5
120	0.1965	57.1
240	0.2145	62.3

4. Ferric Ion concentration

The experimental conditions for the variation of ferric ion concentration were: Fe^{2+} = 0 ; 20 ml cHCl.l^{-1} ; 2.5 g sample of -50 + 100 mesh Cu_2S ; 40°C ; 900 rpm.

a) 0.25 g.ion Fe^{3+}. l^{-1}

sample time	d mean	%Cu dissolved
5 mins	0.150	43.9
30	0.1705	49.9
60	0.178	52.1
120	0.189	55.2
240	0.203	59.3

b) 0.5 g.ion. Fe^{3+}. l^{-1}

sample time	d mean	%Cu dissolved
5 mins	0.1595	46.4
30	0.1765	51.4
60	0.185	53.8
120	0.1965	57.2
240	0.215	62.5

c) 0.75 g.ion $Fe^{3+}.l^{-1}$

sample time	d mean	%Cu dissolved
5 mins	0.164	47.5
30	0.185	52.3
60	0.189	54.7
120	0.2035	58.9
240	0.2235	64.6

d) 1.0 g.ion $Fe^{2+}.l^{-1}$

sample time	d mean	%Cu dissolved
5 mins	0.167	48.1
30	0.183	52.8
60	0.1945	56.1
120	0.210	60.5
240	0.235	67.6

5. Ferrous ion concentration

The experimental conditions for the variable of ferrous ion concentrations were: Fe^{3+} = 0, 20 ml $cHCl.l^{-1}$; 25g sample of -50 + 100 mesh Cu_2S ; 40°C ; 900 rpm.

a) 1.0 g.ion $Fe^{2+}.l^{-1}$

sample time	d mean	%Cu dissolved
5 mins	0.035	10.1
30	0.072	20.7
60	0.078	22.4
120	0.081	23.2
240	0.085	24.4

6. Ferrous ion in the presence of Ferric Ion

The experimental conditions for the variation of ferrous ion strength in the presence of ferric ion are:

Fe^{3+} = 0.5 g.ion $Fe^{3+}.;^{-1}$; 20 ml. $cHCl^{-1}$; 2.5g sample of -50 mesh Cu_2S ; 40°C ; 900 rpm.

a) 0.05 g.ion $Fe^{2+}.l^{-1}$ as for Table 1(c)

b) 0.25 g.ion $Fe^{2+}.l^{-1}$

sample time	d mean	%Cu dissolved
5 mins	0.163	47.3
30	0.182	52.8
60	0.1905	55.3
120	0.2045	59.3
240	0.2275	65.8

c) 0.5 g.ion $Fe^{2+}.l^{-1}$

sample time	d mean	%Cu dissolved
5 mins	0.1665	48.1
30	0.1855	53.6
60	0.196	56.6
120	0.211	60.9
240	0.2375	68.5

d) 1.0 g.ion $Fe^{2+}.l^{-1}$

sample time	d mean	%Cu dissolved
5 mins	0.1695	48.7
30	0.193	55.4
60	0.204	58.5
120	0.2215	63.5
240	0.248	71.0

7. Acid strength

The experimental conditions for the variation of acid strength were: Fe^{3+}/Fe^{2+} = 10, Fe^{3+} = 0.5 g.ion.l^{-1}; 2.5g sample of -50 mesh Cu_2S ; 40°C ; 900 rpm.

a) 5 ml. cHCl,l^{-1}

sample time	d mean	%Cu dissolved
5 mins	0.1595	46.4
30	0.1765	51.3
60	0.185	53.8
120	0.1955	56.8
240	0.2135	62.0

b) 20 ml. cHCl.l^{-1} as in Table 1(c)

c) 40 ml. cHCl.l^{-1}

sample time	d mean	%Cu dissolved
5 min	0.161	46.9
30	0.1775	51.6
60	0.1855	54.0
120	0.1965	57.1
240	0.215	62.4

d) 80 ml. cHCl.l^{-1}

sample time	d mean	%Cu dissolved
5 min	0.161	46.9
30	0.1765	51.3
60	0.186	54.0
120	0.197	57.3
240	0.2165	62.8

8. Sample Weight

Experimental conditions for the variable of sample weight were: Fe^{3+}/Fe^{2+} = 10, Fe^{3+} = 0.5 g.ion.l^{-1}; 20 ml cHCl.l^{-1} ; -50 + 100 mesh Cu_2S ; 40°C ; 900 rpm.

a) 5.0 g Cu_2S sample

sample time	d mean	%Cu dissolved
5 mins	0.306	43.8
30	0.345	50.3
60	0.365	53.2
120	0.387	56.3
240	0.425	61.8

Appendix 2

a) Determination of the Activation Energy of the First Reaction-half

Experimental conditions $Fe^{3+}/Fe^{2+} = 10$, $Fe^{3+} = 0.5$ g.ion. l^{-1}; 20 ml. cHCl. l^{-1}; -50 + 100 mesh Cu_2S; 900 rpm.

The copper content of the leach liquor was determined after two minutes at 20°C, 40°C and 60°C.

Temperature	20°C	40°C	60°C
Temp °A	293	313	333
$I/T^{\circ}A \times 10^3$	3.413	3.195	3.003
d	0.130	0.143	0.152
%Cu dissolved	37.7	41.8	44.8
log %Cu dissolved	1.576	1.621	1.651

The plot of log [%Cu diss.] vs. $I/T^{\circ}A$, (fig.74), gives a slope of $-\frac{E_A}{2.303R}$

$$\text{Mean slope, } -\frac{E_A}{2.30} = -1.8 \times 10^2$$

$$\therefore \quad E_A = \underline{821 \pm 90 \text{ cals/mole}/^{\circ}C}$$

b) Determination of the Activation Energy of the Second Reaction-half

The values of the rate of reaction, expressed in %Cu dissolved per hour, are taken from figs. 30, 31 and 32, (Appendixes 1(a) and 5)

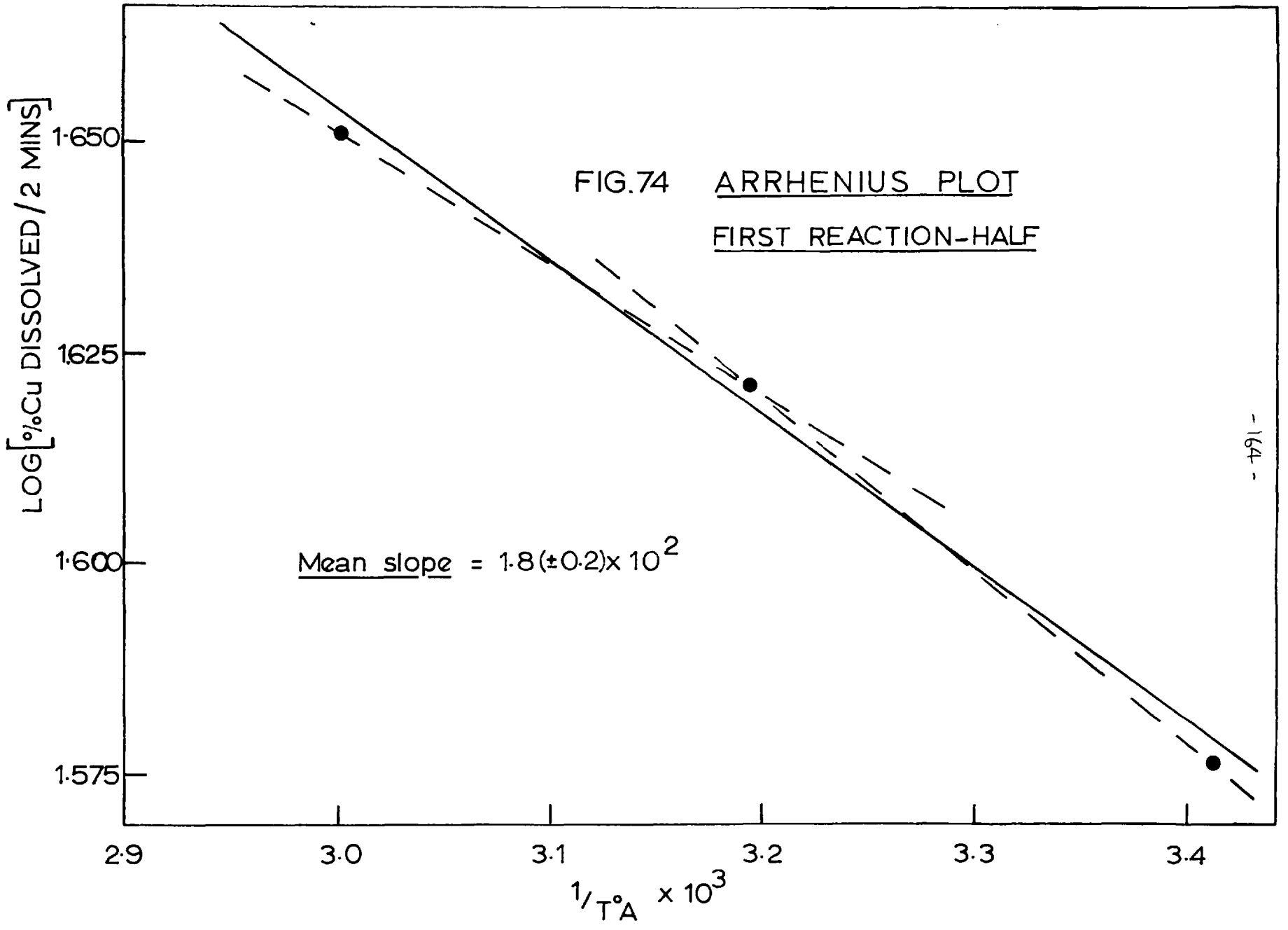


FIG.74 ARRHENIUS PLOT

FIRST REACTION-HALF

Temp ^{o}C	22.5	30	40	50	60	70	80
Temp ^{o}A	295.5	303	313	323	333	343	353
$I/T^{o}A \times 10^{3}$	3.396	3.300	3.195	3.096	3.003	2.916	2.833
Rate(50-60%Cu diss.)	0.67	1.27	3.82	15.4	50.0		
Log Rate(50-60%Cu diss)	-0.174	0.104	0.512	1.188	1.699		
Rate(60-70%Cu diss.)			2.22	7.54	23.6	80.0	180
Log Rate(60-70%Cu diss)			0.346	0.877	1.373	1.903	2.255
Rate(70-80%Cu diss.)			0.853		10.0	44.4	120
Log Rate(70-80%Cu diss)			-0.069		1.0	1.647	2.079
Rate(80-90%Cu diss.)			0.305		4.17	21.1	66.7
Log Rate(80-90%Cu diss)			0.515		0.620	1.324	1.824

The plot of log rate vs $^{1}/T \times 10^{3}$ is shown in fig. 75. E_A is equal to 2.303 x 1.98 x slope.

$$E_{A(50\text{-}60\%Cu\ dissolved)} = \underline{24.2\ kcals}$$

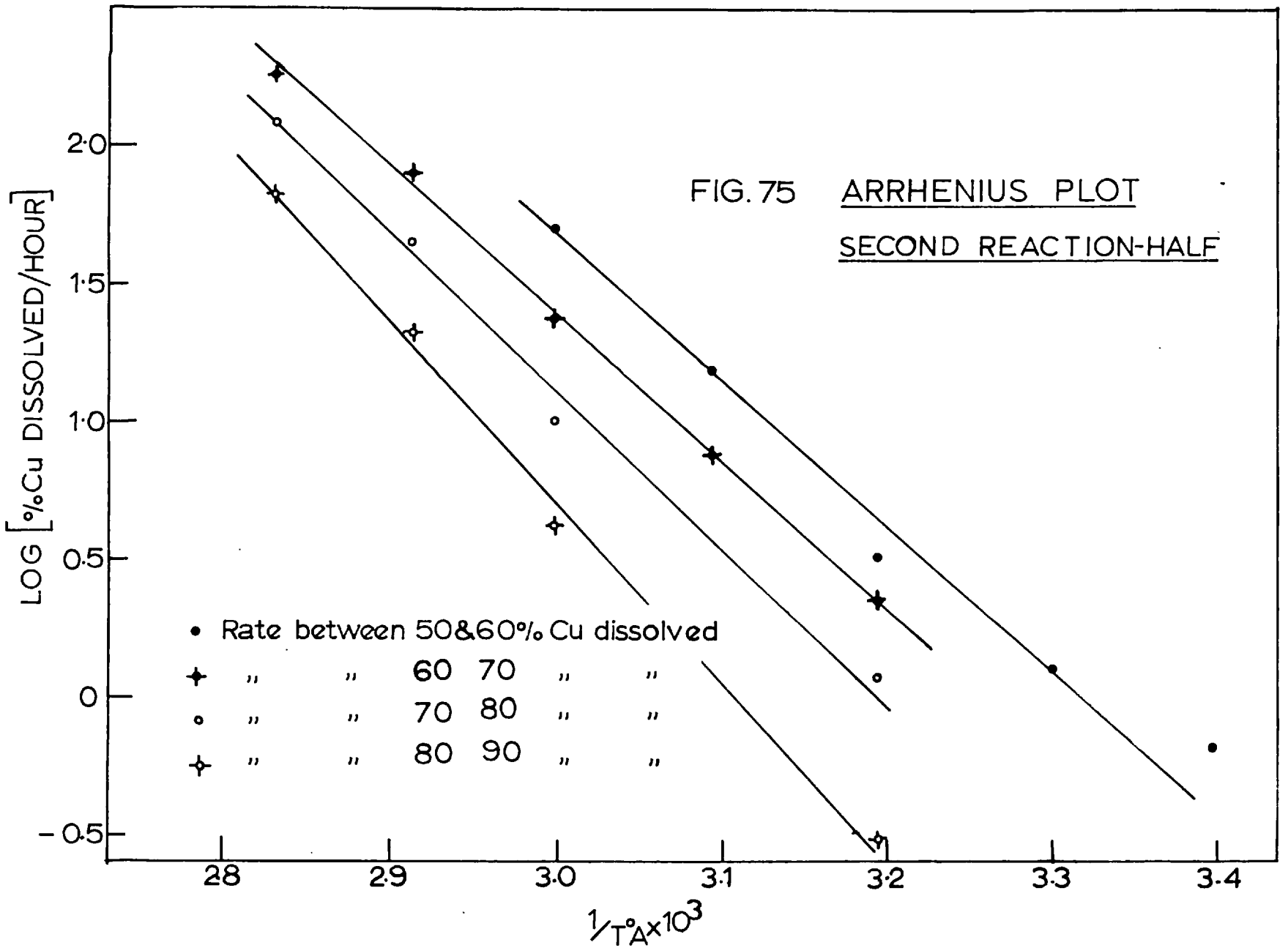
$$E_{A(60\text{-}70\%Cu\ dissolved)} = \underline{24.6\ kcals}$$

$$E_{A(70\text{-}80\%Cu\ dissolved)} = \underline{26.9\ kcals}$$

$$E_{A(80\text{-}90\%Cu\ dissolved)} = \underline{29.2\ kcals}$$

Mean activation energy for the second reaction-half

$$E_A = \underline{26.2\ kcals}$$


FIG. 75 ARRHENIUS PLOT
SECOND REACTION-HALF
LOG [%Cu DISSOLVED/HOUR]
2·0
1·5
1·0
0·5
0
-0·5
• Rate between 50&60% Cu dissolved
" " 60 70 " "
" " 70 80 " "
" " 80 90 " "
2·8
2·9
3·0
3·1
3·2
3·3
3·4
1/T°A x 10³

Appendix 3

Flotation of Screened Chalcocite and Leach Residues in Water and $FeCl_3$aq.

The results are the percentage of a given size fraction that are floated over a Hallimond tube (fig.76) containing water or $FeCl_3$aq, by 100 bursts of bubbles from the rubber bulb. The $FeCl_3$aq contained 0.5 g.ion Fe^{3+}, 0.05 g.ion Fe^{2+}, and 20 mls cHCl/litre. The 'residues' were the residues from the investigation of leaching rate dependence on particle size. (Appendix 1(b))

	H_2O			$FeCl_3$aq		
	Cu_2S		Residue	Cu_2S		Residue
-3/16" + 7##	-		-	-		-
-10 + 14 ##	-		-	-		-
-25 + 36 ##	7.1	9.7 6.4	2.4 4.0 2.1	-		2.16 2.20 1.51
-50 + 100 ##	14.1	12.4 9.8	53.9 48.8 50.7	1.3	2.6 1.7	46.5 43.3 40.0
-150 + 200##	20.3	25.6 21.8	54.4 53.0 50.5	4.6	5.3 5.8	48.0 50.9 47.2

Mesh sizes (British Standard Sieves)

Mesh	Size of Apperture (inches)
7	0.0949
10	0.0660
14	0.0474
25	0.0236
36	0.0166
50	0.0110
100	0.0060
150	0.0041
200	0.0030

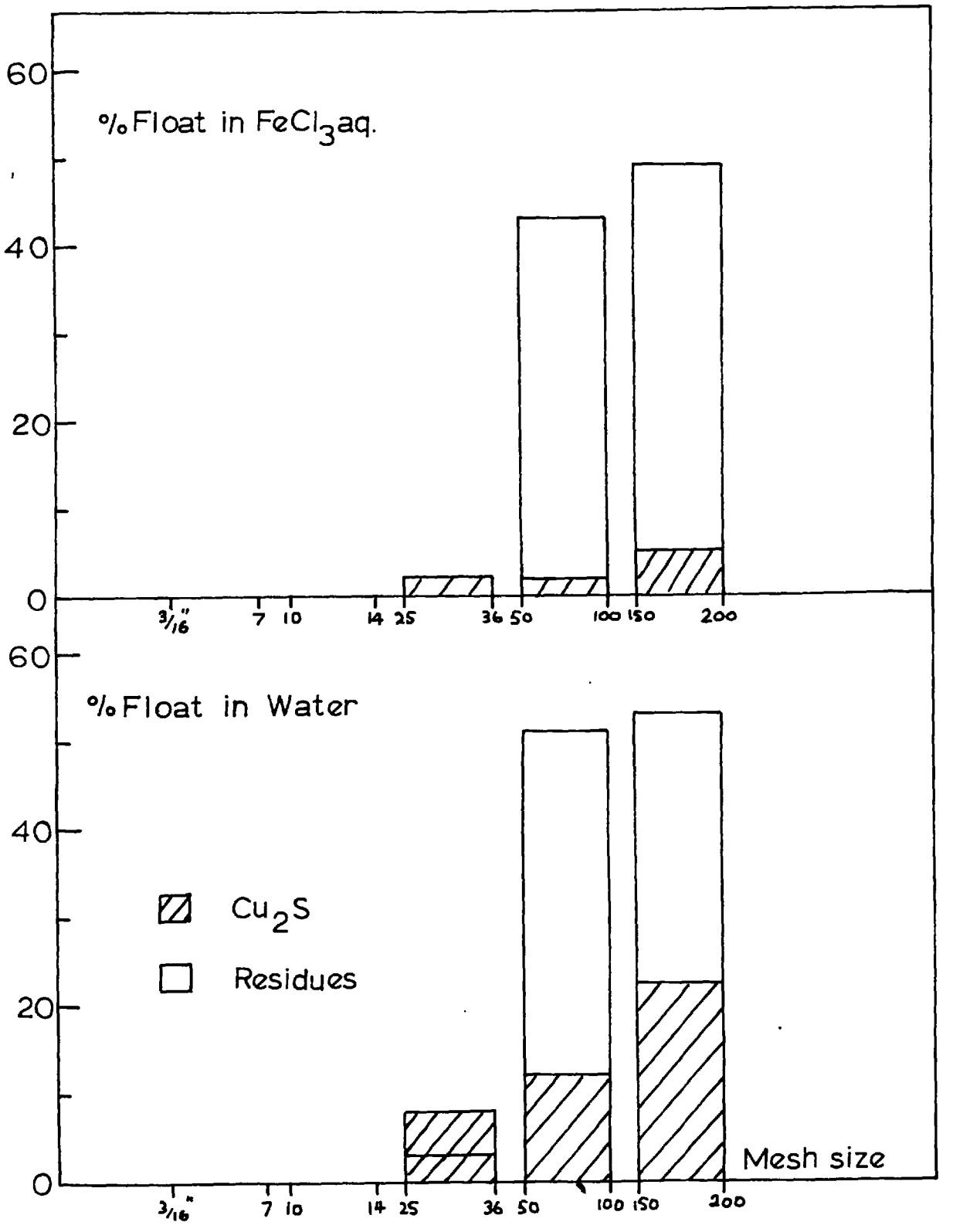


FIG.76 Floatation of Cu_2S and Residue Particles in Water and $FeCl_3$ aq.

Appendix 4

The Densities and Viscosities of Iron Chloride Solutions

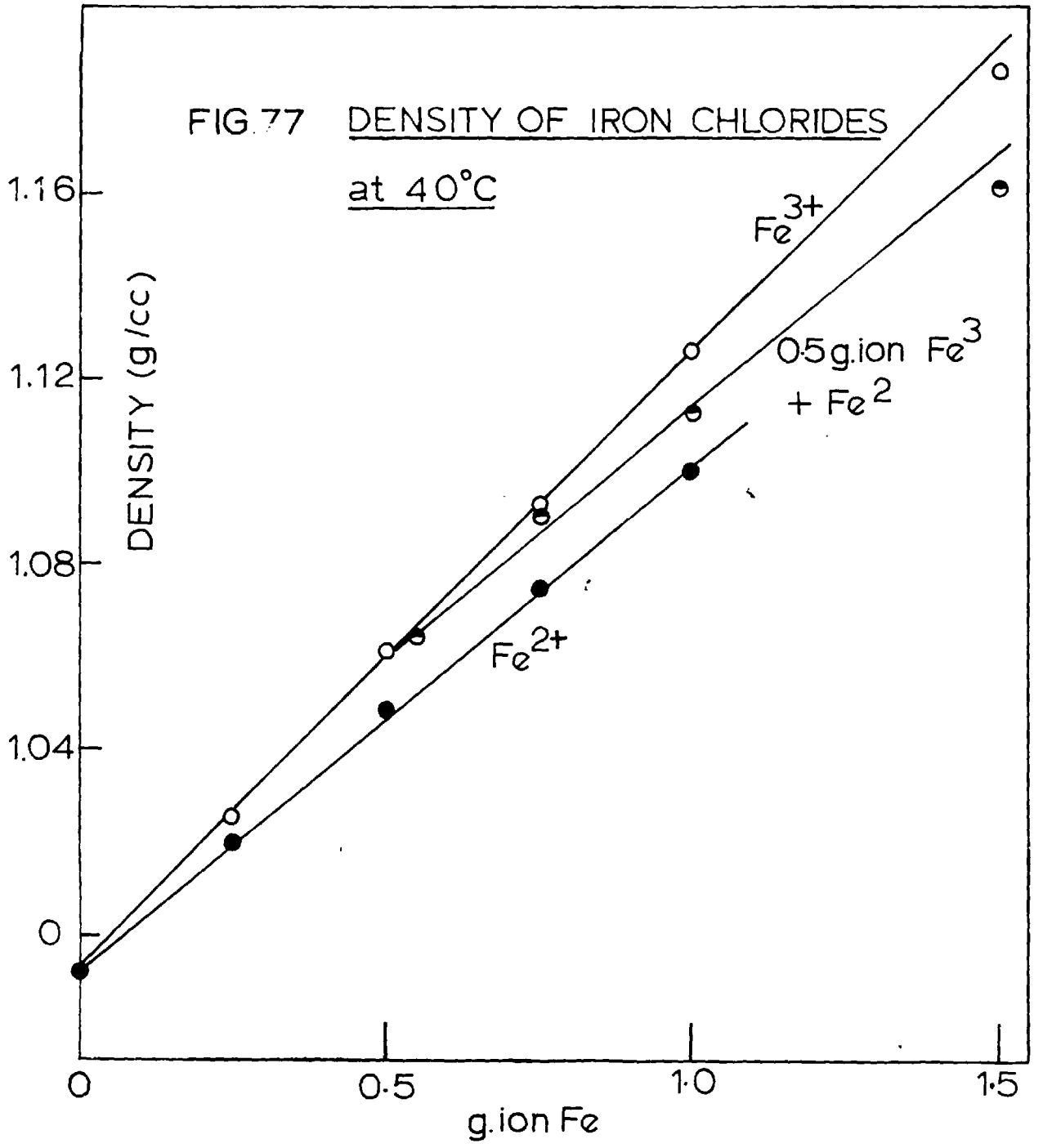
The densities were measured using a glass density bottle with capilliary stopper.

The viscosities were determined using a capilliary U-tube viscometer. The U-tube was kept in water thermostatically maintained at 40°C. 5 mls of solution were pipetted into the viscometer and allowed 20 minutes to come to equilibrium. The liquid was sucked above the top level and released. The time taken for the liquid to fall between two marks on the tube was noted and compared with that of water, of known viscosity:

$$\frac{\eta_1}{\eta_2} = \frac{\rho_1}{\rho_2} \times \frac{t_1}{t_2} \qquad \left[\begin{array}{r}\text{Subscript } 1 - \text{water} \\ 2 - \text{solution}\end{array}\right]$$

Results: (figs 77 and 78)

Liquid	(g/cc)	η (centipoise)
Water	0.9922	0.654
0.05 Fe^{2+} + 0.5Fe^{3+} per litre	1.0645	0.909
0.25 " + "	1.0901	0.988
0.50 " + "	1.1109	1.054
1.0 " + "	1.1615	1.275
0.25 Fe^{2+} per litre	1.0201	0.722
0.50 " " "	1.0485	0.793
0.75 " " "	1.0743	0.876
1.00 " " "	1.1010	0.955
0.25 Fe^{3+} " "	1.0258	0.764
0.50 " " "	1.0616	0.896
0.75 " " "	1.0929	1.036
1.00 " " "	1.1260	1.207
1.50 " " "	1.1855	1.573


FIG.77 DENSITY OF IRON CHLORIDES
at 40°C
1.16
1.12
1.08
1.04
0
DENSITY (g/cc)
Fe^{3+}
0.5 g.ion Fe^{3} + Fe^{2}
Fe^{2+}
0
0.5
1.0
1.5
g.ion Fe

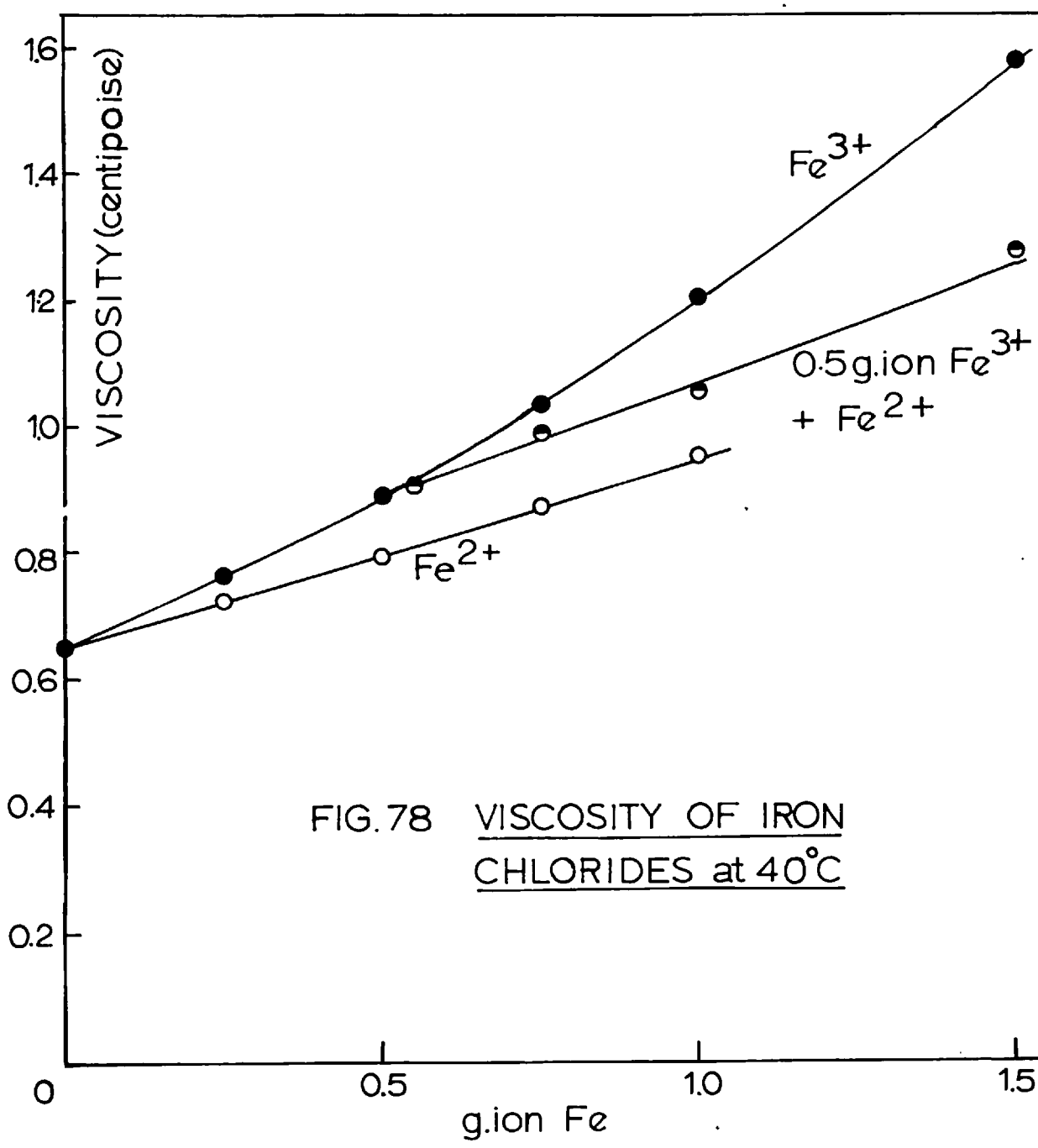


FIG. 78 VISCOSITY OF IRON CHLORIDES at 40°C

Appendix 5 X-ray Powder Photograph Residues

a) First reaction-half

Leach conditions: 2.5g (-50 + 100 mesh) Cu_2S, 900 rpm, 40°C, variable ferric ion concentration, 20 mls c HCl /l, 60 minutes. 20 mls of the leach liquor were analysed in the usual manner.

Film	Fe^{3+} conc.g.ion/l	d	%Cu dissolved
1	-	-	0.0 (Cu_2S)
2	0.0156	0.099	7.28
3	0.0195	0.120	8.83
4	0.0235	0.136	10.0
5	0.0274	0.152	11.2
6	0.0313	0.185	13.6
7	0.0470	0.282	20.7
8	0.0548	0.318	23.4
9	0.0625	0.367	27.0
10	0.0782	0.472	34.7
11	0.0940	0.560	41.2
12	0.125	0.651	47.9

b) Second reaction-half

Leach conditions: 2.5g (-50 + 100 mesh)Cu_2S ; 900 rpm ; Fe^{3+}/Fe^{2+} = 10, Fe^{3+} = 0.5 g.ion /l ; 20 mls cHCl/l.

5 mls of the leach liquor were analysed in the usual manner. The derived rate-curves are shown in figs. 31 and 32.

40°C

Film	sample time	d	%Cu dissolved
13	5 mins	0.1605	46.7
14	45	0.180	52.4
15	2½ hrs	0.2005	58.4
16	5	0.2235	65.1
17	8	0.241	70.2
18	12	0.2545	74.2
19	18	0.271	79.0
20	24	0.282	82.2
21	36	0.295	86.0
22	48	0.304	88.6
23	60	0.3145	91.7

60°C

Film	sample time	d	%Cu dissolved
24	4 mins	0.1745	51.3
25	15	0.2055	60.5
26	30	0.228	67.1
27	1 hr	0.252	74.2
28	2	0.2785	82.0
29	3	0.2935	86.4
30	4	0.3045	89.7
31	6	0.3195	94.1
32	8	0.327	96.3
33	12	0.3315	97.6
34	24	0.337	99.2

80°C

Film	sample time	d	%Cu dissolved
35	4 mins	0.218	64.7
36	10	0.258	76.5
37	20	0.3005	89.2
38	30	0.326	96.8
39	1 hr.	0.3355	99.6
40	4	0.337	100.0

Appendix 6

Diffraction Data on Copper Sulphide Phases

i) Cu_2S III 20°C Djurle[19]

hkl	d	I	hkl	d	I	hkl	d	I
131	6.376	w	442	2.528	m	346	1.879	st
231	4.666	w	135			086		
151			1.10.2	2.476	m	582		
222	4.240	w	413	2.466	m	455	1.876	w
251	3.856	w	193			366		
062	3.775	w	215	2.477	w	237	1.798	w
242	3.3735	m	344	2.404	st	157		
162	3.598	m	084	2.401	st	2.12.4		
233	3.335	w	433	2.392	w	633		
153			373			475	1.778	w
322	3.315	m	235	2.370	w	515		
024	3.275	m	155			4.11.3	1.755	w
262	3.186	m	471	2.330	m	593		
342	3.056	m	2.10.2			4.10.4	1.729	
280	2.966	w	480			317		
400			502	2.242	m	077		
182	2.953	m	255			177	1.710	w
204	2.933	m	522	2.211	m	604		
144			106			3.12.4	1.704	w
411	2.886	m	126	2.181	w	584	1.688	w
173	2.865	w	444	2.120	w	008		
224			2.12.2	2.028		1.15.3		
333	2.826	w	562	2.0.11	w	1.14.4	1.672	w
431	2.765	m	246			028		
362	2.733	m	464	2.003	w	466		
440	2.725	m	600	1.981	m	682	1.661	w
244	2.696	w	3.12.0	1.975	st	0.16.2		
422	2.667	m	580			277	1.658	w
291	2.647	w	435	1.952	m	128		
164			306			722	1.637	w
115	2.616	m	266	1.910	w	048		
353			3.12.2	1.897	w			
451	2.563	w	117					
0.10.2	2.533	m						

ii) $Cu_{1.96}S$ III 20°C Djurle[19]

d	I
4.29	w
3.89	w
3.748	m
3.584	w
3.381	m
3.276	w
3.191	w
3.101	w
3.035	w
3.009	w
2.963	w
2.938	w
2.882	w
2.864	w
2.831	w
2.812	w
2.784	w
2.688	w
2.653	w
2.599	w
2.561	w
2.518	w
2.475	w
2.415	w
2.389	st
2.316	w
2.291	w
2.264	w
2.142	w
2.107	w
2.070	w
2.047	w
1.963	m
1.957	m
1.870	st
1.830	w
1.690	m
1.680	w
1.513	w
1.273	m
1.120	w

iii) $Cu_{1.96}S$ II 20°C Djurle[19]

hkl	d	I
101) 003)	3.76	w
102	3.26	w
110	2.829	w
004	2.812	vw
103) 111)	2.743	st
194	2.304	st
113	2.261	w
200) 114)	1.991	m
201	1.970	m
202	1.888	w
203) 211)	1.767	w
212	1.707	w+
106	1.699	vw
213	1.616	w
214	1.511	vw
107	1.492	w
215) 221)	1.403	m
108) 301) 223)	1.327	w
312	1.235	w
217	1.197	w

iv) Phase $Cu_{1.8}S$ II 20°C Djurle[19]

hkl	Composition							
	$Cu_{1.82}S$		$Cu_{1.78}S$		$Cu_{1.74}S$		$Cu_{1.70}S$	
	d	I	d	I	d	I	d	I
	3.407	vw	3.397	vw			3.394	vw
	3.355	w	3.358	vw	3.355	vw	3.361	vw
							3.267	vw
111	3.212	m+	3.212	m+	3.207	m	3.204	m
	3.010	m	3.019	m	3.031	w	3.040	w
200	2.784	m+	2.780	m+	2.778	m	2.777	m
	2.753	vw	2.736	vw			2.679	vw
	2.556	w	2.543	vw	2.529	vw	2.502	vw
	2.341	w	2.357	vw			2.414	vw
							2.252	vw
	2.145	m	2.151	m	2.161	w	2.175	w
					2.141	vw	2.136	vw
					2.092	vw	2.084	vw
220	1.971	st	1.967	st	1.965	st	1.962	st
	1.816	vw	1.822	vw			1.838	vw
	1.755	w	1.760	w	1.770	w	1.780	w
							1.762	vw
	1.699	vw	1.698	vw			1.699	vw
311	1.679	m	1.677	m	1.676	m	1.673	m
222	1.608	w	1.607	w	1.606	vw	1.604	w
	1.561	vw	1.554	vw				
	1.451	w	1.452	w	1.454	vw	1.457	vw
400	1.393	w	1.391	w+	1.389	w	1.387	w
	1.310	w	1.312	w	1.314	vw	1.318	vw
	1.286	vw	1.285	vw			1.284	vw
	1.278	vw	1.278	vw			1.273	vw
	1.264	vw	1.264	vw			1.262	vw
	1.222	vw	1.222	vw	1.220	vw	1.213	vw
	1.203	vw	1.205	vw				
	1.169	vw	1.168	vw			1.169	vw
422	1.137	m	1.136	m	1.134	m	1.133	m

v) Phase CuS Reference 90

d	I	hkl
8.18	7	002
3.285	14	100
3.220	28	101
3.048	67	102
2.813	100	103
2.724	56	006
2.317	10	105
2.097	6	106
2.043	7	008
1.902	25	107
1.896	75	110
1.735	34	108
1.634	3	201
1.609	8	202
1.572	15	203
1.556	37	116
1.463	6	1.0.10
1.390	6	118
1.354	7	1.0.11
1.343	5	207
1.280	9	208
1.227	5	212
1.210	9	213
1.0998	8	1.0.14
1.0946	10	300
1.0607	9	218
1.0155	7	306

vi) Orthorhombic Sulphur De Wolff[91]

d	I	hkl	d	I	hkl
7.69	6	111	2.404	2	404
5.76	14	113	2.375	4	422
5.68	5	022	2.366	4	335
4.80	2	202	2.288	6	0.2.10
4.19	2	151	2.215	2	048,2.0.10
4.06	11	220	2.146	4	1.1.11
3.91	12	131	2.112	10B	319, 062
3.85	100	222	2.098	2	2.2.10
3.57	8	133	2.057	1	511
3.44	40	026	2.041	1	0.0.12,248
3.38	3	224	2.003	2	353
3.33	25	311	1.988	4	408
3.21	60	206	1.957	2	262
3.11	25	313	1.926	1	444
3.08	17	135	1.900	7B	355,066,515
3.06	±	008	1.856	1	3.1.11
2.842	18	044	1.838	1	159
2.688	2	331	1.823	4	2.4.10
2.673	1	242	1.781	11	266,357
2.621	13	137	1.754	7	535
2.614	4	400	1.725	8	602
2.569	8	333	1.698	7	1.3.13
2.501	7	244	1.665	2	
2.424	13	317	1.658	2	
			1.647	5	

Appendix 7

Measurement and Calculation of Residue X-ray Powder Photographs

Glass capilliary tubes of 0.5 mm diameter were filled with the ground residues of Appendix 5. X-ray powder photographs were taken using a Phillips 9 cm camera and a Phillips X-ray generator. A copper filter was used at 25 Kv and 20 mA. The exposure time was 6 hours throughout

The camera was calibrated by measuring the lines of spectrographically pure copper. The films of the residues were measured and corrections made for film shrinkage. The calculated d-values, and the intensities of the lines expressed as a percentage of the intensities of the strongest line, are now tabulated hereafter.

a) First reaction-half

Film 1 Original Cu_2S

θ	d	I	θ	d	I
11.90	3.739	5	21.575	2.096	10
12.37	3.599	5	22.985	1.974	100
13.44	3.317	10	23.26	1.952	5
13.615	3.275	10	24.22	1.871	80
13.94	3.200	10	26.855	1.706	20
14.09	3.167	10	27.175	1.688	5
14.635	3.051	5	27.805	1.653	$2\frac{1}{2}$
15.135	2.952	15	28.18	1.632	$2\frac{1}{2}$
15.485	2.887	5	30.335	1.524	5
16.21	2.761	5	31.535	1.474	$2\frac{1}{2}$
16.41	2.729	20	34.58	1.358	$2\frac{1}{2}$
16.76	2.673	10	34.88	1.348	$2\frac{1}{2}$
17.06	2.629	5	36.575	1.294	$2\frac{1}{2}$
17.485	2.567	5	37.00	1.281	5
17.735	2.531	15	37.40	1.269	5
18.135	2.477	15	39.07	1.223	$2\frac{1}{2}$
18.715	2.403	40	41.24	1.169	$2\frac{1}{2}$
19.315	2.331	20	43.23	1.126	$2\frac{1}{2}$
20.12	2.241	20	45.40	1.083	$2\frac{1}{2}$
20.37	2.215	20			
21.30	2.122	10			

Film 2 7.28% Cu dissolved

θ	d	I	θ	d	I
12.825	3.473	$2\frac{1}{2}$	18.085	2.483	5
13.12	3.396	5	18.715	2.403	40
13.865	3.217	5	23.085	1.966	100
14.735	3.031	5	24.295	1.874	70
15.385	2.906	$2\frac{1}{2}$	27.03	1.696	15
15.76	2.838	$2\frac{1}{2}$	27.28	1.682	15
16.01	2.795	$2\frac{1}{2}$	27.88	1.649	10
16.535	2.709	5	30.51	1.518	5
16.76	2.673	5	37.12	1.277	10
17.435	2.573	5	45.80	1.075	5
17.735	2.531	5			

Film 3 8.83% Cu dissolved

θ	d	I
13.145	3.390	5
13.84	3.223	20
14.735	3.031	10
16.035	2.791	20
18.77	2.396	20
23.085	1.966	100
24.32	1.872	20
27.055	1.695	5
27.30	1.681	15
42.66	1.138	5
46.025	1.071	10
15.51	2.882	5
15.73	2.844	5

Film 4 10.0% Cu dissolved

θ	d	I
13.12	3.396	5
13.865	3.217	20
14.69	3.040	10
15.46	2.892	5
15.785	2.835	5
16.085	2.782	20
18.77	2.396	20
23.135	1.962	100
24.32	1.872	20
27.08	1.693	5
27.33	1.679	15
42.635	1.138	5
46.025	1.071	10

Film 5 11.2% Cu dissolved

θ	d	I
13.84	3.223	20
14.665	3.045	5
16.085	2.782	20
18.77	2.396	15
20.87	2.164	5
23.085	1.966	100
24.295	1.874	15
27.13	1.691	5
27.355	1.678	15
42.635	1.138	5
46.00	1.072	10

Film 6 13.6% Cu dissolved

θ	d	I
13.865	3.217	35
14.665	3.045	5
16.11	2.778	35
20.82	2.169	5
23.135	1.962	100
27.43	1.673	25
33.76	1.387	10
42.91	1.132	15
46.125	1.069	10

Film 7 20.7% Cu dissolved

θ	d	I
13.88	3.214	30
14.46	3.087	5
14.635	3.051	5
16.11	2.778	30
20.77	2.174	5
23.135	1.962	100
23.665	1.921	20
25.175	1.812	2½
27.455	1.672	20
28.81	1.500	2½
33.785	1.386	2½
35.85	1.316	2½
42.955	1.131	10
46.20	1.068	5

Film 8 23.4% Cu dissolved

θ	d	I
13.84	3.223	20
14.44	3.091	5
14.585	3.002	5
16.135	2.774	30
20.77	2.174	5
23.16	1.960	100
23.665	1.921	40
25.175	1.812	5
27.43	1.673	30
28.81	1.600	5
33.805	1.386	5
35.85	1.316	5
42.91	1.132	5

Film 9 27.0% Cu dissolved

θ	d	I
13.865	3.217	20
14.44	3.091	30
15.385	2.906	5
16.135	2.774	35
20.72	2.174	2½
23.135	1.962	100
23.74	1.915	60
25.20	1.811	5
27.455	1.672	5
28.785	1.601	5

Film 10 34.7% Cu dissolved

θ	d	I
14.44	3.091	40
15.435	2,896	30
16.185	2.766	30
23.16	1.960	30
23.84	1.907	100
25.225	1.809	15
29.005	1.590	20

Film 11 41.2% Cu dissolved

θ	d	I
13.565	3.287	2½
13.765	3.240	2½
14.485	3.082	50
15.56	2.874	40
16.235	2.757	20
23.915	1.902	100
25.32	1.803	10
26.45	1.731	5
28.58	1.611	5
29.105	1.585	30
38.72	1.232	5
44.625	1.098	5

Film 12 47.9% Cu dissolved

θ	d	I
13.59	3.281	5
13.765	3.240	5
14.235	3.135	5
14.51	3.077	50
15.585	2.869	40
16.26	2.753	20
23.94	1.900	100
25.345	1.801	10
26.425	1.732	10
28.53	1.614	10
29.13	1.584	30
38.90	1.228	5
44.725	1.096	5

b) Second reaction-half

Film 24 51.3% Cu dissolved

θ	d	I
13.565	3.287	10
13.74	3.246	10
14.51	3.077	50
15.61	2.865	40
16.235	2.757	30
23.97	1.897	100
25.345	1.801	10
26.375	1.735	5
28.605	1.610	5
29.185	1.581	20
38.90	1.228	5
44.755	1.095	5

Film 25 60.5% Cu dissolved

θ	d	I
11.50	3.867	5
13.565	3.287	10
13.765	3.240	10
14.315	3.118	5
14.51	3.077	40
15.635	2.860	30
16.235	2.757	20
23.995	1.896	100
25.395	1.798	10
26.425	1.732	5
28.58	1.611	5
29.235	1.578	20
38.845	1.229	5
44.78	1.094	5

Film 26 67.1% Cu dissolved

θ	d	I
11.28	3.941	5
11.475	3.875	10
13.59	3.281	10
13.765	4.240	10
14.315	3.118	10
14.485	3.082	40
15.66	2.856	30
16.26	2.753	15
23.97	1.897	100
25.50	1.791	10
26.475	1.729	5
28.605	1.610	5
29.31	1.575	15
38.90	1.228	5
44.83	1.0934	5

Film 27 74.2% Cu dissolved

θ	d	I
11.305	3.932	10
11.475	3.875	15
12.865	3.462	5
13.34	3.341	$2\frac{1}{2}$
13.615	3.275	5
13.815	3.228	10
14.315	3.118	10
14.51	3.077	30
15.66	2.856	20
16.26	2.753	15
23.995	1.896	100
25.52	1.789	5
26.475	1.729	5
28.555	1.613	5
29.285	1.576	15
38.795	1.230	5
44.88	1.092	5

Film 28 82.0% Cu dissolved

θ	d	I
11.35	3.917	5
11.50	3.867	30
12.89	3.456	15
13.365	3.335	10
13.815	3.228	20
14.29	3.123	15
14.535	3.072	25
15.685	2.851	25
17.035	2.631	5
17.935	2.503	5
18.435	2.438	5
18.935	2.376	5
19.615	2.296	5
21.40	2.113	5
23.995	1.896	100
25.60	1.784	5
26.00	1.759	$2\frac{1}{2}$
26.475	1.729	5
27.03	1.696	$2\frac{1}{2}$
28.38	1.622	5
28.63	1.609	5
29.285	1.576	10
34.58	1.358	5
38.82	1.230	5
44.755	1.095	10

Film 29 86.4% Cu dissolved

θ	d	I
7.66	5.783	5
10.93	4.066	5
11.13	3.994	5
11.305	3.932	5
11.50	3.867	80
12.915	3.449	15
13.34	3.341	5
13.815	3.228	15
14.29	3.123	10
14.535	3.072	10
15.685	2.851	10
17.06	2.628	5
17.935	2.503	5
18.435	2.438	5
18.91	2.379	5
19.64	2.294	5
21.30	2.123	5
23.97	1.897	100
25.60	1.784	5
25.975	1.760	$2\frac{1}{2}$
26.475	1.729	5
26.98	1.699	$2\frac{1}{2}$
27.605	1.664	$2\frac{1}{2}$
27.88	1.649	$2\frac{1}{2}$
28.33	1.624	5
28.58	1.611	5
29.385	1.571	5
34.58	1.358	5
38.845	1.229	$2\frac{1}{2}$
44.88	1.092	5

Film 30 89.7% Cu dissolved

A	d	I
7.685	5.765	5
10.88	4.084	5
11.305	3.932	30
11.475	3.875	100
12.42	3.584	5
12.89	3.456	20
13.34	3.341	10
13.815	3.228	20
14.29	3.123	10
15.635	2.860	10
17.035	2.631	10
17.885	2.510	10
18.46	2.435	10
18.935	2.376	10
19.615	2.296	10
21.30	2.123	10
23.995	1.896	30
25.02	1.823	5
25.60	1.784	10
26.025	1.757	5
26.525	1.726	10
26.98	1.699	5
27.53	1.668	5
27.905	1.647	5
28.305	1.626	10
28.655	1.608	10
32.285	1.443	5
32.785	1.424	5
34.53	1.360	5
44.78	1.094	5

Film 31 94.1% Cu dissolved

A	d	I
5.835	7.582	5
7.44	5.953	5
7.71	5.746	10
10.93	4.066	5
11.305	3.932	30
11.50	3.867	100
12.42	3.584	5
12.915	3.449	30
13.165	3.365	5
13.34	3.341	10
13.815	3.228	30
14.315	3.118	10
14.44	3.091	10
15.685	2.851	10
17.085	2.624	10
17.385	2.580	5
17.885	2.510	10
18.46	2.435	10
18.91	2.379	10
19.665	2.291	10
21.325	2.120	20
23.945	1.899	20
24.945	1.828	5
25.55	1.787	10
26.05	1.755	5
26.55	1.725	10
27.005	1.698	5
27.555	1.666	5
27.855	1.650	5
28.355	1.623	10
28.68	1.606	10
32.36	1.440	5
32.785	1.424	5
34.58	1.358	5

Film 32 96.3% Cu dissolved

θ	d	I
7.49	5.914	5
7.635	3.924	10
10.88	4.084	10
11.28	3.941	30
11.475	3.875	100
12.395	3.591	5
12.865	3.462	20
13.12	3.396	5
13.29	3.353	10
13.59	3.281	5
13.765	3.240	25
14.265	3.128	10
14.39	3.102	10
15.635	2.860	10
17.01	2.635	10
17.435	2.573	5
17.935	2.503	10
18.46	2.435	10
18.91	2.379	10
19.615	2.296	10
20.195	2.233	5
20.995	2.152	5
21.325	2.120	10
22.58	2.008	5
22.785	1.991	5
23.11	1.964	5
23.865	1.905	10
24.92	1.830	5
25.575	1.786	10
25.975	1.760	10
26.425	1.732	10
26.955	1.701	10
27.555	1.666	5
27.805	1.653	5
28.33	1.624	10
28.605	1.610	10
32.31	1.442	5
32.81	1.423	5
34.605	1.357	5

Film 33 97.6% Cu dissolved

θ	d	I
5.49	8.057	5
5.76	7.680	5
7.465	5.934	5
7.685	5.765	10
10.98	4.048	10
11.28	3.941	30
11.525	3.858	100
12.47	3.572	5
12.865	3.462	20
13.12	3.396	5
13.34	3.341	10
13.59	3.281	5
13.84	3.223	25
14.29	3.123	15
14.39	3.102	15
15.66	2.856	15
17.06	2.628	10
17.435	2.573	5
18.01	2.493	10
18.51	2.428	10
18.91	2.379	10
19.64	2.294	10
20.295	2.222	5
21.045	2.147	5
21.40	2.113	10
22.605	2.006	5
22.86	1.984	5
23.21	1.956	5
23.945	1.899	10
25.02	1.823	5
25.675	1.779	10
26.075	1.754	10
26.575	1.723	10
27.03	1.696	10
27.605	1.664	5
27.93	1.646	5
28.38	1.622	10
28.655	1.608	10
32.36	1.440	10
32.86	1.421	10
34.68	1.355	5

Film 34 99.2% Cu dissolved

θ	d	I
5.76	7.680	5
7.515	5.895	5
7.66	5.783	10
10.93	4.066	10
11.305	3.932	30
11.50	3.867	100
12.42	3.584	5
12.62	3.516	2½
12.845	3.467	30
13.12	3.396	5
13.34	3.341	10
13.615	3.275	5
14.79	3.234	30
14.265	3.128	10
14.37	3.108	5
15.635	2.860	10
17.01	2.635	10
17.36	2.584	2½
17.935	2.503	10
18.435	2.438	10
19.935	2.376	10
19.615	2.296	10
20.22	2.230	2½
20.97	2.154	2½
21.325	2.120	10
22.58	2.008	5
22.785	1.991	5
23.11	1.964	5
23.84	1.907	10
24.945	1.828	5
25.55	1.787	10
26.00	1.759	10
26.50	1.728	10
26.955	1.701	10
27.555	1.666	5
27.88	1.649	5
28.33	1.624	5
28.555	1.613	5
32.385	1.439	5
32.76	1.425	5
34.58	1.358	5

Appendix 8

Electron Probe Calibration Curves for Copper and Sulphur

The mean point counts on spectrographically pure copper, recrystalised chalcocite, and leach residues of Appendix 5(a), are tabulated below. The specimen current (6.1×10^{-6} mA) was constant throughout.

Figs. 79 and 80 are the calibration curves for copper and sulphur respectively.

Material	Copper counts per second.	Sulphur counts per second
Spec. pure copper	11.13×10^3	108
Cu_2S (79.86 Wt%Cu)	8.64	6.62×10^2
Residue of Film 2 (78.7 Wt%Cu)	8.46	6.95
Residue of Film 7 (74.5 Wt%Cu)	7.92	8.42
Residue of Film 12 (67.6 Wt%Cu)	6.97	10.14

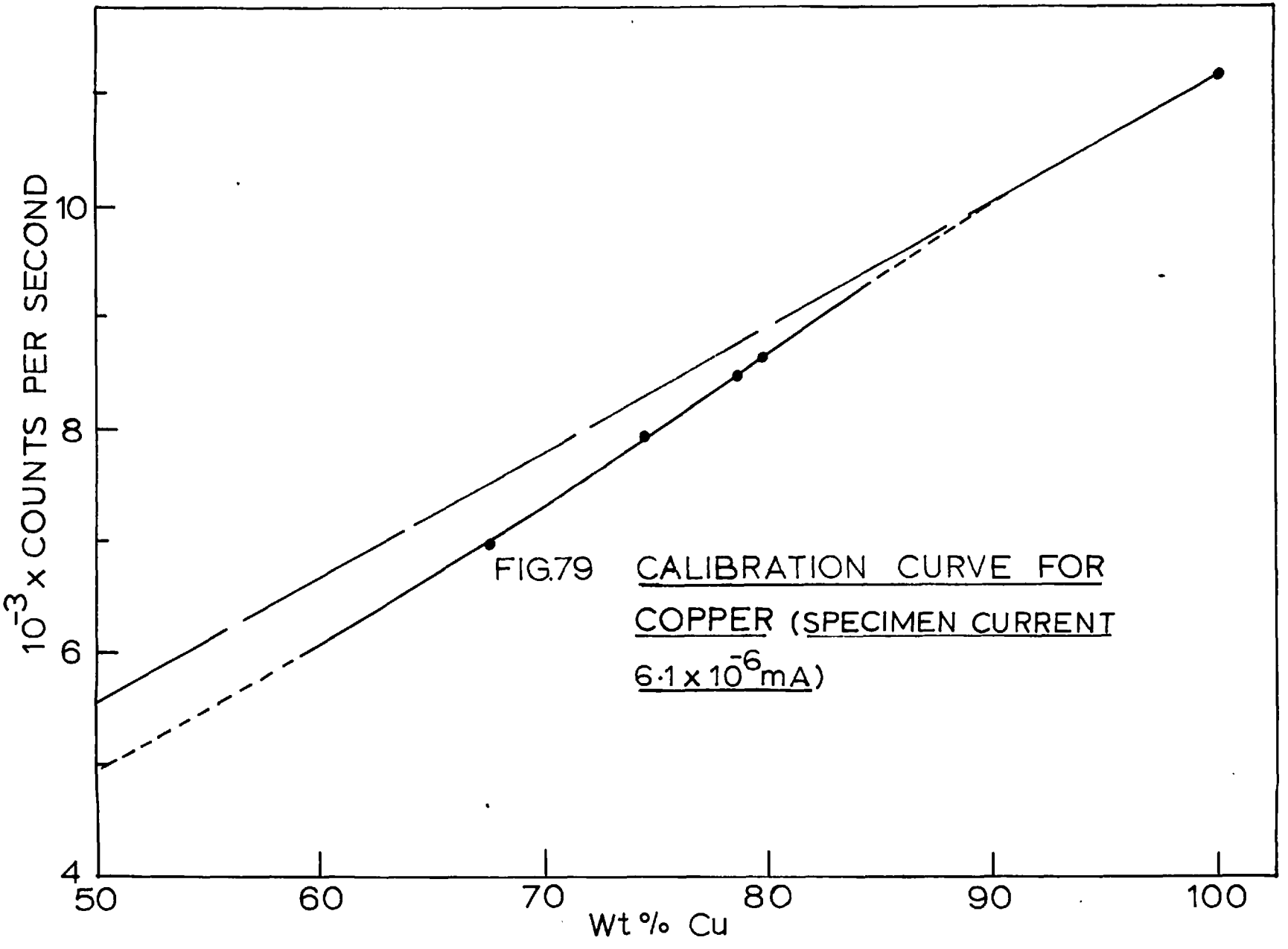


FIG.79 CALIBRATION CURVE FOR COPPER (SPECIMEN CURRENT 6.1×10^{-6} mA)

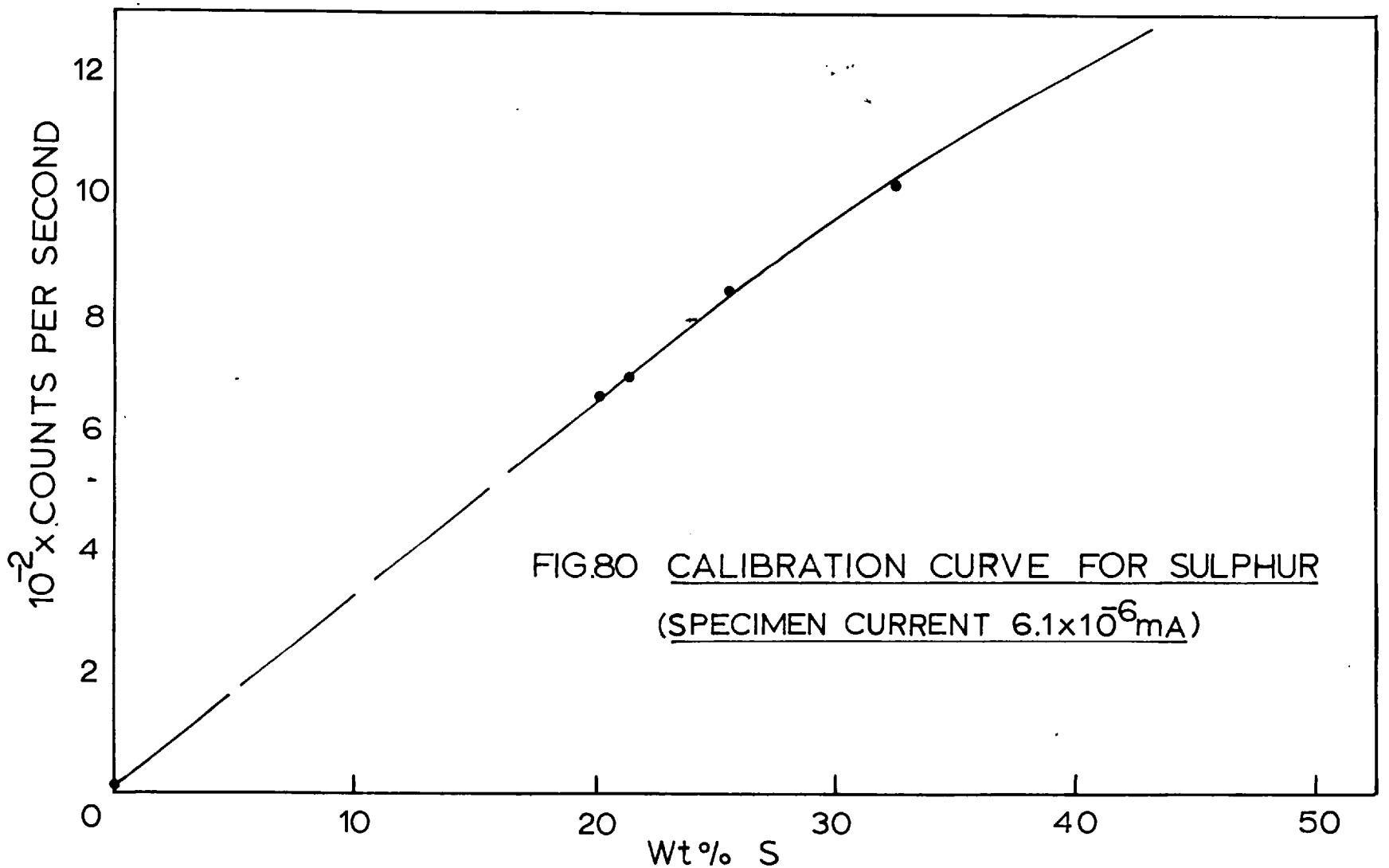


FIG.80 CALIBRATION CURVE FOR SULPHUR
(SPECIMEN CURRENT 6.1×10^{-6} mA)

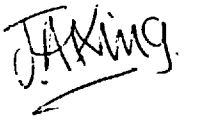
ACKNOWLEDGEMENTS

Primarily, the author wishes to convey sincere gratitude to his supervisor, Dr. A. R. Burkin for the encouragement and guidance given throughout the research project.

The author is indebted to the Science Research Council for financial assistance during the period 1963 - 1966.

Thanks are due to Mr. N. Ware for valuable assistance given with the JEOL Electron Probe Microanalyser, and to Mrs. E. King for typing the thesis and checking the proofs.

Finally, the author thanks his colleagues in the Nuffield Research Group for many valuable discussions and the permanent laboratory staff for their co-operation.



Royal School of Mines,
London, S.W.7

REFERENCES

1. Sullivan J.D. U.S.Bureau of Mines, 1930, Technical papers 473, 487, et al.
2. Warren I.H. Aust. J. App. Sci., 1958, 9, p.36
3. Warren B.E. & Burwell J.T. J. Chem. Phys., 1935 3, p.6
4. Abrahams S.C. Acta Cryst., 1955, 8, p.661.
5. Oftedal I. Zeits. Krist., 1932, 83, p.9.
6. Roberts H.S. & Ksanda C.J. Am. J. Sci., 1929, 17, p.489.
7. Gossner B. & Mussgnug F. Cbl. Min., Abt.A, 1927, p.410.
8. Wyckoff - Crystal Structures. Chap. III, fig. III, 14.
9. Berry L. G. Am. Min., 1954, 39, p.504.
10. Oftedal I. Norsk. Geol. Tidsk., 1945, 24, p.114.
11. Buerger N.W. Econ. Geol., 1941, 36, p.19.
12. Buerger N.W. & Buerger M.J. Am. Mineral., 1944, 27, p.712.
13. Belov N.V. & Butuzov V.P. C.R. Acad. Sci. USSR, 1946, 54, p.717.
14. Weunsch B.J. & Buerger M.J. Science, 1963, 141, p.276.
15. Weunsch B.J. & Buerger M.J. Mineral Soc. Am. Spec. Paper No. 1, 1963, p.164.
16. Hirahara F. T. Phys. Soc. Japan, 1949, 2, p.211.

17. Ueda R. J. Phys. Socl Japan, 1949, 3, p.287.

18. Djurle S. Acta Chem. Scand., 1958, 12, p.1415.

19. Wuensch B.J. Professor of Ceramics, Private communication, M.I.T. December, 1965.

20. Johannsen F. & Vollmer H. Z. Erzbergban Metallhuettenw, 1960, 13, p.313.

21. Bornemann K. & Wagenmann K. Ferrum, 1913/14, 10, p.976.

22. Schuhmann R. & Moles O.W. Trans. A.I.M.E., 1951, 191, p.235.

23. Heyn E. & Bauer O. Metallurgie, 1906, 3, p.73.

24. Smith D. Unpublished Thesis, M.I.T., 1952.

25. Sudo K. Science Reports of the Research Institutes, Tohoku University, 1950, (A), 2, No 3, p.519.

26. Krivsky W.A. Unpublished Thesis, M.I.T., 1954.

27. Smith C.S. Trans A.I.M.E., 1938, 128, p.325.

28. Friedrich K. & Wachlert M. Metall.u. Erz., 1913, 10, p.976.

29. Joukoff J.G. Metall. u Erz., 1929, 26, p.137.

30. Jensen E. Norske Videnskaps - Akad., Oslo, Mat. Naturv. Klasse, 6. 1947.

31. Posnjack E., Allen E.T., & Mervin H. Z. anorg. allg. Chem., 1916, 94, p.95.

32. Ruhl W. & Saur E. Ber. Oberhess. Ges. Natur - Heilk. Giessen, Naturw. Abt., 1957, 28, p.35.

33. Elliot R.P. 'Constitution of Binary Alloys' 1962 McGraw - Hill.

34. Lamb A.B. & Jacques A.G. J.Am. Chem. Soc., 1938, p.967.

35. Siddall T.H. & Vosburgh W.C. J.Am. Chem. Soc., 1951, p.4270.

36. Olson A.R. & Simonson T.R. J. Chem. Phys., 1949, 17, p.1322.

37. Bray W.C. & Hershey A.V. J.Am. Chem. Soc., 1934, p.1889.

38. Milburn R.M. J. Am. Chem Soc., 1957, p.537.

39. Hedstrom B.O.A. Arkiv for Kemi 1953, Bd 6, Nr 1, p.1.

40. Milburn R.M & Vosburgh W.C. J. Am. Chem. Soc., 1955, 77, p.1352.

41. Rabinovitch E. & Stockmayer W.H. J. Am Chem. Soc., 1942, 64, p.335.

42. Lamb A.B. & Jacques A.G. J. Am. Chem. Soc., 1938, p.1215.

43. Mulay L.N & Selwood P.W. J.Am Chem. Soc., 1955, 77, p.2693.

44. Bronsted J.N. & Volgnartz K. Z. phys. Chem., 1928, 134, p.97.

45. Lindstrand F. Svensk Kem. Tidskr., 1944, 56, p.14.

46. Brosset C. Svensk Kem. Tidskr., 1941, 53, p.434.

47. Arden T.V. J. Chem Soc., 1951, p.350.

48. Barb W.G., Baxendale J. H., George P., Hargrave K.R. Trans. Farad. Soc., 1951, 47, p.591.

49. Connick R.E. & Tsao M.S. J.Am. Chem Soc., 1954, 76, p.5311.

50. Wilson A.S. & Taube H. J. Am. Chem Soc., 1952, 74, p.3509.

51. Ito. T., & Tui N. Sci. Reports, Tchuku Univ., 1953, 37, p.19.

52. Connick R.E., Hepler L.G., Hugus Z. Z., Kury J.W., Latimer W.M., J. Am. Chem Soc., 1956, 78, p.1827.

53. Broersma S. J. Chem Phus., 1957, 26, p.1405.

54. Turner R.C. & Miles K.E. Canad. J. Chem., 1957, 35, p.1002.

55. Perrin D. D. J. Chem. Soc., 1959, p.1710.

56. Richards D. H. & Sykes D.W. J. Chem. Soc., 1960, p.3626.

57. Schlyter K. Trans. Roy. Inst. Technol. Stockholm, 1962, Nr 195 & 196.

58. Popa G., Luca C & Iosif E. Z. phus. Chem (Leipzig), 1963, 222, p.49.

59. Biedermann G. Private Communication to Schlyter K, quoted in reference 57.

60. Lindstrand F. Dissertation. Lund (1939).

61. Hedstrom B.O.A. Arkiv Kemi, 1953, 5, p.457.

62. Lenssing D.L. & Koltoff I.M. J.Am. Chem. Soc., 1953, 75, p.2476.

63. Gayer K.H. & Wootner L. J. Am Chem. Soc., 1956, 78, p.3944.

64. Bolzan J. A. & Arvia A. Electrochim. Acta, 1963, 8, p.375.

65. Krans K. A. & Moore G.E. J. Am. Chem Soc., 1953, 75, p.1460.

66. McConnell H. & Davidson N. J. Am. Chem. Soc., 1950, 72, p.3164.

67. Bray W.C. & Hershey J. Am Chem. Soc., 1934, 56, p.1889.

68. Moller M. J. Phys. Chem., 1937, 41, p.1123

69. Bent H. E. & French C. L. J.Am Chem. Soc., 1941, 63, p.568.

70. Brosset C. Naturwiss, 1941, 29, p.455.

71. Rabinovitch E. & Stockmeyer W. H. J. Am. Chem Soc., 1942, 64, p.335.

72. Olerup H. Svensk Kem. Tidskr., 1943, 55, p.13.

73. Badoz - Lambling J. Bull. Soc. Chim. France, 1950, p.552.

74. Moore G. E. & Krans K. A. J. Am Chem Soc., 1950, 72, p.5792.

75. Li J.C.M. & Gregory N.W. J. Am Chem Soc., 1952, 74, p.4671.

76. Friedman H. L. J. Am Chem. Soc., 1952, 74, p.5.

77. Gamlen G. A. & Jordan D. O. J. Chem. Soc., 1953, p.1435.

78. Lister M. W. & Rivington D. E. Canad. J. Chem., 1955, 33, p.1603.

79. Brady G. W. J. Chem Phys., 1958, 29, p.1371.

80. Coll H., Nauman R. V. & West P. W. J. Am. Chem. Soc., 1959, 81, p.1284.

81. Marcus T. J. Inorg. Nucl. Chem., 1960, 12, p.287.

82. Sutin N. Rowley J. K. & Dodson R. W. J. Chem. Phys., 1961, 65, p.1248.

83. Standley C. L. & Kruh R. F. J. Chem Phys., 1961, 34, p.1450.

84. White J. M. Kelly P. & Li N. C. J, Inorg. Nuclear Chem., 1961, 16, p.337.

85. Lindstrand F. Dissertation, Lund, 1939.

86. Mattoo B. N. Z. phys. Chem. (Frankfurt) 1959, 19, p.156.

87. Olerup H. Dissertation, Lund. 1944.

88. Woods Gallagher & King. Inorg. Chem., 1962, 1, p.55.

89. Read H. H. Rutley's 'Elements of Mineralogy', Murby 1957.

90. A.S.T.M X-ray Indix Files. No.60464.

91. A.S.T.M. X-ray Index Files No.8247.

92. Betts R. H. Gilmour H.S. A, and Liegh R. K., J. Am. Chem. Soc., 1950, 72, p.4978.

93. Richardson F.D. & Jeffes J. H. E., J. Iron Steel Inst., 1952, 171, p.167.

94. Jost W. 'Diffusion', Wiley N.Y. 1961.